AD-A264 762

‖‖‖‖‖‖‖‖‖‖‖‖‖‖‖

WL-TR-92-4079

Internal Structural Characterization

R. Klaassen
M. Bashyam

General Electric Aircraft Engine
Quality Technology Center
One Neumann Way
Cincinnati, OH 45215-6301

August 1992

Final Report for 09/01/88 - 03/30/92

DTIC
ELECTE
MAY 26 1993
S E D

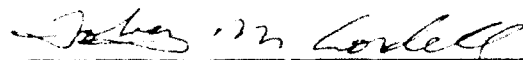93-11819
‖‖‖‖‖‖‖‖‖‖‖‖‖‖‖

93 5 25 229

NOTICE

When Government drawings, specifications, or other data are used for any other purpose other than in connection with a definitely Government-related procurement, the United States Government incurs no responsibility or any obligation whatsoever. The fact that the government may have formulated or in any way supplied the said drawings, specifications, or other data, is not to be regarded by implication, or otherwise in any manner construed, as licensing the holder, or any other person or corporation; or as conveying any rights or permission to manufacture, use, or sell any patented invention that may be related thereto.

This report is releasable to the National Technical Information Service (NTIS). At NTIS, it will be available to the general public, including foreign nations.

This technical report has been reviewed and is approved for publication.

CHARLES F. BUYNAK
Nondestructive Evaluation Branch
Metals and Ceramics Division

TOBEY M. CORDELL, Chief
Nondestructive Evaluation Branch
Metals and Ceramics Division

FOR THE COMMANDER

NORMAN N. TALLAN, Chief
Metals and Ceramics Division
Materials Directorate

If your address has changed, if you wish to be removed from our mailing list, or if the addressee is no longer employed by your organization please notify WL/MLLP Bldg 655, 2230 Tenth St Ste 1, WPAFB, OH 45433-7817 to help us maintain a current mailing list.

Copies of this report should not be returned unless return is required by security considerations, contractual obligations, or notice on a specific document.

REPORT DOCUMENTATION PAGE

Public reporting burden for this collection of information is estimated to average 1 hour per response, including the time for reviewing instructions, searching existing data sources, gathering and maintaining the data needed, and completing and reviewing the collection of information. Send comments regarding this burden estimate or any other aspect of this collection of information, including suggestions for reducing this burden, to Washington Headquarters Services, Directorate for Information Operations and Reports, 1215 Jefferson Davis Highway, Suite 1204, Arlington, VA 22202-4302, and to the Office of Management and Budget, Paperwork Reduction Project (0704-0188), Washington, DC 20503.

1. AGENCY USE ONLY (Leave blank)	2. REPORT DATE August 1992	3. REPORT TYPE AND DATES COVERED Final Report September 1988-March 1992

4. TITLE AND SUBTITLE Internal Structural Characterization	5. FUNDING NUMBERS F33615-88-C-5433 PE: 62102F PR: 2418 TA: 02 WU: 41
6. AUTHOR(S) R. Klaassen & M. Bashyam	

7. PERFORMING ORGANIZATION NAME(S) AND ADDRESS(ES) General Electric Aircraft Engine Quality Technology Center One Neumann Way Cincinnati OH 45215-6301	8. PERFORMING ORGANIZATION REPORT NUMBER

9. SPONSORING/MONITORING AGENCY NAME(S) AND ADDRESS(ES) Charles F. Buynak (513) 255-9807 Materials Directorate (WL/MLLP) Wright Laboratory Air Force Materiel Command Wright-Patterson AF Base OH 45433-6533	10. SPONSORING/MONITORING AGENCY REPORT NUMBER WL-TR-92-4079

11. SUPPLEMENTARY NOTES

12a. DISTRIBUTION/AVAILABILITY STATEMENT Approved for Public Release; Distribution is Unlimited.	12b. DISTRIBUTION CODE

13. ABSTRACT (Maximum 200 words) The nondestructive evaluation (NDE) techniques most appropriate for the detection of a variety of defects in metal-and ceramic matrix composites (MMC and CMC's) are described. NDE techniques which were investigated for application to these materials include acoustic microscopy, ultrasonic pulse-echo, ultrasonic through-transmission, ultrasonic velocity, ultrasonic backscatter, ultrasonic surface wave velocity, ultrasonic surface wave attenuation, film radiography, microtomographic radiography, and dual-energy microtomographic radiography. Types of defects for which optimized techniques are summarized include delaminations, broken fibers, fiber spacing, fiber orientation, fiber/matrix interface, matrix cracks and voids/porosity. Further NDE development is needed for these materials in the areas of basic development for other NDE modalities, advanced development for nondestructive material characterization, and the scale-up of proven NDE techniques for full scale components, to accommodate cost and geometry limitations.

14. SUBJECT TERMS Ultrasonics Radiography Cracks Characterization Metal Matrix Composite Nondestructive Evaluation (NDE) Defect Ceramic Matrix Composite Computed Tomography Detection	15. NUMBER OF PAGES 130
	16. PRICE CODE

17. SECURITY CLASSIFICATION OF REPORT UNCLASSIFIED	18. SECURITY CLASSIFICATION OF THIS PAGE UNCLASSIFIED	19. SECURITY CLASSIFICATION OF ABSTRACT UNCLASSIFIED	20. LIMITATION OF ABSTRACT UNCLASSIFIED

NSN 7540-01-280-5500

Standard Form 298 (Rev 2-89)
Prescribed by ANSI Std Z39-18
298-102

FOREWORD

This Final Technical Report of the Internal Structural Characterization program describes the technical effort from September 28, 1988 through March 31, 1992. The program objective was to investigate the potential of using nondestructive evaluation (NDE) techniques for the evaluation of the internal structure of high-temperature Metal Matrix Composites (MMCs), and Ceramic Matrix Composites (CMCs), proposed for use in advanced aircraft turbine engines. This program was sponsored by the Air Force Systems Command, Aeronautical Systems Division/MLKM, Wright-Patterson Air Force Base, Ohio.

This program was performed under the technical direction of Mr. Charles Buynak of the Nondestructive Evaluation Branch, Materials Directorate of Wright Laboratory, Wright-Patterson Air Force Base, Ohio. The program was conducted by the Quality Technology Center of GE Aircraft Engines, (GEAE), Cincinnati, Ohio. The GEAE Technical Program Manager was Mr. R.E. Klaassen. The Principal Investigator for Ultrasonic Development was Mr. M. Bashyam. The subcontracted X-Ray Development effort was under the technical direction of Mr. D.C. Copley who interfaced with Dr. Qizhi Cao of ARACOR (Advanced Research and Applications Corporation). Dr. Cao was ARACOR's Program Manager and responsible for all NDE efforts at ARACOR.

Textron Speciality Materials manufactured the metal matrix composite panels. Their contribution to the program was directed by Mr. Horst Gigerenzer. Corning Glass Works manufactured the ceramic matrix composite panels and provided consultation on defining and introducing simulated defects. Their contribution to the program was directed by Ms. Jane Adams.

Accesion For		
NTIS CRA&I		☒
DTIC TAB		☐
Unannounced		☐
Justification		
By		
Distribution /		
Availability Codes		
Dist	Avail and / or Special	
A-1		

TABLE OF CONTENTS

TABLE OF CONTENTS (Cont.)

TABLE OF CONTENTS (Cont.)

LIST OF ILLUSTRATIONS

Page

LIST OF ILLUSTRATIONS (Cont.)

LIST OF ILLUSTRATIONS (Cont.)

LIST OF TABLES

1.0 Introduction

The need exists to extend the capability of future military aircraft engine materials to operate at higher temperatures and higher stresses and for longer service lives than now possible. The dual requirements of higher temperatures and longer life place stringent conditions on the types of advanced materials that can be used in these engines. Meeting this need requires significant advances in the physical and mechanical characteristics of these materials, like those projected for the advanced metal matrix composites (MMCs), and ceramic matrix composites (CMCs). However, before these anisotropic materials can be reliably applied, the mechanical behavior, failure modes and internal structure must be better understood.

The evaluation of properties of matrix, fiber and fiber/matrix interfaces in such complex materials, both during material manufacture and service life, has presented a challenging task to the NDE community. The Internal Structural Characterization (ISC) program addressed the development of the capabilities of selected inspection techniques for the specific problem of evaluating the internal structure of the MMC and CMC materials.

The ISC program approach included the following central features:

- Fabrication of MMC and CMC specimens with defects introduced intentionally.
- Development of ultrasonic and radiographic techniques to characterize the material and the defect states.
- Evaluation of the fiber/matrix interface condition using advanced NDE techniques.
- Establishment of controlled experiments and analytical methods to evaluate the experimental results.
- Correlation between the observed NDE test results and the destructive measurements.

1.1 Program Highlights

The Internal Structural Characterization program made significant progress in advancing the NDE of composite materials. The development of acoustic microscopy techniques under this program provided a revolutionary advance for the NDE of MMCs. This technique is able to image details smaller than those believed possible as recent as early 1991. Even before the conclusion of the ISC program, this new technology has played a key role in understanding the structure and performance of these materials. Methods to detect minute structural details, such as broken fibers and voids, were developed under this program. By applying this technology to concurrent MMC material development programs, damage

from mechanical property tests has been detected, including fiber/matrix debonds and cracks, which is leading to an improved understanding of failure mechanisms. As this technology is applied to more composite specimens, additional capabilities are being discovered.

High resolution radiographic computed tomography (microtomography) techniques have been investigated under this program, which supplement the high resolution ultrasonic techniques. The Tomoscope and Synchrotron provide details about fiber location, orientation and integrity within both CMC and MMC materials. Details as small as the fiber core were imaged with these techniques.

In general, the techniques developed for MMCs and CMCs are widely applicable composite components. In addition to the acoustic microscopy and microtomography, general ultrasonic and radiographic techniques were developed. Once scaled-up, with respect to economic and defect detectability issues, these techniques should provide wide-ranging capabilities for the inspection of full sized components.

2

2.0 Background

Whenever new materials are developed for applications having stringent operating requirements, NDE is needed for three purposes: Material characterization for manufacturing process control, failure mechanism characterization for property/damage understanding, and defect detection and characterization. The specific NDE requirements for each of these three applications are rooted in the dimensions and properties of the features that influence the performance of the material. The sizes of the constituent components of a composite, (fibers or particulate), dictate the resolution of the NDE inspection needed to verify manufacturing process control. The size of the constituent components also places a lower limit on the resolution requirements for damage characterization, as damage initiation is likely to interact with the smallest of components. The types of defects that are expected to be possible, and the extent of those defects that are believed to significantly impact the performance of the material dictate the NDE resolution limits for defect detection and characterization.

NDE parameters are typically difficult to define up front, because the exact nature of the material, damage mechanisms, and defects are not initially known. This uncertainty dictates that the material be over-inspected initially to establish the limits of NDE needs, and then requirements can be relaxed as properties are better understood. This program sought to avoid this difficulty by controlling the types and the extent of defects present in the specimens.

NDE development can be simplified by minimizing the number of variables present in the material. NDE development is most difficult when the basic structure of specimens is unknown, and the geometry is hostile. Once basic NDE techniques have been developed for the simple case, then they can be extended to apply to the more difficult cases. This program was designed for simplicity by isolating the individual defects, and providing the most accommodating geometry possible.

2.1 MMC Issues

The most significant difficulties associated with NDE for MMCs are rooted in the inhomogeneity and the general lack of knowledge about the performance of the material. The ductile matrix and brittle fiber cause severe scattering of ultrasonic energy, and the differing levels of density tend to blur radiographic images. The basic properties and mechanisms of failure of the material are not fully characterized, although they seem to be tied to matrix cracking and fiber/matrix interface quality. Manufacturing is in its infancy; the unknown natural defect distribution adds uncertainty to the NDE needs. Furthermore, existing

3

manufacturing processes result in surface roughness that adds noise to the data in nearly all types of NDE methods.

2.2 CMC Issues

While CMCs can also be described as inhomogeneous, the fibers and matrix are both ceramic, and thus have many similarities. As a result, discrimination between the two components of the structure is difficult. The lack of knowledge about these materials leave them vulnerable to the same difficulties as MMCs. The basic properties and mechanisms of failure of the material are not fully characterized, although they seem to be tied to matrix cracking and fiber/matrix interface damage. Manufacturing is in its infancy; the unknown natural defect distribution adds uncertainty to the NDE needs. Furthermore, existing manufacturing processes result in surface roughness which adds noise to data for nearly all types of NDE methods.

3.0 Program Plan

The overall program was comprised of three time-sequenced tasks. The objective was to investigate the potential of using NDE techniques for the evaluation of high-temperature MMC and CMC materials. The techniques investigated needed to have the capability to evaluate physical and geometric parameters of the internal structure of these materials. The effort was conducted in three tasks described below, with Tasks I and II conducted concurrently.

3.1 Task I - Inspection Technique Development

The purpose of Task I was to develop advanced ultrasonic and radiographic techniques for the interrogation and evaluation of high-temperature MMCs and CMCs typical of those materials used in advanced turbine engines. Basic material characteristics evaluated by the NDE methods included information concerning the fibers, the matrix, and the fiber/matrix interface, such as fiber distribution, fiber misalignment, fiber breakage, delaminations, porosity, and fiber coatings.

This Task represented the largest portion of the effort under this program. The results from this Task are organized by NDE technique used in Section 5 of this report, and are organized by detected defects in Section 6.

3.2 Task II - Experimental Plan

The purpose of Task II, which was conducted concurrently with Task I, was to plan the final experimental phase of the program, Task III. The specific MMC and CMC materials to be studied were identified along with the types of material properties and defect types to be evaluated. Seeded defect specimens from both MMC and CMC materials were fabricated to the specifications described in Section 5 of this report. The manufactured defects did not always match the original intentions, and several unintentional defects resulted as well. Each of the resulting types of defects are also described in Section 5 of this report.

3.3 Task III - Demonstration of Inspection Capability

The purpose of Task III was to demonstrate the inspection capabilities of the ultrasonic and radiographic techniques developed according to the experimental plan. This included destructive examination and correlation with the NDE test results. Based on the results of this NDE development program, the benefits and shortcomings of each of the tested techniques are described (Section 6). Finally, recommendations for further research and development efforts needed to produce practical, cost-effective inspection techniques in realistic development, production, and service situations (Section 9).

5

4.0 Description of Materials and Defects

Specimens were designed and manufactured to provide well-defined targets for NDE development. Based on the known properties of these targets, the NDE parameters could be optimized for identification and detectability. The specific types of targets were chosen to represent the range of defects deemed possible given the existing manufacturing techniques. The following subsections describe these specimens in more detail.

4.1 Metal Matrix Composite Specimens

Eight MMC test panels were manufactured by Textron Inc. The panels were made of plasma sprayed titanium 6Al-4V (Ti 6-4) matrix and Silicon Carbide (SCS-6), continuous fibers. The Ti 6-4 matrix material was used because its properties and manufacturing capability were best understood relative to other metallic/intermetallic matrix systems. SCS-6 fibers were used because they were less reactive with the titanium matrix than other fibers.

The SCS-6 fiber is a double pass fiber, 142 microns (5.6 mils) in diameter, with a 33-micron (1.3-mil) carbon core, and has an ultimate tensile strength of 500 ksi. In producing the fiber, a 33-micron carbon filament unwinds from a drum and passes through a segmented reaction chamber approximately 10 feet long. A rolling contact electrode at each end of the chamber heats the filament to a high temperature as it slowly moves through the gas filled chamber. Silicon carbide from the gas is coated on the filament and in the final stages of the process, the atmosphere is changed in the segmented tube to enrich the carbon content of the silicon carbide coating. This 1-micron-thick enriched coating of the outside layer protects the fiber from degradation from the surrounding titanium. The "double pass" fiber refers to a pass through a second chamber segment to increase the thickness of the enriched carbon coating. As processing of the MMC may damage this coating layer, the additional thickness acts as insurance of maintaining an intact protective coating. The finished fiber exits the chamber and is cooled and wound on a take-up spool.

MMC monotapes were produced by winding the SCS-6 fiber around a steel drum at a predetermined spacing, inserting the drum into a plasma spray chamber, and spraying molten titanium over the fibers. The fiber spacing on the drum and the thickness of the sprayed titanium layer are used to calculate the volume percent of fiber with respect to matrix in the final layup.

The monotape was cut into (nominal) 150 mm by 150 mm squares, along the axial dimension. The MMC panels were made by stacking a series of these monotapes,

and consolidating the stack using a hot isostatic pressing technique. Anomalies were intentionally introduced in the panels prior to consolidation to simulate the type of flaws that could potentially occur in production.

Eight MMC test panels were produced with a nominal fiber volume fraction of 0.35. Four panels had 8 plies, three had 16 plies, and one had 24 plies, giving them a thickness of 1.6 mm, 3.2 mm, and 4.9 mm, respectively. Defects were introduced into the panels as follows:

4.1.1 Delaminations

Delaminations between plies were introduced by spraying a thin coating of contaminant through a circle template overlaid on the monotape. Boron nitride and yttrium oxide were used as contaminants. Three panels of different thicknesses were made with delaminations, with locations and orientations as shown in Figures 4.1, 4.2 and 4.3. Figure 4.4 shows destructive characterization of two boron nitride (BN) induced delaminations, one in which the contaminant remained as a planar defect and another, in which the contaminant broke into many voids. These two variations of delaminations are representative of those seen in these panels. Figure 4.5 shows a typical yttrium oxide induced defect, in which the contaminant broke into many voids.

4.1.2 Bunched Fibers

A monotape was made with a 25-mm-wide strip of closely spaced fibers. Voids were expected to result from the inability of the titanium matrix to fit in the narrow gaps between the fibers. This type of bunched fibers was introduced at three different plies, in two panels of differing thicknesses, as shown in Figures 4.6 and 4.7. Destructive verification of the resulting bunching is shown in Figure 4.8. Unintentional bunched fiber defects were found in MMC panel 5, and destructive verification of these is shown in Figure 4.9.

4.1.3 Single-Pass Fibers

A monotape was made using fibers with only a single-pass enriched carbon coating, in an effort to produce a condition of fiber/matrix interface damage. This single-pass monotape was used in place of one-half of the monotape of two different plies of one panel, as shown in Figure 4.10. Although the fiber coating differed from the double pass coatings, as shown in Figure 4.11, the fiber/matrix interface did not appear to be affected.
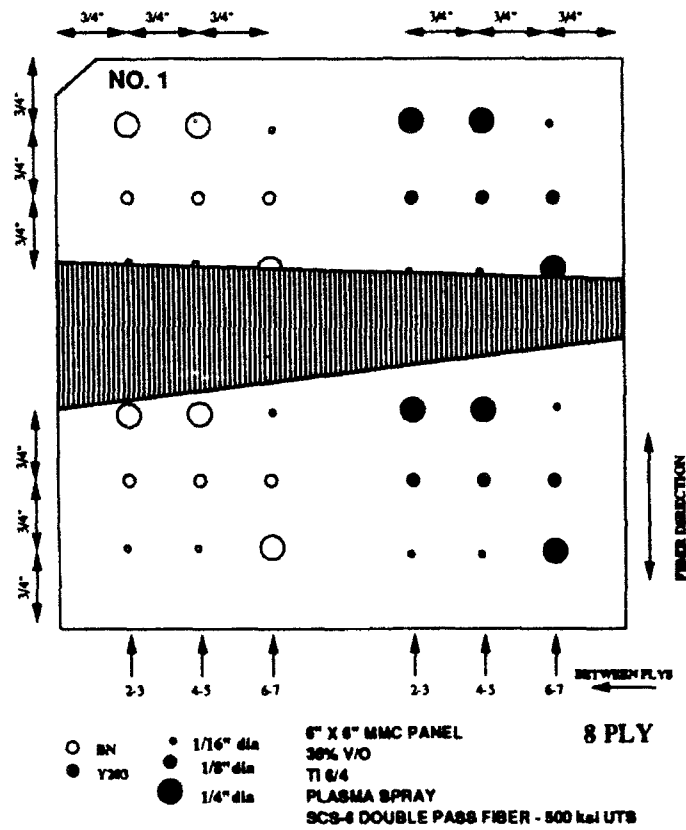
Figure 4.1   MMC panel 1 with delaminations.
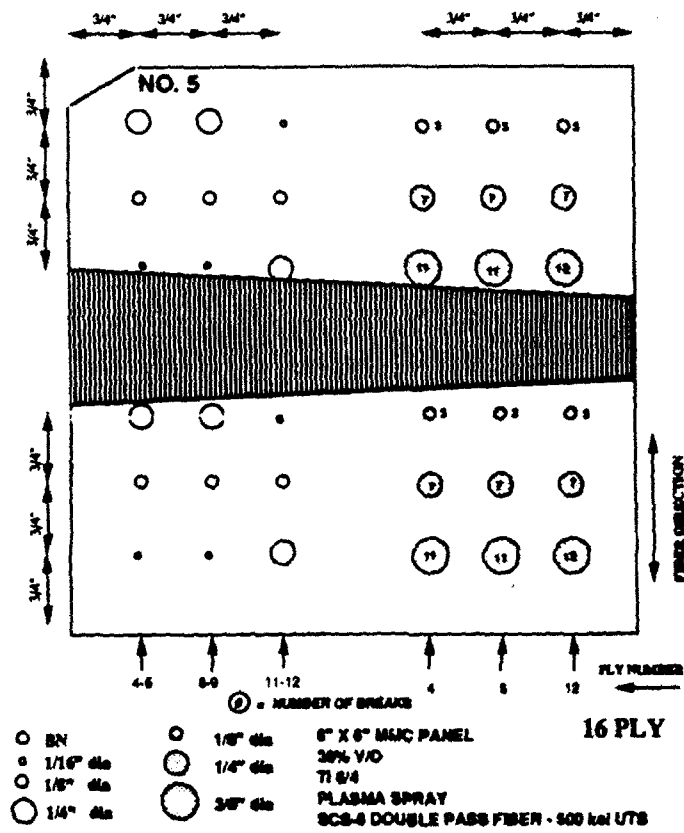
Figure 4.2 MMC panel 5 with delaminations and broken fibers.

9

Figure 4.3 MMC panel 8 with delaminations and broken fibers.

Planar Delamination

Figure 4.4.a

Ti 6/4 Matrix

Carbon Core Fibers

Delamination/Voids

Figure 4.4.b

|——————————|
0.020 inch
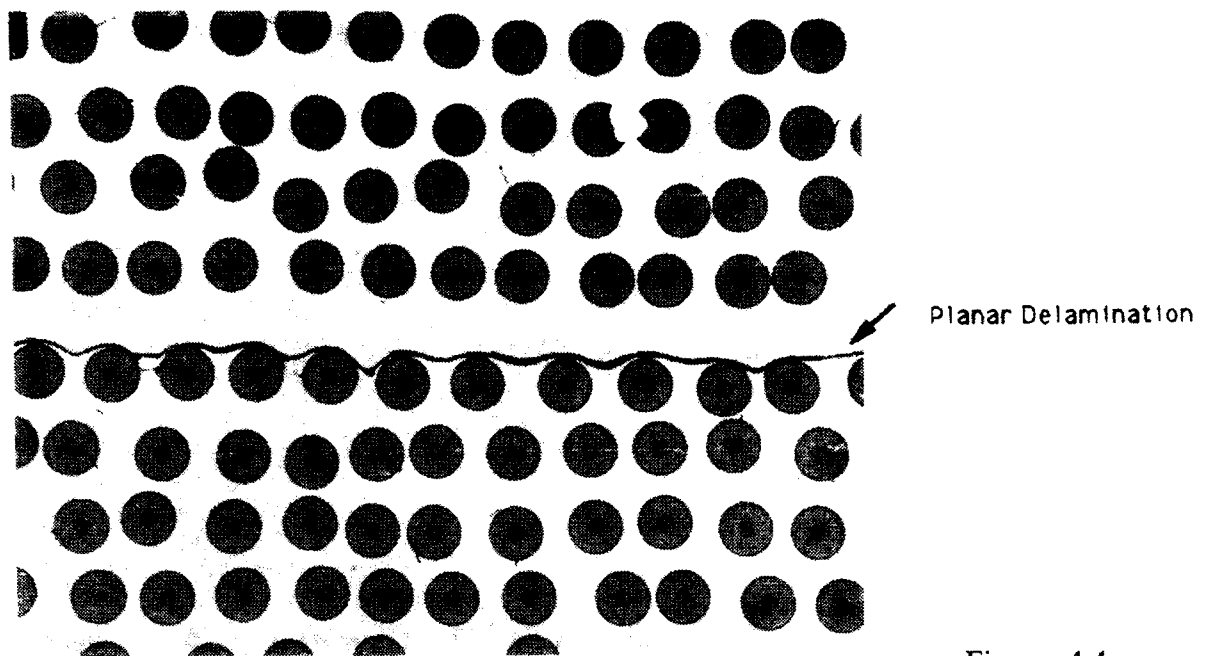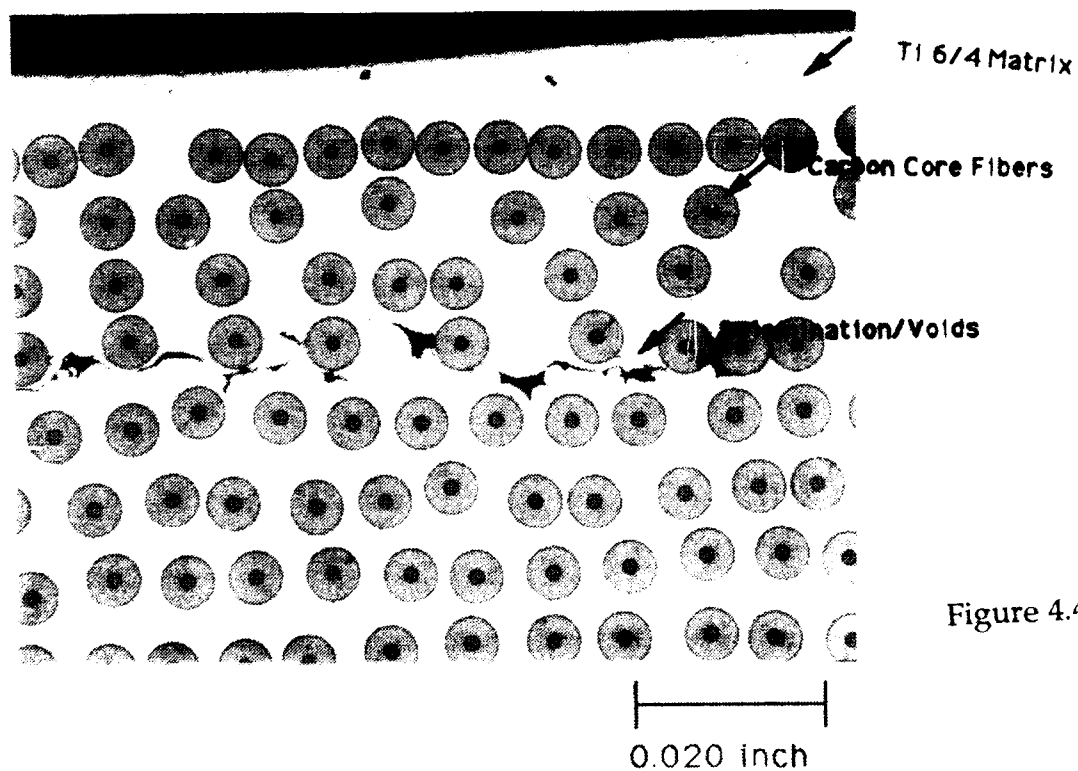
Figure 4.4 Cross sections of boron nitride induced delaminations
in SiC/Ti MMC panel 1. Figure 4.4.a represents the
intended planar delamination, while Figure 4.4.b shows
how some delaminations split to form voided regions.

11
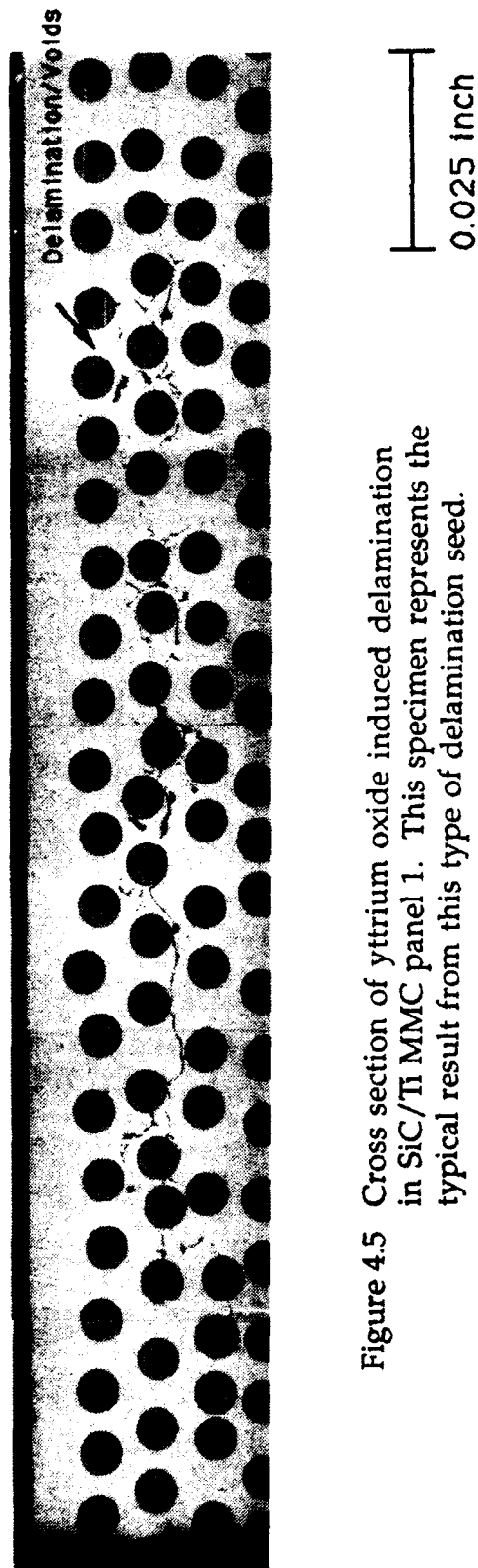
Figure 4.5 Cross section of yttrium oxide induced delamination in SiC/Ti MMC panel 1. This specimen represents the typical result from this type of delamination seed.
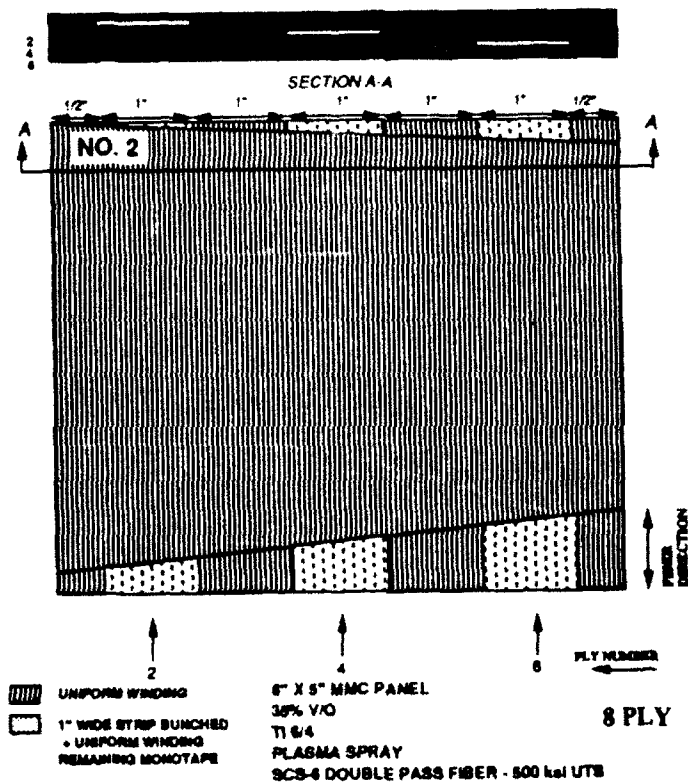
Figure 4.6 MMC panel 2 with bunched fibers and voids.

13

Figure 4.7 MMC panel 6 with bunched fibers and voids.

4th Ply Bunched Fibers
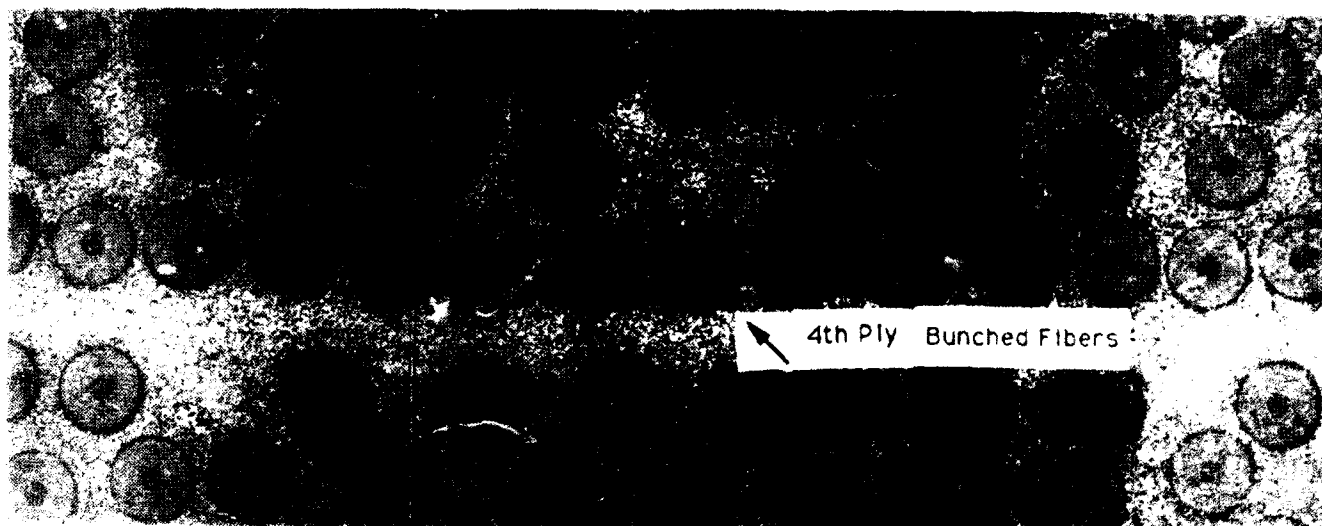
Figure 4.8 Bunched fibers in the fourth ply of SiC/Ti MMC
panel 2. Fibers are not noticeably damaged.

Bunched Fibers

Figure 4.9.a

|—— 0.020 inch ——|
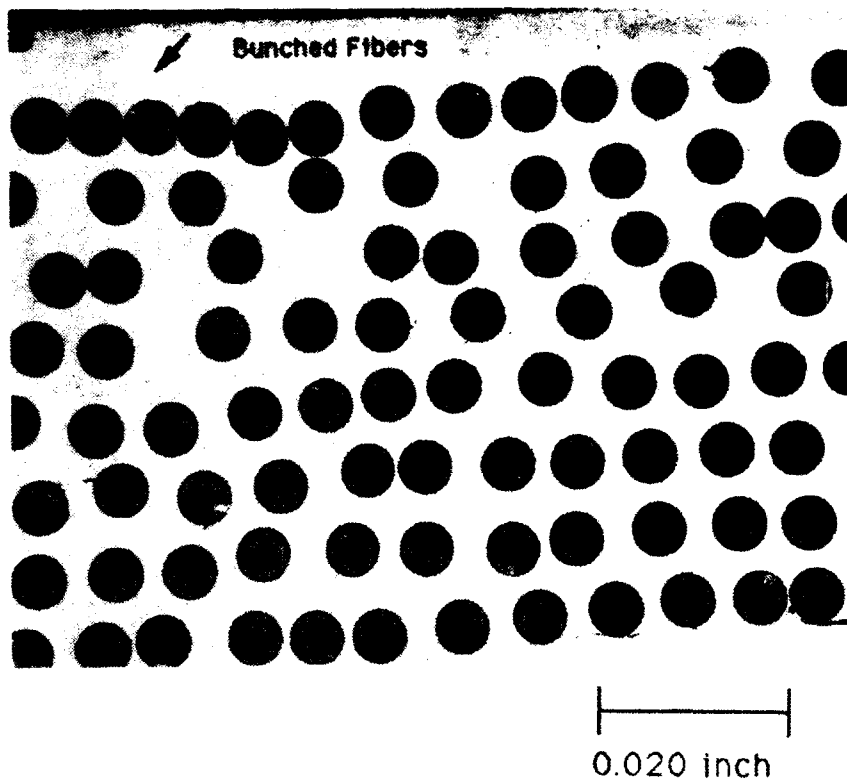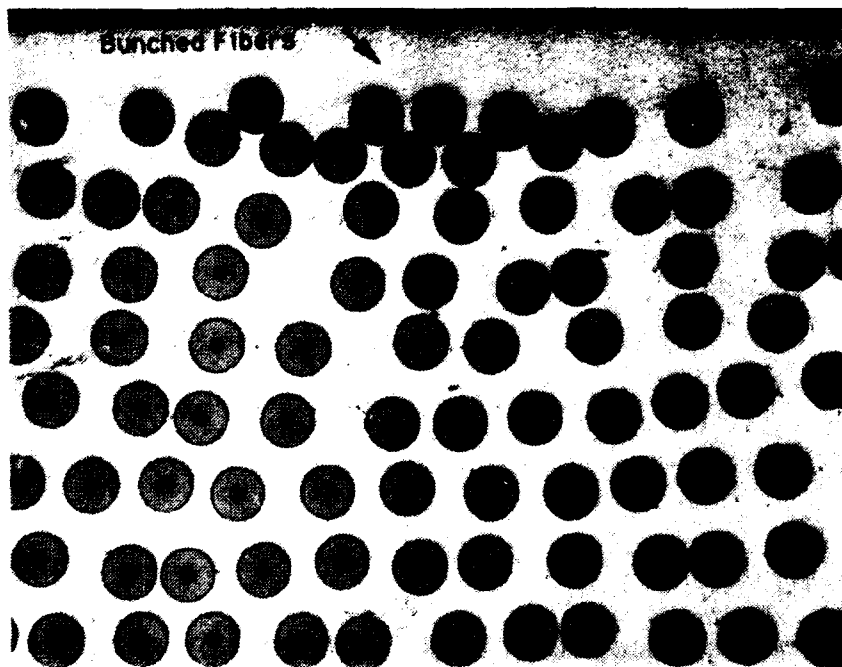
Bunched Fibers

Figure 4.9.b

Figure 4.9· Unintentional bunched fibers in SiC/Ti MMC panel 5.
Figure 4.9.a shows fibers which are well bonded to
the matrix, in spite of close proximity. Figure 4.9.b
shows fibers which are packed together so that the
matrix was unable to flow around them.
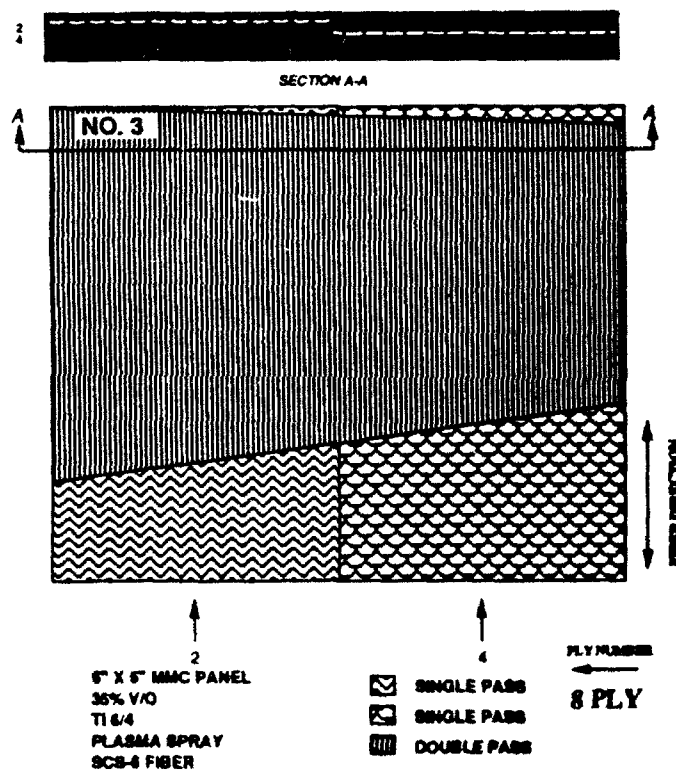
Figure 4.10 MMC panel 3 with single-pass fibers.
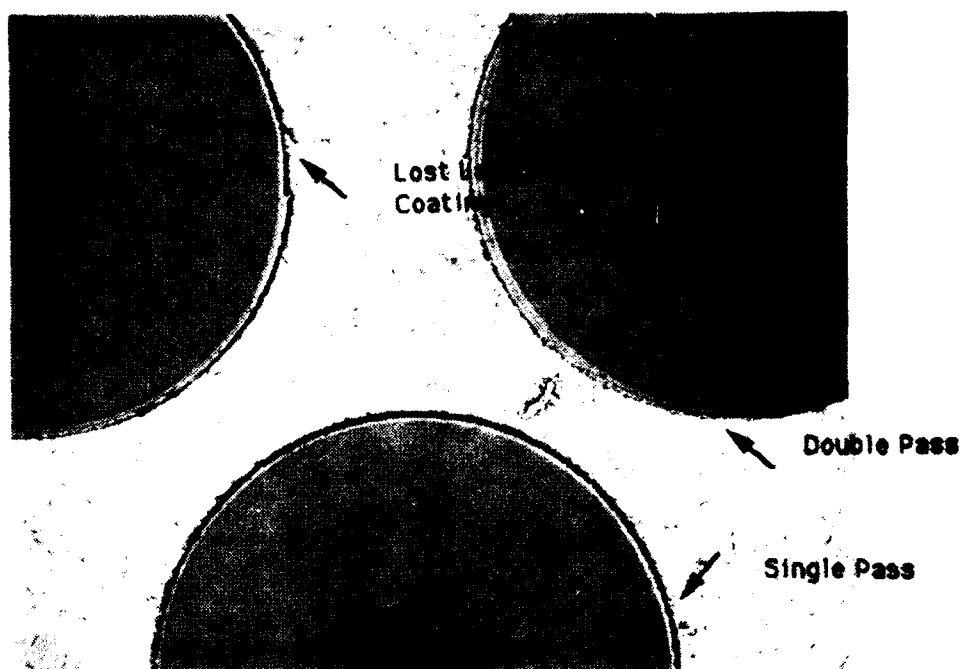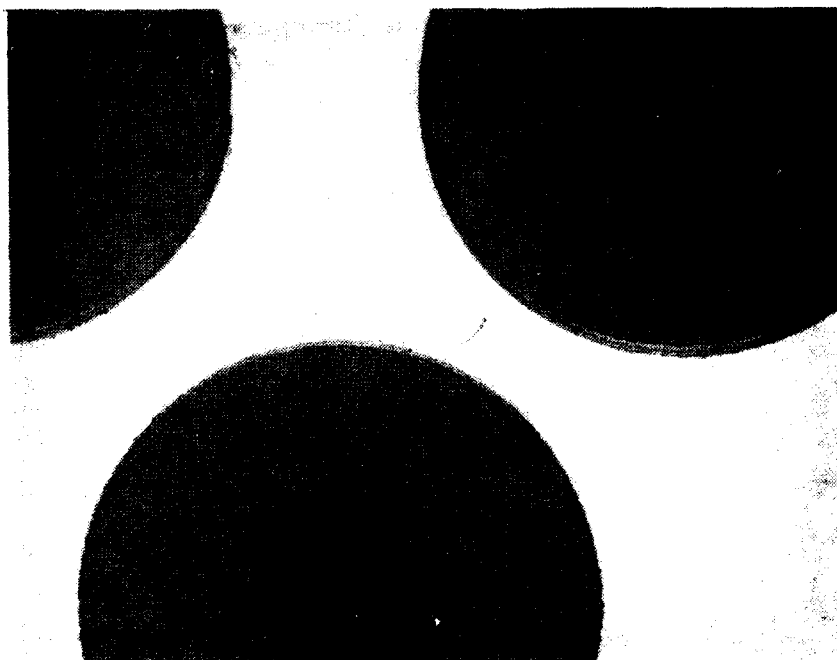
Figure 4.11 Cross section of single-pass and double pass fibers
in SiC/Ti MMC panel 3. The two photographs are
from the same region, with different light settings.

4.1.4 Broken Fibers

A template with three different size holes was placed on a monotape. The corner of a sharp razor blade was used to break the fibers where they were exposed. These defects were inserted in three panels, and the locations of the intentional breaks are shown in Figures 4.2, 4.3 and 4.12. In those Figures, the numbers within the circles correspond to the number of locations where fibers were broken within each given circled area. Figure 4.13 shows one such group of intentional breaks. In addition to these intentional broken fibers, Each MMC panel contained an overwhelming number of unintentionally broken fibers. Figure 4.14 shows a typical distribution of unintentional fiber breaks.

4.1.5 Cross Ply Layup

Plies were cut and laid in a 16 ply, [0,0,+45,0,0,-45,0,0]Symetric sequence. Figure 4.15 shows this pictorially.

4.2 Ceramic Matrix Composite Specimens

Corning Glass Works manufactured 24 test panels. Of these, 16 were made from Nicalon fibers and calcium aluminum silicate (CAS) matrix, and eight panels were made from SCS-6 fibers and CAS matrix. Anomalies were introduced during the manufacturing process to simulate a variety of defects that could potentially occur in production.

The CAS matrix material was selected for study because it was the most developed and best understood CMC system. The lamination and hot-press manufacturing route is well controlled and is suitable for introducing controlled defects. The 10-to-15 micron diameter Nicalon fiber is a commonly used fiber, and is representative of other small, high temperature fibers such as Nextel and Sumitomo. The 142-micron SCS-6 fiber was the best high temperature fiber, and was expected to respond to NDE measurements in a manner similar to other proposed high temperature fibers, such as single crystal alumina.

The CAS/Nicalon test panels were nominally 100 mm by 100 mm by 8 plies, with a nominal thickness of 3 mm. The fibers were bundled into fiber tows, which were then passed through a slurry of glass and binder, and were wound on to a mandrel for drying. Single layers of pre-impregnated material can then be cut from the mandrel and stacked to produce a laminate. Binders are then burned out, and the laminate is placed in a mold and hot pressed to consolidate to the final form. Panels had a symmetrical layup ([0,90,0,90]Sym.), except for panel N2. Fiber volume fractions were in the range of 35 to 40 percent, as estimated by Corning Glass Works.

19
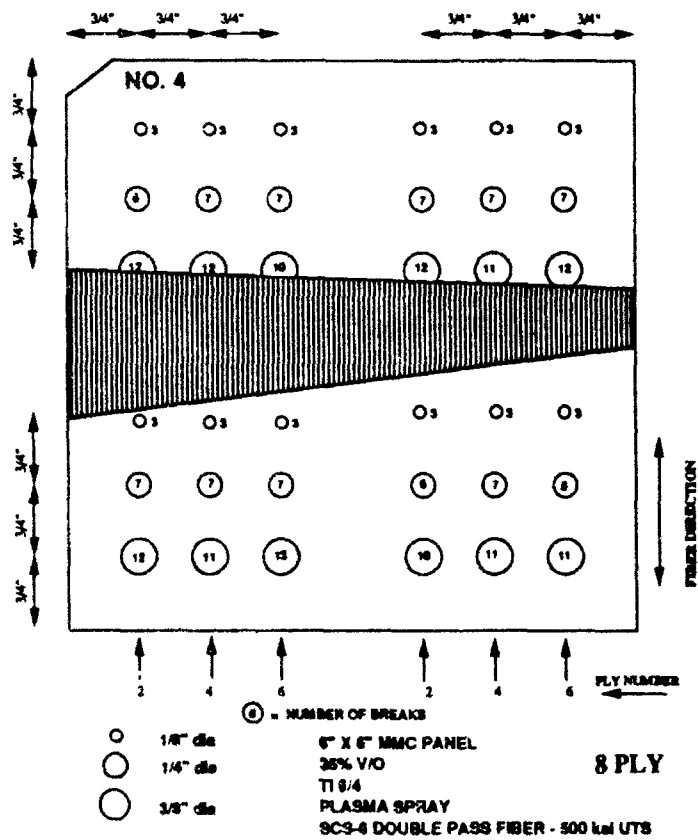
Figure 4.12 MMC panel 4 with broken fibers.

Broken fibers

broken chips within a 6 mm circle.

0.6 cm

Photograph of Top Ply

Fiber

Lower Right Broken Fiber
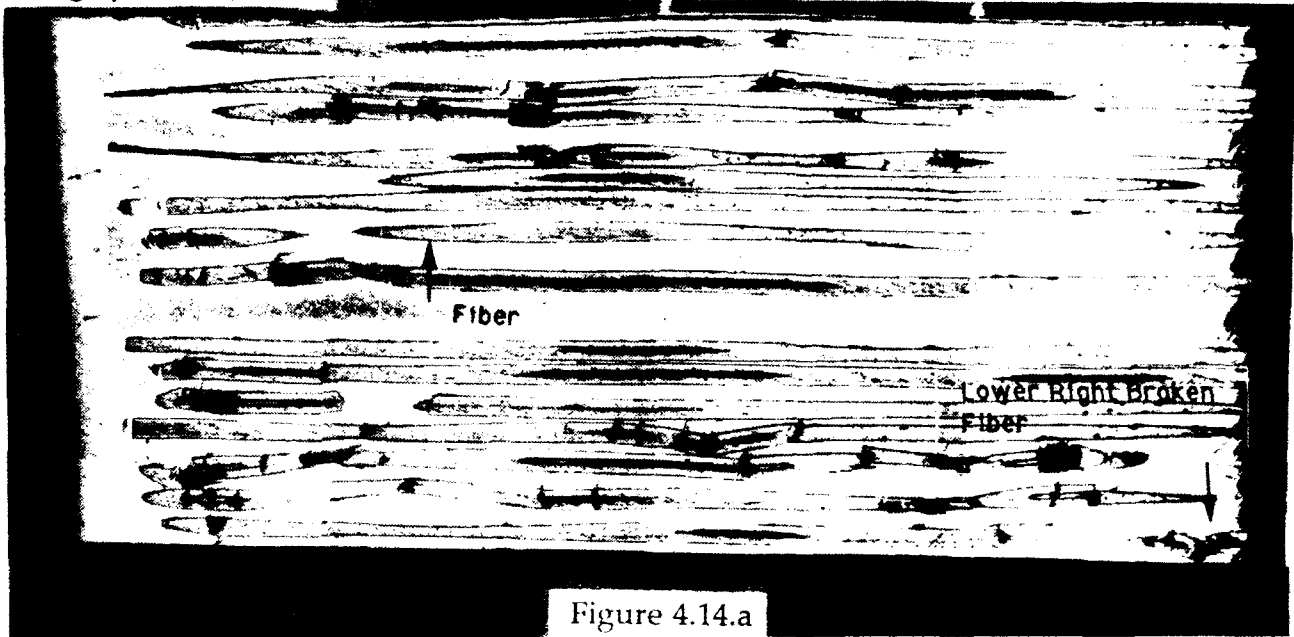
Figure 4.14.a

Ultrasonic Image of Top Ply   Area = .31 X .13 in

Fiber

Lower Right Broken Fiber

Black = Fiber or Defect

Figure 4.14.b

0.050 inch
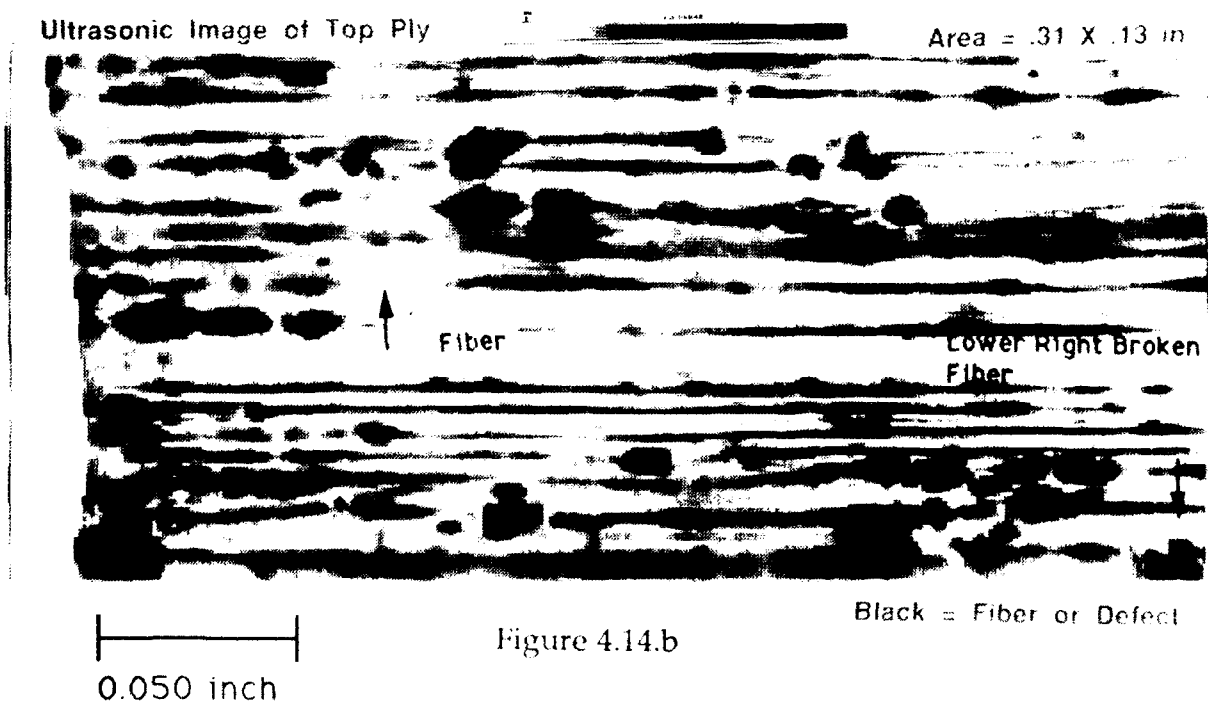
Figure 4.14 Correlation between acoustic microscope indications
and broken fibers in SiC/Ti MMC panel 2. Figure 4.14.a
shows the typical incidence of broken fibers in the
MMC panels made for this program. Figure 4.14.b is the
corresponding acoustic microscope image, made prior to
the removal of the Titanium outer layer. This
demonstrates the detectability of broken fibers.

CENTER

0 0 +45 0 0 -45 0 0 0 0 -45 0 0 +45 0 0

NO. 7

16 PLY
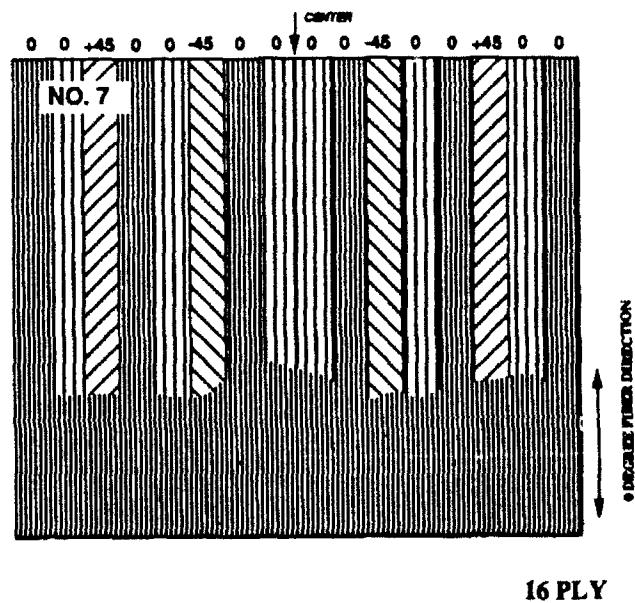
6" X 6" MMC PANEL - layup
0,0,+45,0,0,-45,0,0,0,0,-45,0,0,+45,0,0
38% V/O
TI 6/4
PLASMA SPRAY
SCS-6 DOUBLE PASS FIBER - 500 ksi UTS

Figure 4.15 MMC panel 7 with cross ply lay-up.

23

The CAS/SCS-6 panels were nominally 100 mm by 100 mm, by eight plies, with a resulting thickness of approximately 1.7 mm. The larger diameter, stiffer fiber required a different manufacturing route from the Nicalon panels. Panels were produced by stacking alternate layers of tape-cast green-state glass-ceramic sheets, and single layers of fibers. The stack was then burned to remove binders, and hot-pressed in a mold for consolidation. Simulated defects were generally similar to those in the Nicalon panels, with variations due to the different manufacturing routes. Except for panel S2, stacking sequence was [0,90,0,90]Sym., and fiber volume fractions were in the range of 20 to 30 percent, as estimated by Corning Glass. The CAS/SCS-6 panels were used for supplemental verification of NDE techniques, because this material is similar in nature to the CAS/Nicalon composite. As a result, less information was obtained for these panels.

4.2.1 Delaminations

Planar delaminations were created in the CAS/Nicalon material by inserting dry fiber between various plies. Their sizes and locations were specified as shown in Figure 4.16.

Planar delaminations were produced in the CAS/SCS-6 material by punching holes in one glass layer. Their sizes and locations were specified as shown in Figure 4.17.

4.2.2 Incorrect Stacking Sequence

The sequence [0,90,90,0,90,0,90,0]was substituted for the symmetrical layup ([0,90,0,90]Sym.). One such panel was made from both CAS/Nicalon and CAS/SCS-6 materials.

4.2.3 Misaligned Fibers

One CAS/Nicalon panel was made with misaligned fibers. Two bands of fibers, approximately 6.3 mm wide were misaligned in a single layer, as shown in Figure 4.18. The fiber bundles were flexible enough to be bent easily to produce this misalignment.

One CAS/SCS-6 panel was made with misaligned fibers. In two locations, two to three fibers were misaligned by approximately 5 degrees in the fourth layer, as shown in Figure 4.19. The crossed fibers were expected to remain straight because of their stiffness.

SIMULATED DELAMINATION
(DRY FIBER INSERT)

4" X 4" CMC PANEL
CAS-2 MATRIX
NICALON FIBER
8 PLY
LAYUP (0/90)s

BETWEEN PLYS

1-2   4-5   1-2   4-5

● 1/4" dia
◉ 3/8" dia   S/N N1
⬤ 1/2" dia
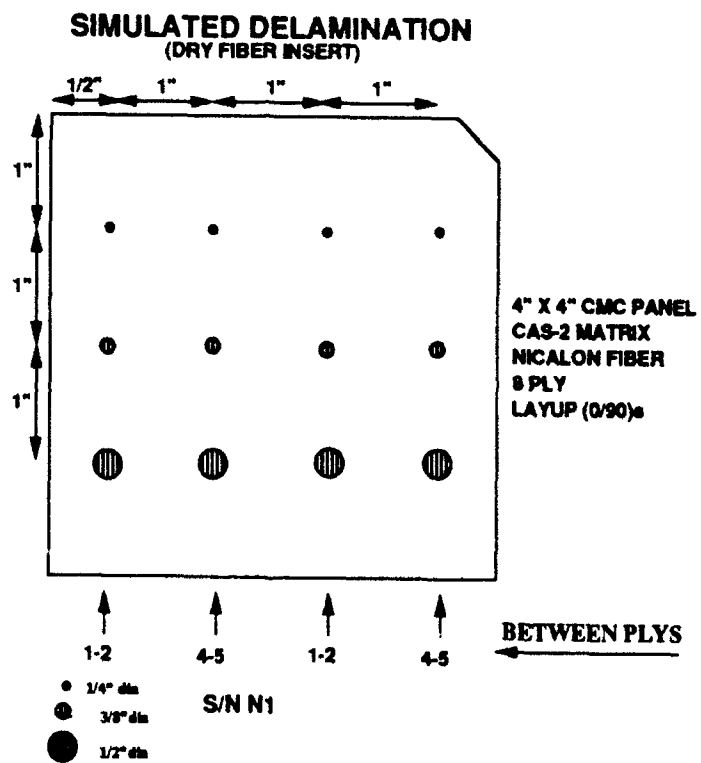
Figure 4.16 CMC panel N1 with delaminations.

SIMULATED DELAMINATION

4" X 4" CMC PANEL
CAS-2 MATRIX
SCS-6 FIBER
8 PLY
LAYUP (0/90)s

1-2   4-5   1-2   4-5   ◄—— (HOLES PUNCHED IN LAYER)

○ 1/4" dia
○ 3/8" dia   S/N S1
○ 1/2" dia
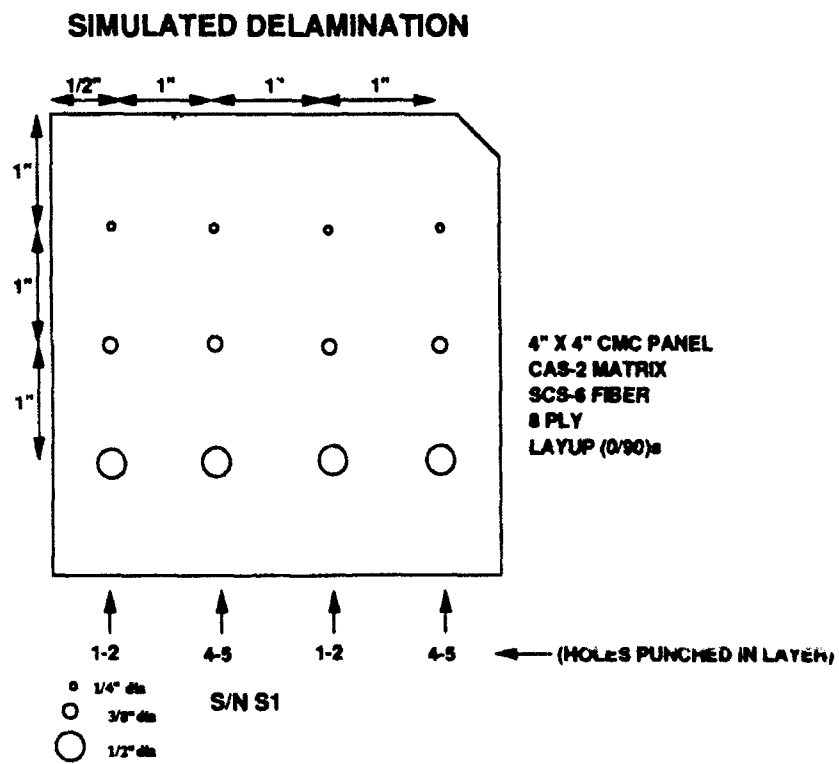
Figure 4.17 CMC panel S1 with delaminations.

MISALIGNED FIBER

1/4"   1/4"

BANDS OF
MISALIGNED
FIBERS IN
LAYER 4

4" X 4" CMC PANEL
CAS-2 MATRIX
NICALON FIBER
8 PLY
LAYUP (0/90)s

1"   2"

S/N N3
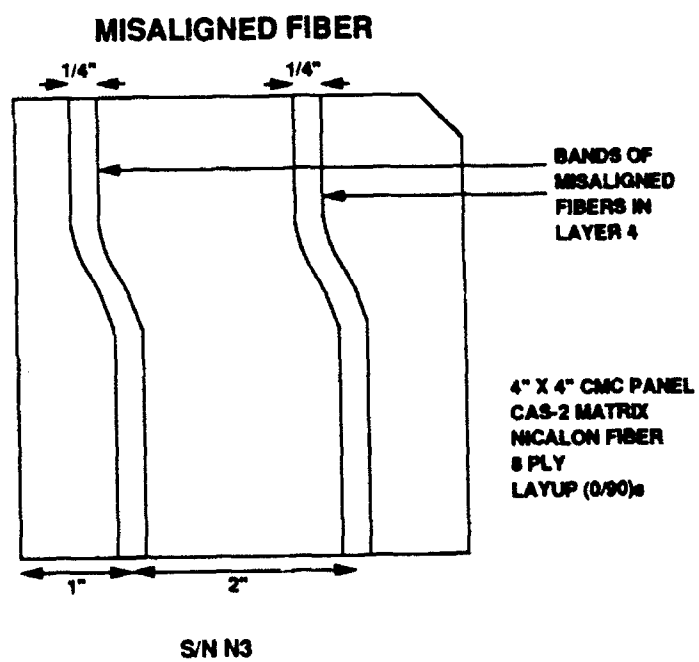
Figure 4.18 CMC panel N3 with misaligned fibers.

CROSSED FIBERS

1"   2"

2-3 CROSSED FIBERS
IN EACH LOCATION.
~5° MISALIGNMENT.
LAYER 4.

4" X 4" CMC PANEL
CAS-2 MATRIX
SCS-6 FIBER
8 PLY
LAYUP (0/90)s

S/N S3
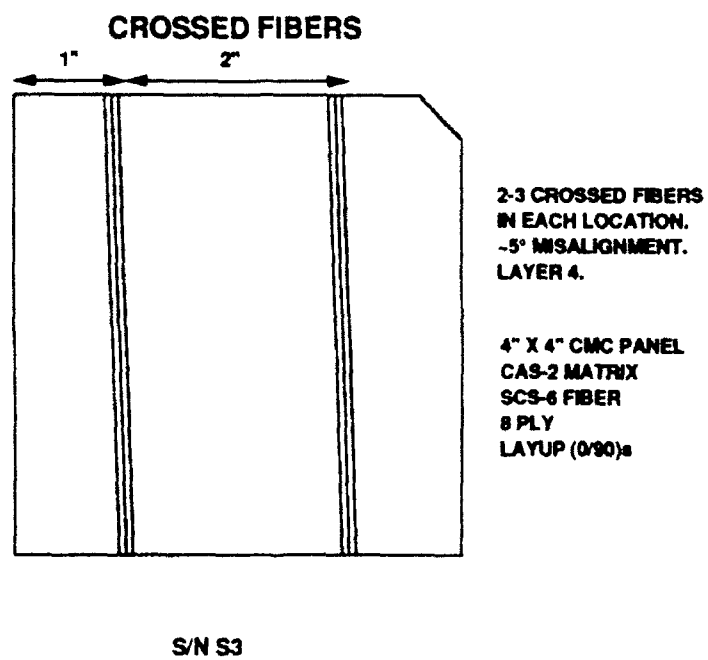
Figure 4.19 CMC panel S3 with misaligned fibers.

4.2.4 Broken Fibers and Splice

One CAS/Nicalon panel was made with two examples of broken/spliced fibers. One band of fibers was broken and then consolidated with no intentional gap at the break. Another band was broken and then consolidated with the pieces separated by a 1.3-mm gap, as shown in Figure 4.20. A fiber splice occurs when the fiber bundle breaks as it is wound onto the drum. This is corrected by tacking the broken ends onto the drum with a small overlap.

One CAS/SCS-6 panel was made with broken/spliced fibers. Fibers in a single layer were broken, and then consolidated with no intentional gap at the break. Another band was broken and then consolidated with the pieces separated by a 1.3-mm gap. The location and orientation of these defects are shown in Figure 4.21.

4.2.5 Minor Porosity and Uniform Fiber Distribution

Incomplete consolidation was achieved in a CAS/Nicalonpasnel and a CAS/SCS-6 panel by reducing process temperature. Figure 4.22 shows the resulting consolidation for the CAS/Nicalon panel: actual porosity was estimated to be less than 1 percent. Uniform fiber distribution was also represented in this CAS/Nicalon panel, as shown in Figure 4.23.

4.2.6 Moderate Porosity, Poor Fiber Distribution and Microcracks

Moderate porosity is defined as that which affects both the matrix within the fiber tow and outside of the fiber tow. This was manufactured by incomplete removal of the residual binder, for CAS/Nicalon andCAS/SCS-6 panels. Figure 4.24 shows the resulting consolidation for a CAS/Nicalon panel: actual porosity was estimated to be between 3 and 6 percent. Also present in this panel are poor fiber distribution (Figure 4.25), and a high incidence of unintentional microcracking, (Figure 4.26).

4.2.7 Well Bonded Fiber--Level One

Fibers were oxidized for one CAS/Nicalon panel and one CAS/SCS-6 panel by increasing the temperature used to burn out the binder. This method was used to generate one level of poor fiber/matrix interface properties.

4.2.8 Well Bonded Fiber--Level Two

Nicalon fibers were oxidized by increasing the temperature used to burn out the binder, in the same way as described in 4.2.7 above, except that a higher processing temperature was used. This method was used to generate a second level of poor fiber/matrix interface properties in a CAS/Nicalon panel.

BROKEN FIBERS AND SPLICE

1"   1/2"   1"   1/2"

3/2"

1"

BROKEN FIBERS
WITH -.05" GAP
BETWEEN BROKEN
ENDS

SPLICE

4" X 4" CMC PANEL
CAS-2 MATRIX
NICALON FIBER
8 PLY
LAYUP (0/90)s

S/N N4
DEFECTS IN LAYER 4
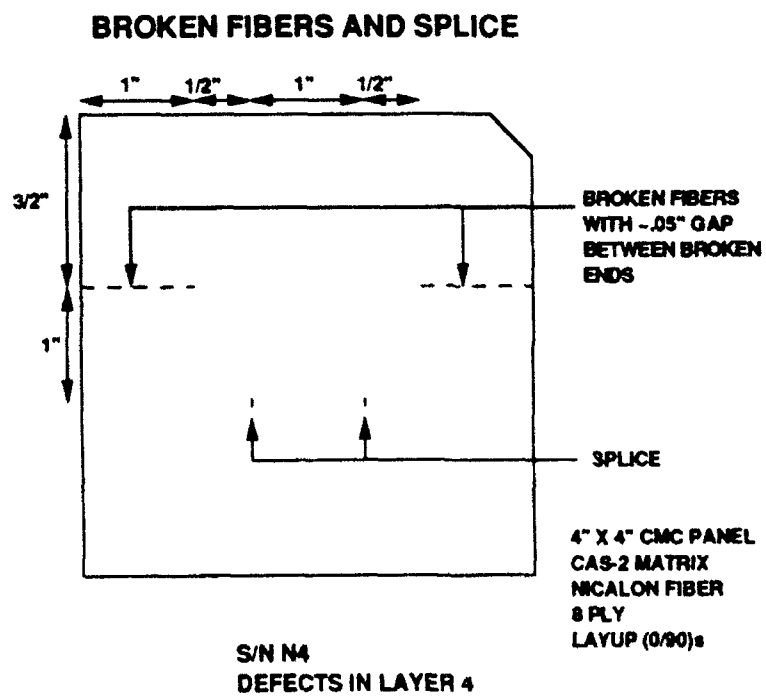
Figure 4.20 CMC panel N4 with broken fibers and splice.

BROKEN FIBERS

1" 2"

2"

BROKEN FIBERS
WITH -.05" GAP
BETWEEN BROKEN
ENDS.
LAYER 4.

4" X 4" CMC PANEL
CAS-2 MATRIX
SCS-6 FIBER
8 PLY
LAYUP (0/90)s

S/N S4
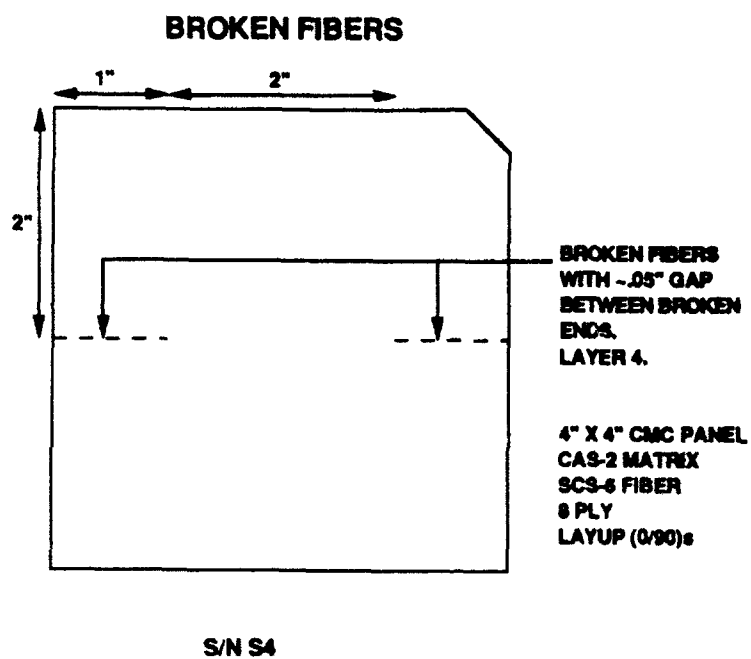
Figure 4.21 CMC panel S4 with broken fibers and splice.
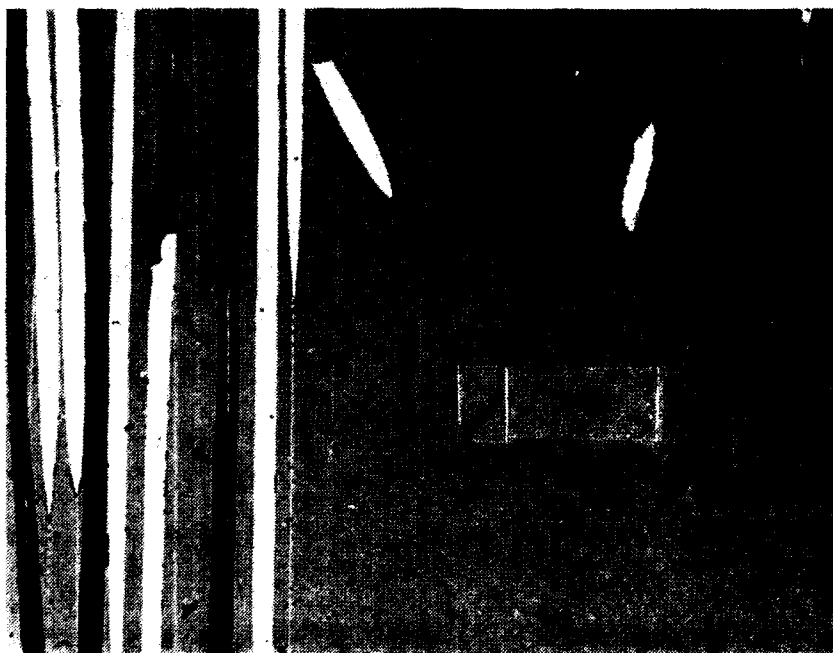
200X

Figure 4.22 CAS/Nicalon CMC panel N5 exhibiting less than 1% porosity.
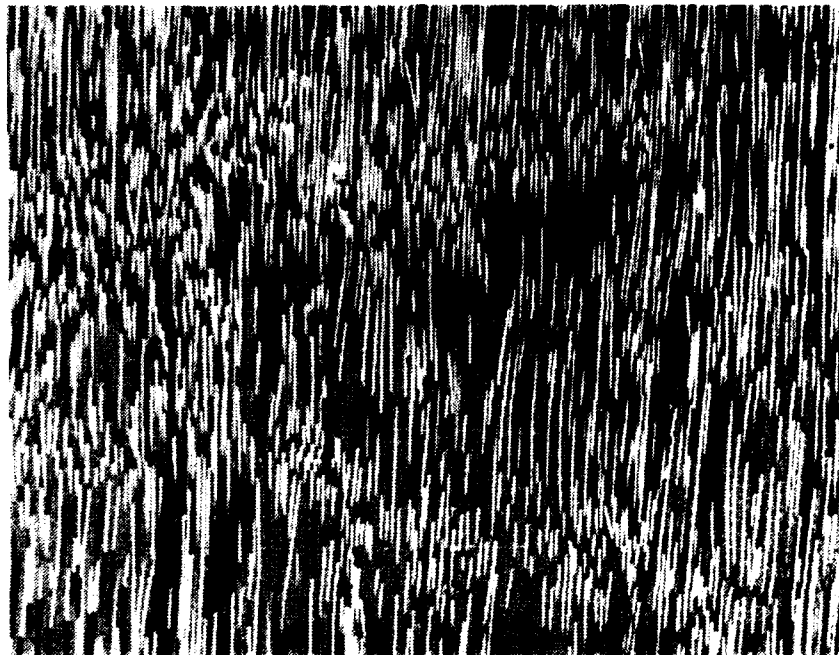
25X

Figure 4.23 CAS.Nicalon CMC panel N5 exhibiting uniform fiber
distribution.
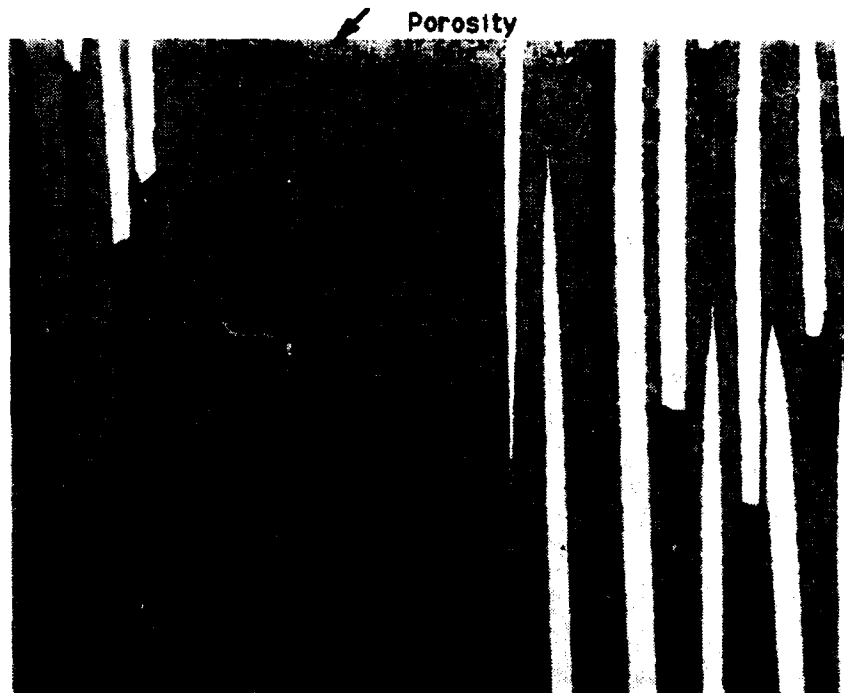
Figure 4.24 CAS/Nicalon CMC panel N6 exhibiting porosity between 3% and 6%.
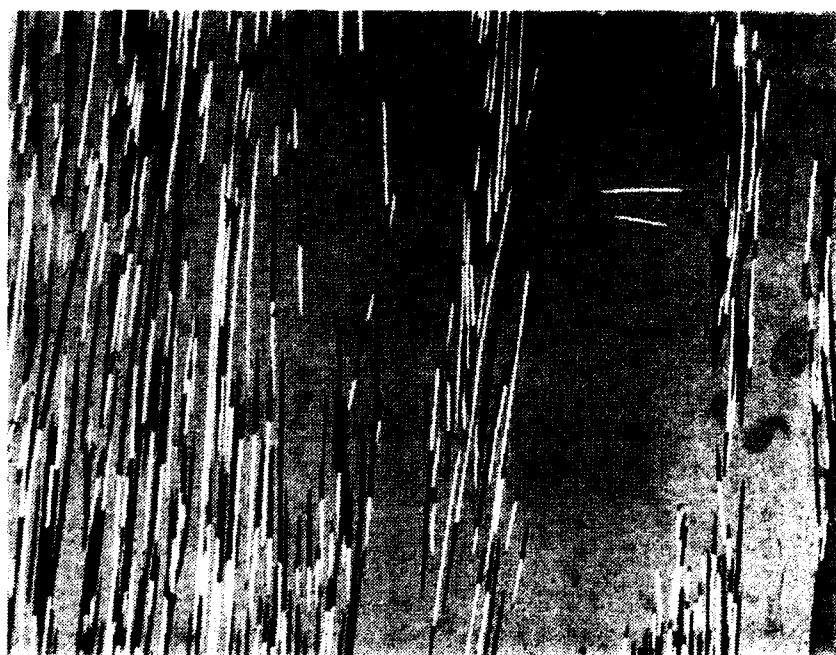
25X

Figure 4.25 CAS/Nicalon CMC panel N6 exhibiting uneven fiber   XX
distribution.
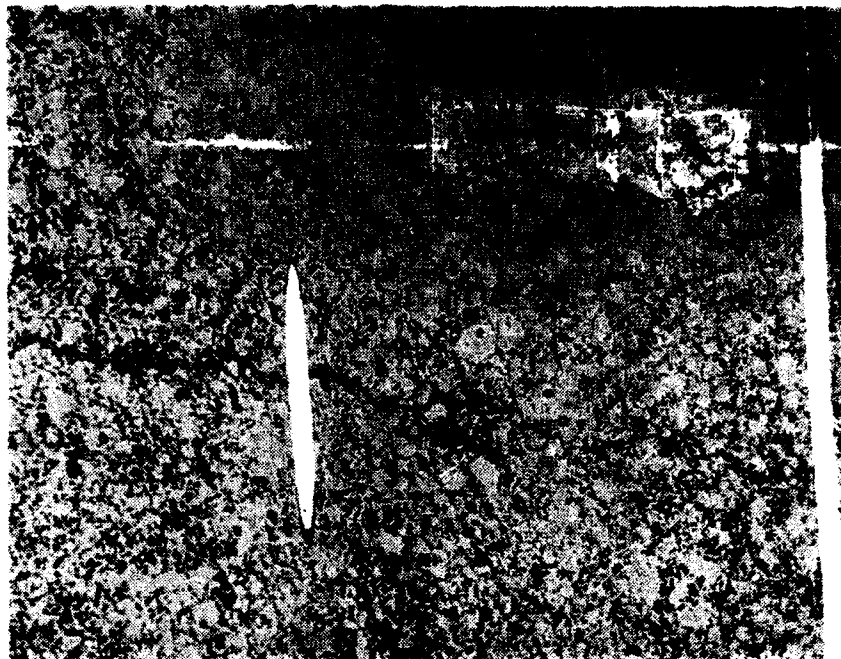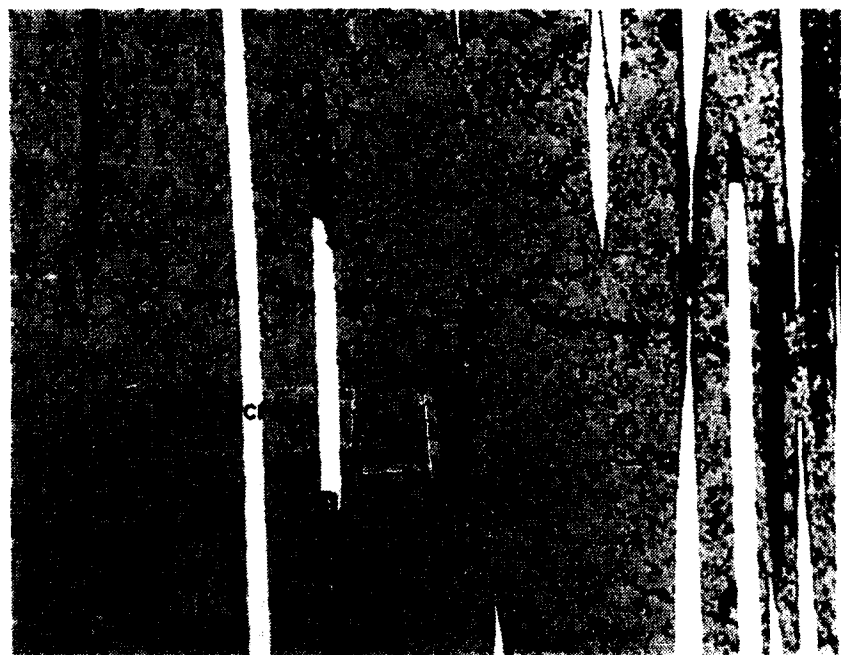
200X

200X

Figure 4.26 CAS/Nicalon CMC panel N6 showing microcracks

4.2.9 25% Fiber Fraction, Low Porosity

One CAS/Nicalon panel was manufactured to contain the low fiber/volume fraction of 25%, and good consolidation. Figure 4.27 shows the porosity which was measured at approximately 1 to 2 percent. Crushed fibers were also inadvertently included, as is shown in Figure 4.28.

4.2.10 40% Fiber Fraction, Minimum Porosity

One CAS/Nicalon panel was manufactured to contain a moderate fiber/volume fraction of 40%, and the best possible consolidation. Figure 4.29 shows the resulting structure.

4.2.11 25% Fiber Fraction, Low Porosity, Cracks

One CAS/Nicalon panel was manufactured to contain the low fiber/volume fraction of 25%, good consolidation and matrix cracks. Figure 4.30 shows the fiber spacing and porosity, which was measured at under 2 percent. The nature of the matrix cracks is shown in Figure 4.31.

4.2.12 40% Fiber Fraction, Porosity "Strings"

One CAS/Nicalon panel was manufactured to contain a moderate fiber/volume fraction of 40%, and a moderate case of porosity. Figure 4.32 shows that the actual fiber fraction is approximately 30%, and Figure 4.33 shows that porosity, although low at 2 percent, occurred in formations denoted as "strings."

4.2.13 55% Fiber Fraction, Good Consolidation

One CAS/Nicalon panel was manufactured to contain the high fiber/volume fraction of 55%, and good consolidation. The actual fiber fraction was estimated at approximately 40%, and a single large matrix crack was also present in panel, as shown in Figure 4.34.

4.2.14 35% Fiber Fraction, Good Consolidation

One CAS/Nicalon panel was manufactured to contain the low fiber/volume fraction and good consolidation. The actual fiber fraction was 35%.

4.2.15 40% Fiber Fraction, Good Consolidation

One CAS/Nicalon panel was manufactured to contain the moderate fiber/volume fraction and good consolidation. The actual fiber fraction was 40%.
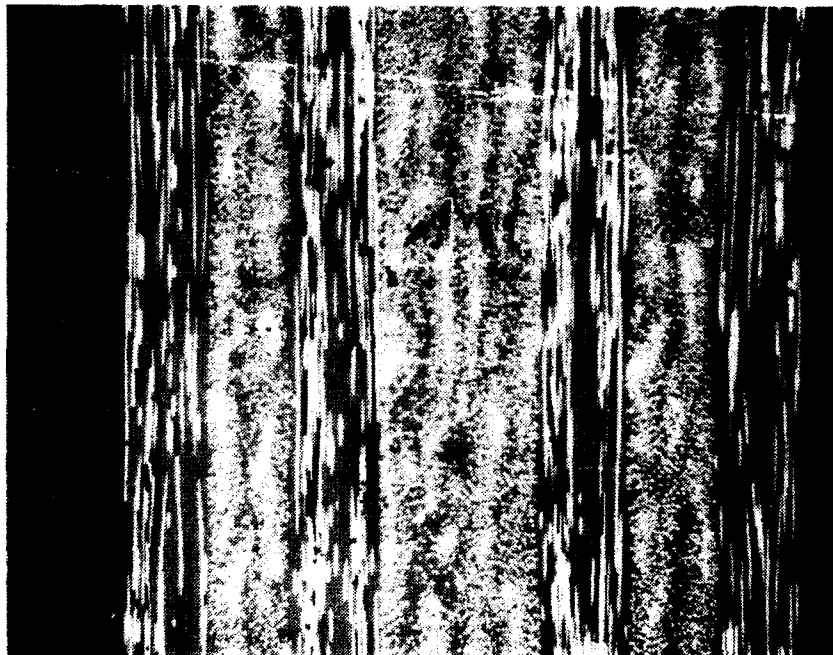
25X

Figure 4.27 CAS/Nicalon CMC panel N9 showing 1 to 2% porosity.
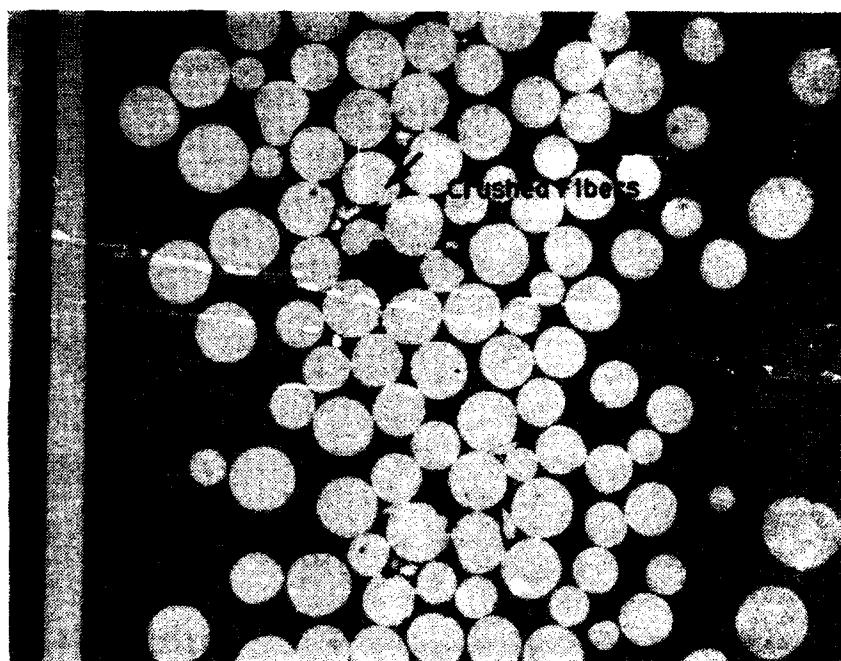
500X

Figure 4.28 CAS-Nicalon CMC panel N9 showing crushed fibers
and uneven fiber distribution.
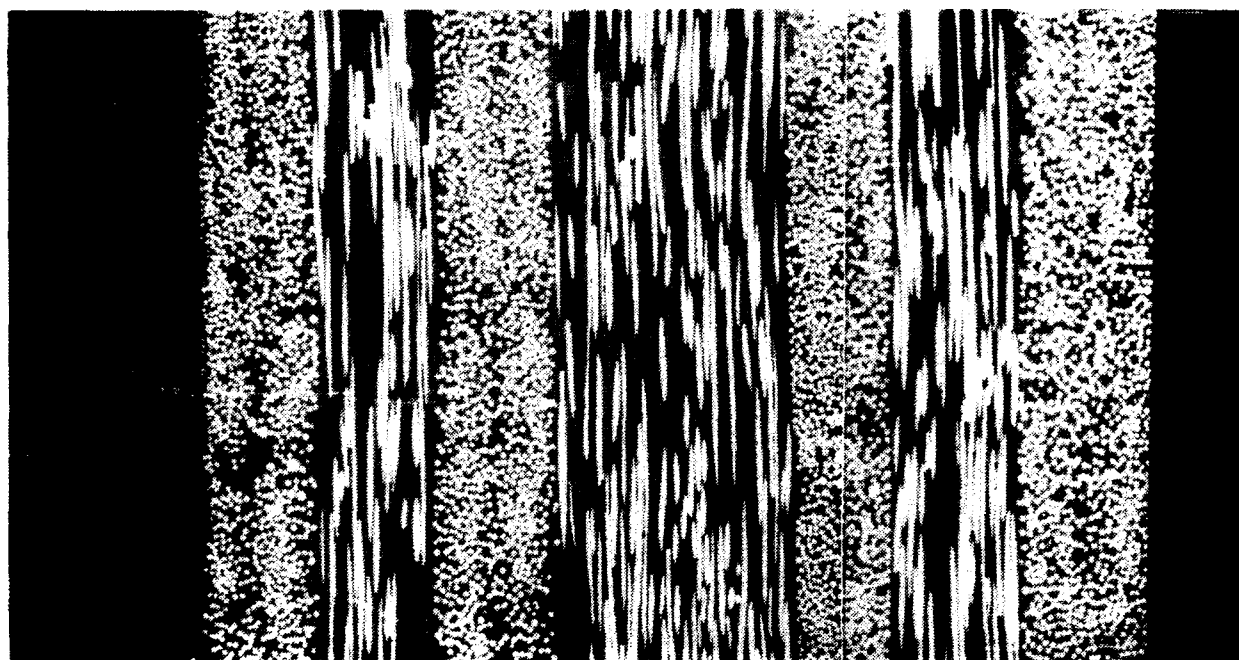
50X

Figure 4.29 .CAS/Nicalon CMC panel N10; well-processed material.
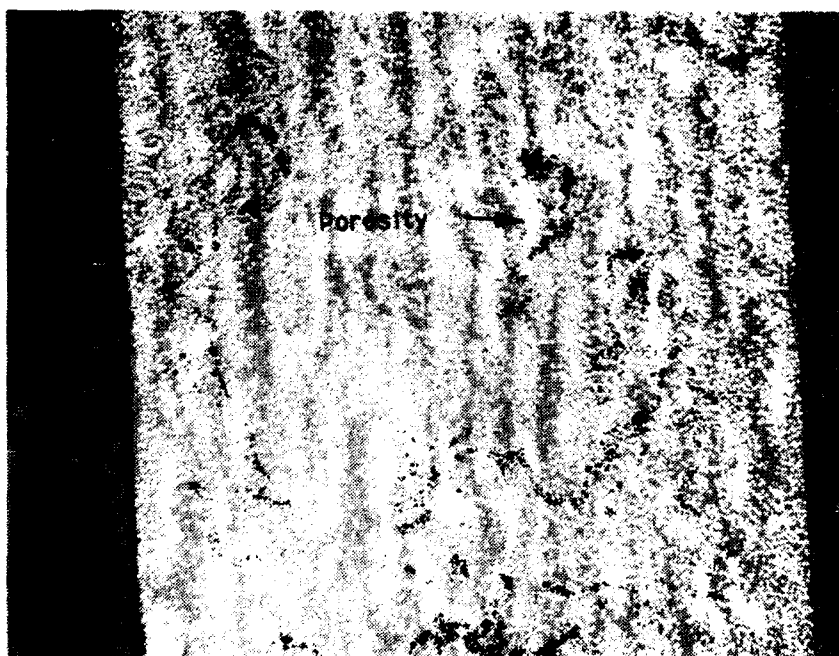
porosity

25X

Figure 4.30 CAS-Nicalon CMC panel N11 showing porosity under
2% and uneven fiber distribution.

25X

Figure 4.31 CAS/Nicalon CMC panel N11 showing a crack
propagating along the fibers.

Low Fiber Density
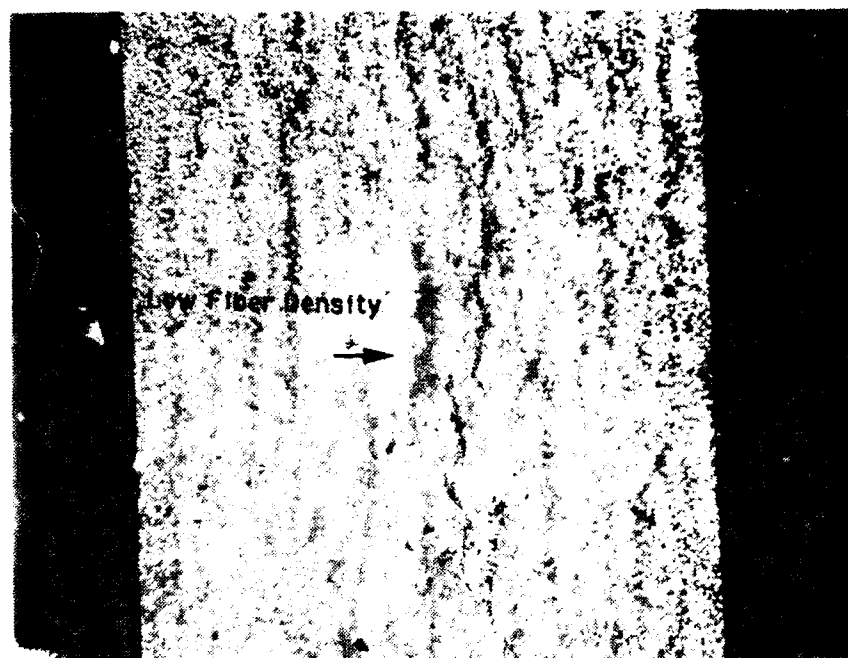
25X

Figure 4.32 CAS/Nicalon CMC panel N12, with low porosity.
and uneven fiber distribution.
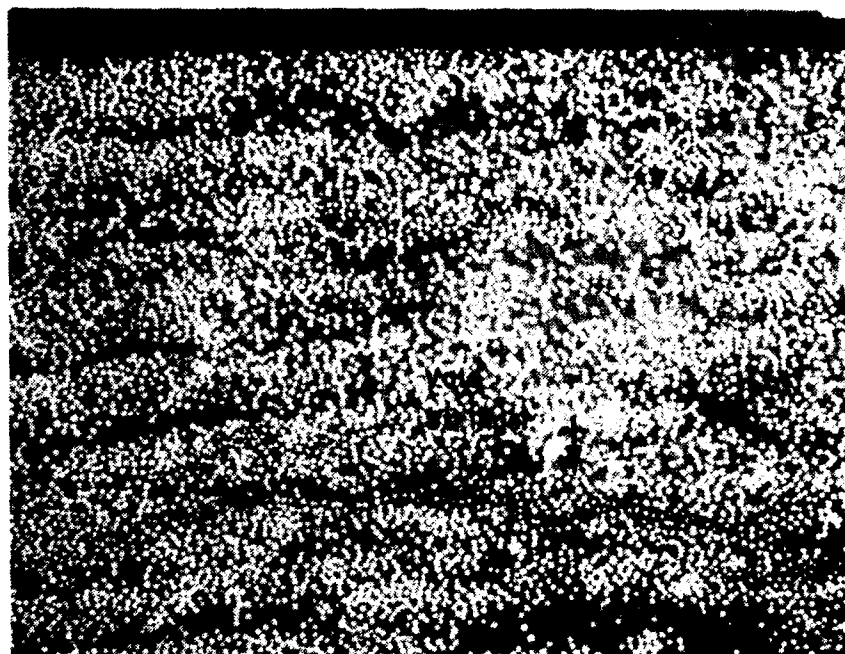
50X

Figure 4.33 CAS/Nicalon CMC panel N12 with example of "stringer" pattern of porosity.
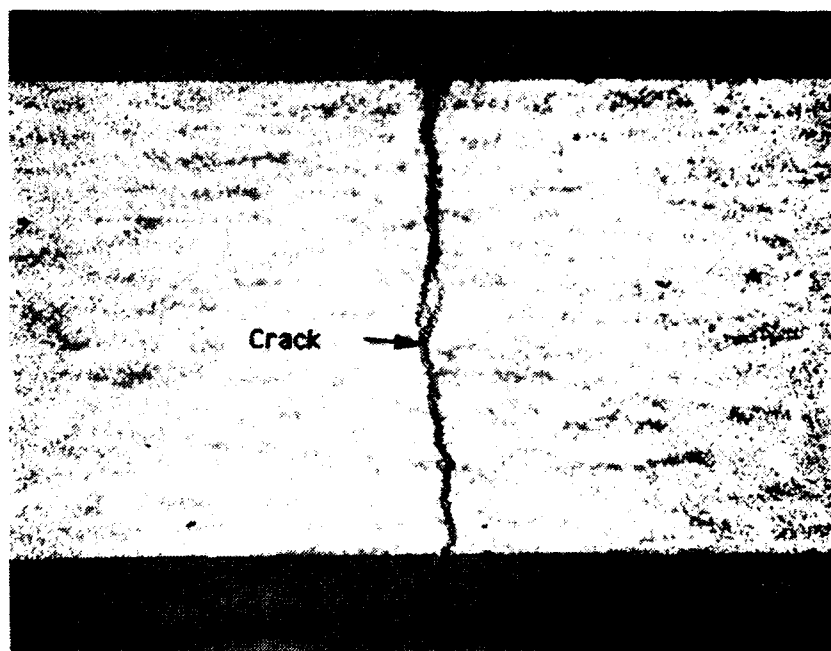
Figure 4.34 CAS/Nicalon CMC panel N13 showing crack propagating through all 16 plies.

4.2.16 51% Fiber Fraction, Good Consolidation

One CAS/Nicalon panel was manufactured to contain the high fiber/volume fraction and good consolidation. The actual fiber fraction was 51%.

4.2.17 Standard CAS/SCS-6 Panel

No defects were introduced to one CAS/SCS-6 panel. It was intended io serve as a control for comparison to other panels.

5.0 NDE Techniques for Composites

Once the types of defects were selected and manufactured, nondestructive evaluation techniques were chosen which were expected to yield the best detection. Ultrasonic and radiographic techniques were chosen for their abilities to penetrate inhomogeneous structures and evaluate density and modulus variations. A subset of these two modalities was explored in an effort to optimize the detection of each type of defect in a variety of configurations. Low resolution ultrasonic pulse echo and through transmission techniques were chosen for inspection of large-area defects such as delaminations. A higher resolution ultrasonic technique, acoustic microscopy, was chosen to find smaller defects including broken fibers and fiber/matrix interface characteristics. Ultrasonic surface waves were chosen to find near surface anomalies which were obscured by near-surface ringdown or scattering for the other ultrasonic techniques. Film radiography was chosen for large volume variations, including fiber orientation. Higher resolution microtomography was chosen to evaluate smaller details such as fiber integrity and fiber coating charateristics. Each NDE technique is described with respect to its basic physical mechanics, its capabilities for defect detection for MMCs and CMCs, and its limiting factors which must be considered during its application.

5.1 Acoustic Microscopy

Basic Technique:
Scanning acoustic microscopy is a high resolution adaptation of pulse-echo ultrasonics. High frequency, sharply focused transducers are selected to provide an interrogating beam diameter that is smaller than the size of the structures which need to be detected. The resulting beam of sound interacts with structural characteristics in the same manner as any other sound beam. Any structure that causes a change in density or modulus will change the acoustic impedance, and will produce an echo for detection. This basic property indicates that a wide variety of structural/defect conditions should be detectable in MMCs and CMCs.

The first step in applying acoustic microscopy is identifying the size of the defect or structure of interest. The smallest defect of interest in the acquired MMC panels was an individual broken fiber. A transducer was chosen with a beam diameter smaller than the 140-micron-diameter fiber. To avoid problems due to the scatter of sound, the lowest possible frequency was selected. Given these two constraints, and the estimation of transducer beam properties, as described by Gilmore [1], two transducers were chosen: 40-MHz, 12-mm focal length, 6-mm lens diameter; and 25-MHz, 25-mm focal length, 10-mm lens diameter. The 40-MHz transducer was chosen for high resolution imaging of fibers in the outer ply, and the 25-MHz transducer was chosen for inspection of deeper plies. The higher frequency

transducer provided exceptional resolution for the imaging of fibers near the surface. Fibers several plies below the surface required the lower frequency transducer to reduce the effects of scattering on the sound beam.

Given the optimized choice of transducers, additional care was required to avoid signal degradation during acquisition. The mechanical scanning device needed to have indexing repeatability and accuracy finer than the beam diameter. A 25-micron accuracy scanning device was used in this program. The electronic signal receiver specifications were of greater importance than the mechanical scanning de ice. Due to weakness of signal strength, the electronic noise of the receiver can obscure the echoes of interest. This problem was minimized by selecting a low-noise amplifier, whose RMS electronic noise amplitude was less than twice the amplitude of room temperature thermal noise. Likewise, the gating circuitry must be able to select a signal segment with an accuracy better than one-half the period of the central transducer frequency.

Assessed Abilities of the Technique for MMCs:
The SCS-6 fiber is composed mostly of silicon carbide, which has an approximate acoustic impedance of 35.8×10^6 kg/m^{2}sec [2]. Because the Ti 6-4 matrix has an approximate impedance of 27.8×10^6 kg/m^{2}sec [3], 12.6 percent of the sound incident to the fiber will be reflected. These numbers indicate that the fibers can be detected, and that much of the incident sound can penetrate for inspection of deeper plies. When imaging the fiber signal, incontinuities in linear fiber indications point to fiber breaks (Figure 4.14), and the position of the fiber indications suggest fiber orientation and spacing. Two examples of bunched fiber indications are shown in Figure 5.1, and their respective causes are shown in Figure 4.9. An indication of fiber orientation is shown in Figure 5.2, for the third ply of a cross-ply laminate. The actual orientation of this ply was -45 degrees, and it was located below two zero-degree plies. Figure 4.14 shows the orientation of shallower plies as detected with this technique.

Another class of structures/defects is the air-backed interface. Delaminations, voids, fiber/matrix debonds and cracks fall into this category. Each of these conditions can be characterized as a transition from a solid (either titanium or silicon carbide) to air. This interface is a perfect reflector, and thus all of the incident sound energy is reflected. The image resulting from this type of structure can suggest the source of the indication. If the indication falls on a fiber, then it may be linked to the fiber, such as a fiber/matrix debond, (Figure 5.3) or fiber crack, (Figure 4.14). If the indication is between fibers, then it must be matrix-based, such as a void, (Figure 5.4). If the indication covers an area larger than the fiber diameter, then it is likely due to a delamination, (Figure 5.5). Photographs of the actual delaminations are shown in Figures 4.4 and 4.5.
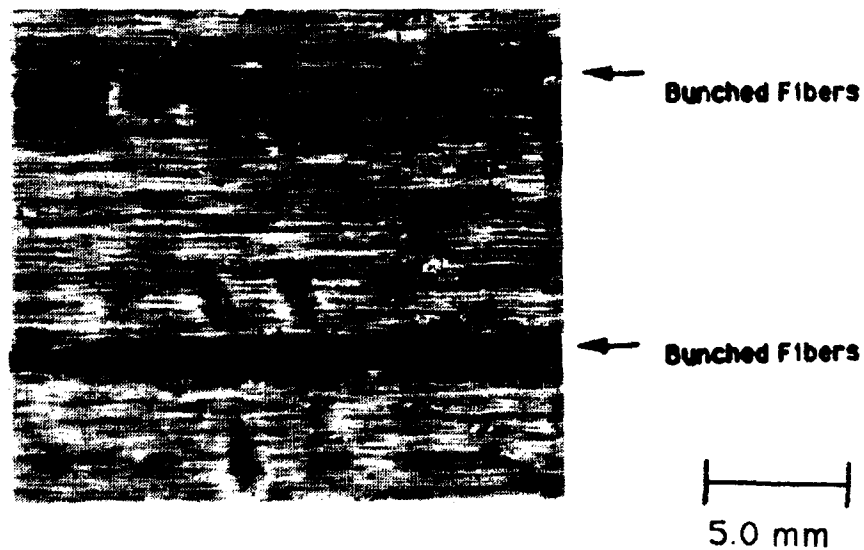
Figure 5.1 Acoustic microscope image of bunched fibers in SiC/Ti
MMC panel 5. Upper band of fibers corresponds to
Fig. 4.9.a. Lower band corresponds to Fig. 4.9.b.

-45 Degree Direction

SCALE ├─────┤=1.9200mm v2.2 rectangle 25 X 16 X .02 isc 7 ply 3 25 MHz
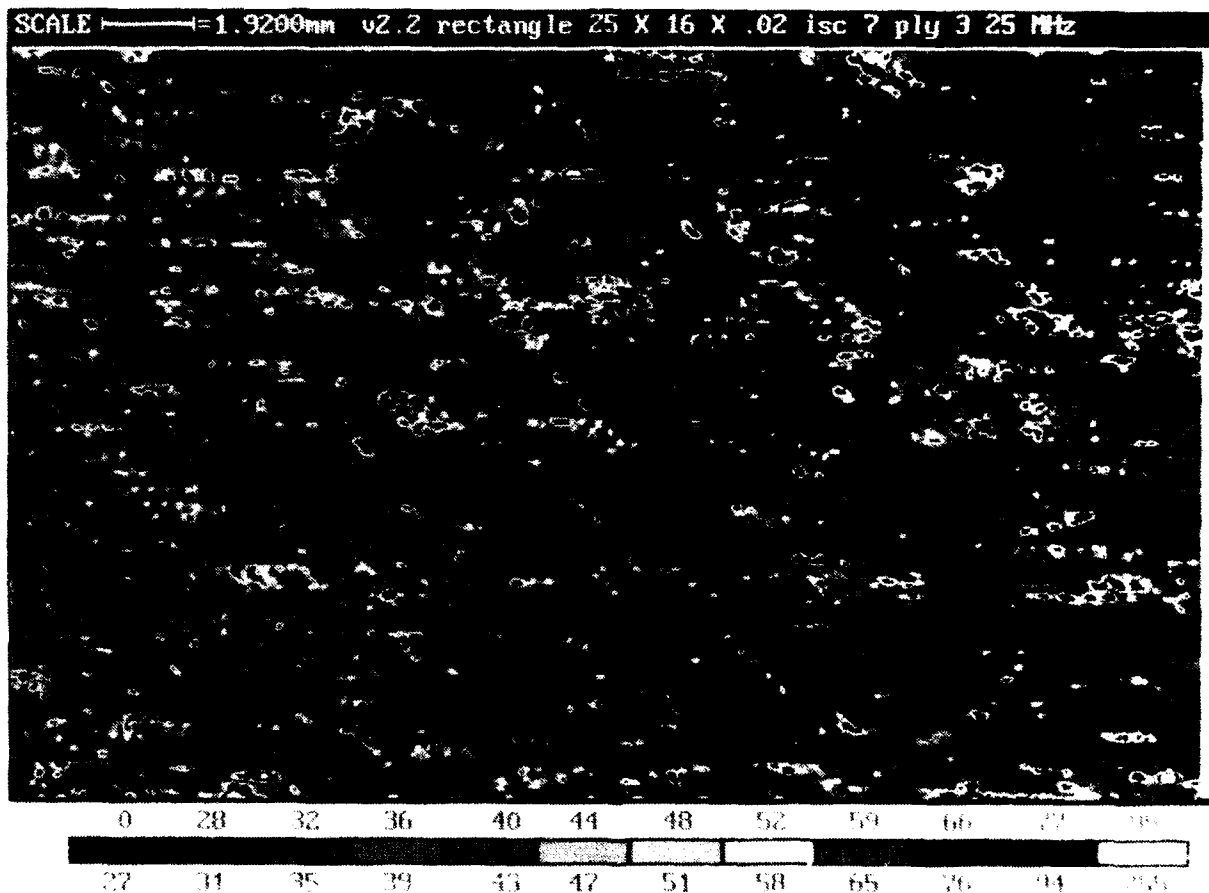
Figure 5.2 Acoustic microscope image of third ply in SiC/Ti MMC
panel 7. Fiber orientation is -45 degrees, as viewed
through two outer plies at zero degrees.
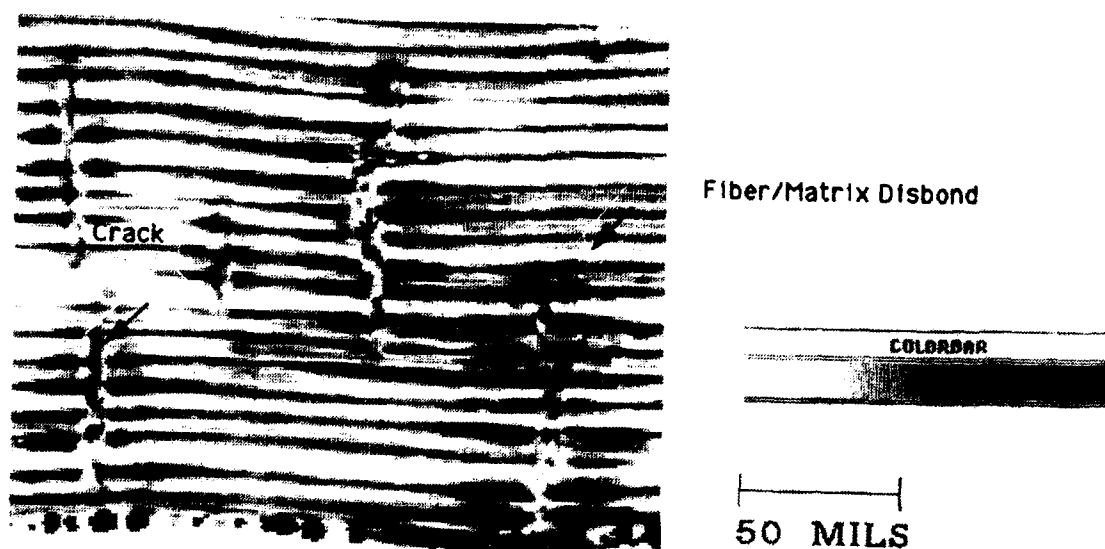
Figure 5.3 Acoustic microscope image of cracks and fiber/matrix
debonds in SiC/TI MMC specimen.

51
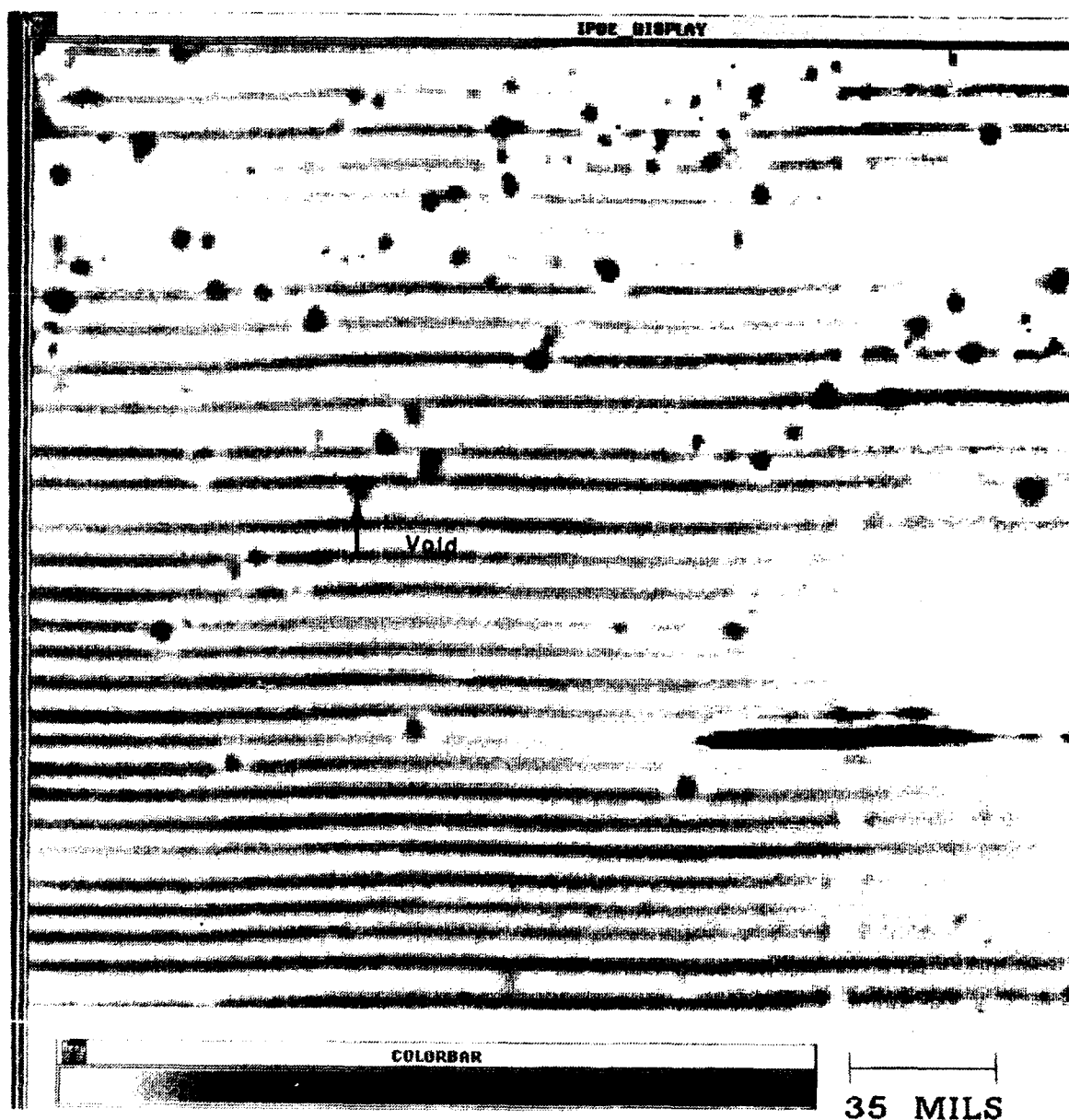
Figure 5.4 Acoustic microscope image of pores in SiC/Ti MMC specimen.

Figure 5.5.a

5.0 mm
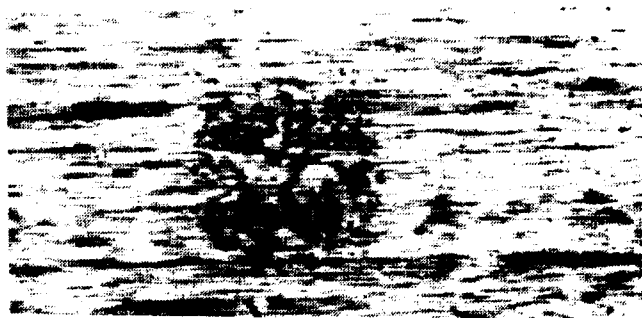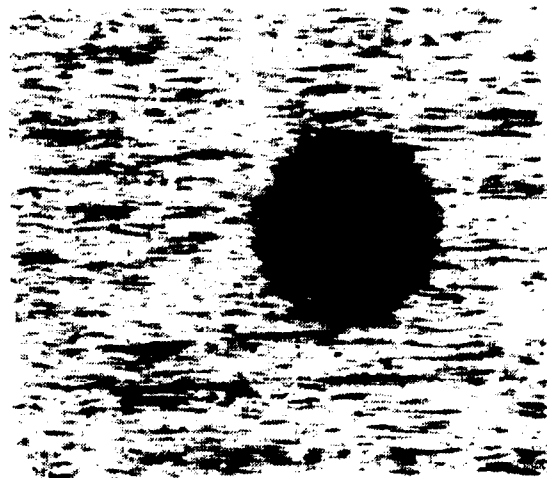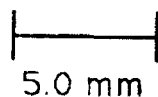
Figure 5.5.b

Delamination

Figure 5.5.c

Figure 5.5 Examples of ultrasonic detection of delaminations in
SiC/Ti MMC panel 5. The indication in Fig. 5.5.a is the
image of the partial delamination shown in Fig. 4.4.b.
The indication in Fig. 5.5.b is the image of the planar
delamination shown in Fig. 4.4.a. Figure 5.5.c shows
a 1.3 mm delamination detected through 17 plies of MMC.

Assessed Abilities of the Technique for CMCs:
The difference in acoustic impedances is not as great between CAS/silicon carbide as for titanium/silicon carbide, and as a result, the detectability of fibers is not expected to be as great. Other features in CMCs, such as air-backed interfaces, should be as easily detected as in MMCs. These abilities were not demonstrated, however, because the surface roughness of the specimens severely scattered the sharply focused sound beam. This technique should be pursued further, if smooth-surfaced specimens become available.

Limitations:
The most severe limitation of acoustic microscopy is the ability of the sound to penetrate an anisotropic material. The fiber/matrix structure is a natural scatterer, and the effect is significant when one tries to inspect volumes well below the specimen surface. Because the fiber only reflects 12.5 percent of the incident sound energy, fibers below the second ply are difficult to image. Figure 5.2 shows how the third ply can be imaged to indicate fiber orientation, but individual fibers are difficult to discern. Air-backed interfaces can be detected at greater depths, and their detectability degrades as a function of depth. A 3-mm delamination could be detected in the seventeenth ply (Figure 5.5), while a void in the order of 25-50 microns could be detected in the outer ply (Figure 5.4). These limits were based on the results of inspecting MMC panels manufactured for this program. These numbers may be too conservative, due to the fact that the fibers in these panels were severely broken, as shown in Figure 4.14, and these breaks scatter sound more severely than high integrity fibers. Thus, the detectability described above represents a worst-case scenario.

A secondary limitation to achieving effective results using this technique is due to the difficulty in placing the focal zone of the sound beam at the proper depth to interrogate the desired volume. Care must be taken in selecting the waterpath, so that the transducer focal point is coincident with the ply under test. An offset of 500 microns can blur together all of the structural details. To select the proper waterpath, one should start with the beam focus on the component surface, and then shorten the travel in water by 4.7 times the desired depth of inspection (4.7 is the approximate ratio of velocities between water: 1.5 mm/μsec and MMC: 7.0 mm/μsec.) (MMC velocity measured on panels made for this program)

The final limitation of acoustic microscopy is cost. Obtaining volumetric data of a full sized component would require excessive scanning times to acquire the large amounts of data to produce a high resolution image. Further development may lead to improved efficiency, or the technique may be limited to spot checks. Regardless, the technique is extremely valuable for material characterization efforts for material development and manufacturing process development.

54

5.2 Ultrasonic Pulse Echo

Basic Technique:
This technique is similar to acoustic microscopy, except that a different transducer is chosen for improved penetration and shorter inspection times, with the trade-off being degraded defect detectability. Penetration and inspection time are both improved as the transducer frequency is decreased, and the lens radius of curvature is increased. The longer wavelengths associated with the lower frequencies, (2.5 to 15 MHz) are not scattered as severely by the fibers, fiber breaks, or other small structures, as compared to the higher frequencies (20 to 50 MHz). As a result, the sound is able to penetrate deeper into the material and detect large structures well below the surface. A larger radius of curvature for the lens means that the sound beam will not be as sharply focused as for acoustic microscopy. Because of this, the beam diameter at the focus is larger, and thus is more easily able to penetrate (bypass) small reflectors. The key to optimizing this technique is to select a transducer with a beam diameter no larger than the critical defect, a -6 dB depth of field approximately equal to the thickness of the area to be inspected, and a wavelength greater than 4 times the size of the inconsequential structure (the fibers). Gilmore [1], discusses the beam diameter and depth of field as a function of frequency, focal length, and lens radius of curvature. This application of pulse-echo ultrasonics is different from many conventional applications in the fact that the far field of the beam cannot used for the inspection. This is a direct result of the scattering caused by the inhomogeneous structure.

Assessed Abilities of the Technique for MMCs:
This technique is especially effective for large delaminations, (Figure 5.5), or other large structural defects or populations of defects. The wide variety of transducers that could be chosen for this technique means that a wide range of detection probabilities is available for any given delamination. The best resolution possible corresponds to that shown in Figure 5.5, for acoustic microscopy, and then as depth of inspection is increased, the size of delamination sought must increase, because the resulting data will be more blurred.

Assessed Abilities of the Technique for CMCs:
This technique is especially effective for large delaminations or other large structural defects or populations of defects, (e.g., porosity), in CMCs. Sound has difficulty penetrating the specimen at the water/specimen interface because of the high acoustic impedance of the matrix. Once the sound is inside the specimen, its attenuation is dominated by porosity rather than the fibrous structure. Porosity is common condition in CMC's, which acts as a severe attenuator of sound. The acoustic impedance of the fiber is nearly equivalent to that of the matrix, so that anisotropic structure has little effect.

Limitations:
Small defects are easily overlooked by this technique, because the fibers and porosity scatter the sound so severely. The fiber/matrix structure in CMCs is not observable with the high resolution version of this technique because the fiber/matrix interface typically does not act as a strong sound reflector. Geometry is an issue to the same extent as for conventional ultrasonics.

5.3 Ultrasonic Through-Transmission/Attenuation

Basic Technique:
Ultrasonic through-transmission inspections can be performed using one of two methods. One method requires that two matched transducers, a transmitter and a receiver, be placed on opposite sides of the specimen. The other method only requires one transducer, and the back surface echo of the component is monitored. This second method assumes that the backwall interface acts as a perfect reflector, such that the amplitude of the signal received is directly related to the attenuation properties of the specimen under test. The effective difference between these techniques and ultrasonic pulse-echo is that they describe how the sound is attenuated (scattered), and thus does not require a coherent back-reflected signal from the defect. This makes through-transmission less dependent on defect geometry, and more dependent on defect size and acoustic impedance.

To optimize the use of ultrasonic through-transmission, one must know the scattering characteristics of the critical defect. Then the transducer must be chosen to ensure that a sufficient amount of the sound beam will be scattered by the defect to allow detection. If the specimen is well consolidated and has a smooth surface, then slight variations in the internal structure are detectable. If the surface is rough, then the scatter due to that roughness will impair the signal-to-noise ratio, and small defects will not be detectable. For optimum results, the surface roughness should be small with respect to the ultrasonic wavelength, and the part surface should remain normal to the transducer axis. An additional variable is the focal characteristic of the transducer. A sharply focused transducer is able to ignore structures in its near field and its far field, while giving optimized signal-to-noise ratio at its focus. This factor must be balanced against the total thickness which needs inspection, as only the region within the -6 dB depth of field will be inspected. Suboptimum inspections will look noisy, as is discussed below in the Assessed Abilities of the Technique for MMCs section.

By analyzing the level of attenuation as a function of signal frequency, the nature of the attenuator can be described. The data from through-transmission tests are normally imaged according to signal amplitude. For CMCs under this program, however, the signal amplitude was decomposed by frequency to characterize the cause of signal attenuation. Large defect structures, such as delaminations should attenuate all frequency components equivalently, while smaller defects, such as

56

voids act as scatterers, and thus attenuate higher frequency components more severely than low frequency components.

Assessed Abilities of the Technique for MMCs:
Large delaminations were detected with this technique, although the location of the focal spot had a significant impact on which defects were detected. In the image shown in Figure 5.6a, that shows a high signal-to-noise ratio, delaminations in only one plane were detected. Delaminations only two pl'es away were completely missed. In order to interrogate the full volume of that same panel, a transducer which had a larger depth of field was used. As seen in Figure 5.6b, the resolution and signal-to-noise ratio were degraded, while delaminations throughout the volume were detected. This technique is believed to hold much promise, as detectability issues are addressed with respect to transducer selection and waterpath selection.

This technique has been shown to be effective in characterizing defect populations (such as porosity) in CMCs, but since such populations were not present in the MMC panels under test, one can only speculate on the relative effectiveness in MMCs. One possible application that should be investigated would be the quantification of broken fibers, as their response should be similar to that of porosity in CMCs.

Assessed Abilities of the Technique for CMCs:
Nondefective materials exhibit low attenuation, with virtually no frequency dependence. Delaminations and porosity exhibit higher levels of attenuation, as shown in Figures. 5.7 and 5.8. Other defects are expected to be detectable by this technique, as their size and reflectivity will define their sound scattering properties. The specific cause of the attenuation can be characterized by a comparison of the attenuation for a number of frequency components. Figure 5.9 shows how the attenuation changes for three configurations. This frequency-based effect can be implemented while a component is being scanned, for full characterization. Other, more economical approaches might be to acquire only a few narrow-band signals over the entire specimen, or to only characterize indications which cross a calibrated attenuation threshold.

Limitations:
As mentioned above, location and orientation of the focal spot of the transducer determine the detectability of defects. For the high resolution image in Figure 5.6a, a 15-MHz transducer with a 38-mm focal length and a 6-mm lens diameter was used. To detect delaminations throughout the panel volume, a 10-MHz, unfocused transducer was used.

Another limitation for ultrasonic through-transmission is its dependence on surface roughness. Because rougher surfaces scatter more sound, and thus yield lower signal-to-noise ratios, they can be deceiving if not tightly controlled.

57

Figure 5.6.a

Delaminations

Figure 5.6.b

25 mm
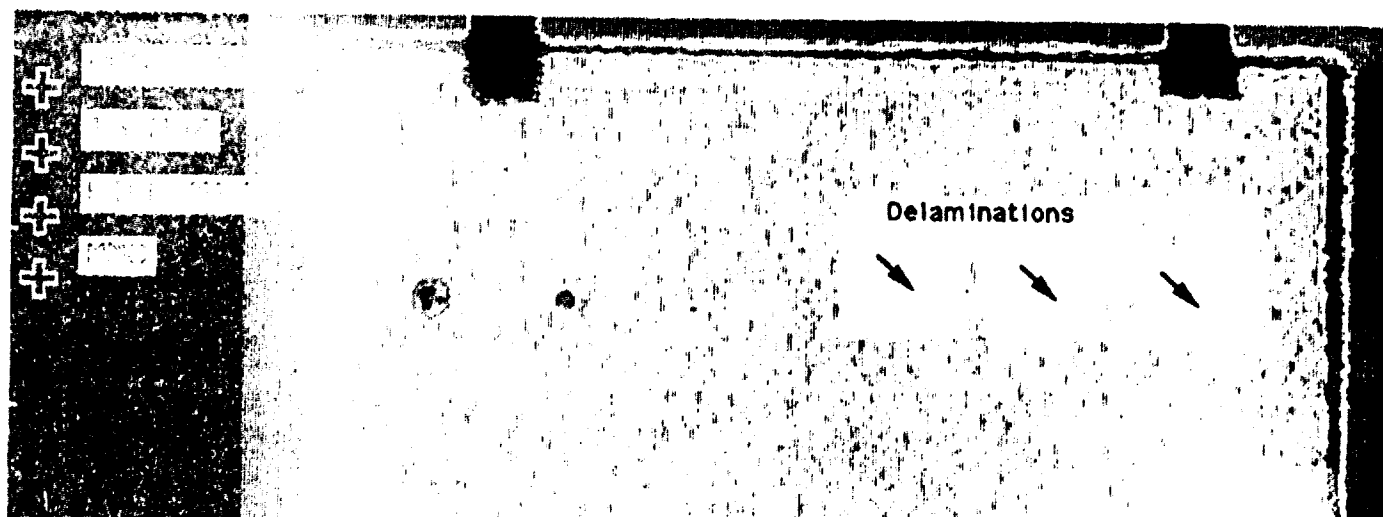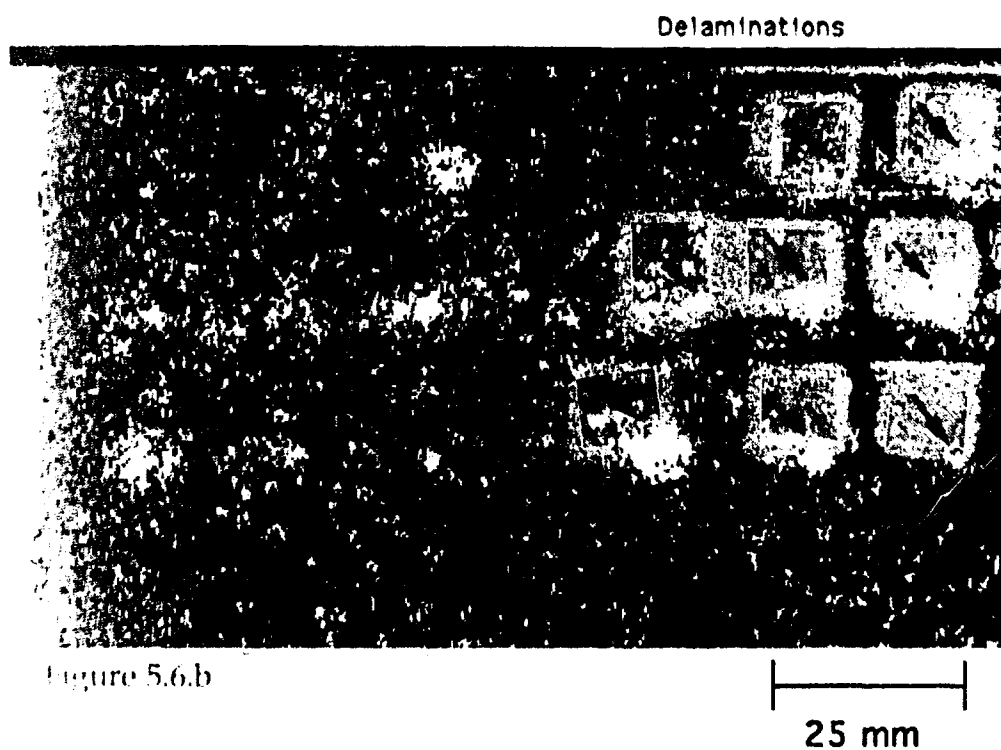
Figure 5.6 Ultrasonic through-transmission images of delaminations in SiC/Ti MMC panel 1. Figure 5.6.a shows the resolution possible with an inspection using focused transducers. Figure 5.6.b shows how structures throughout the volume of a panel can be detected.

58
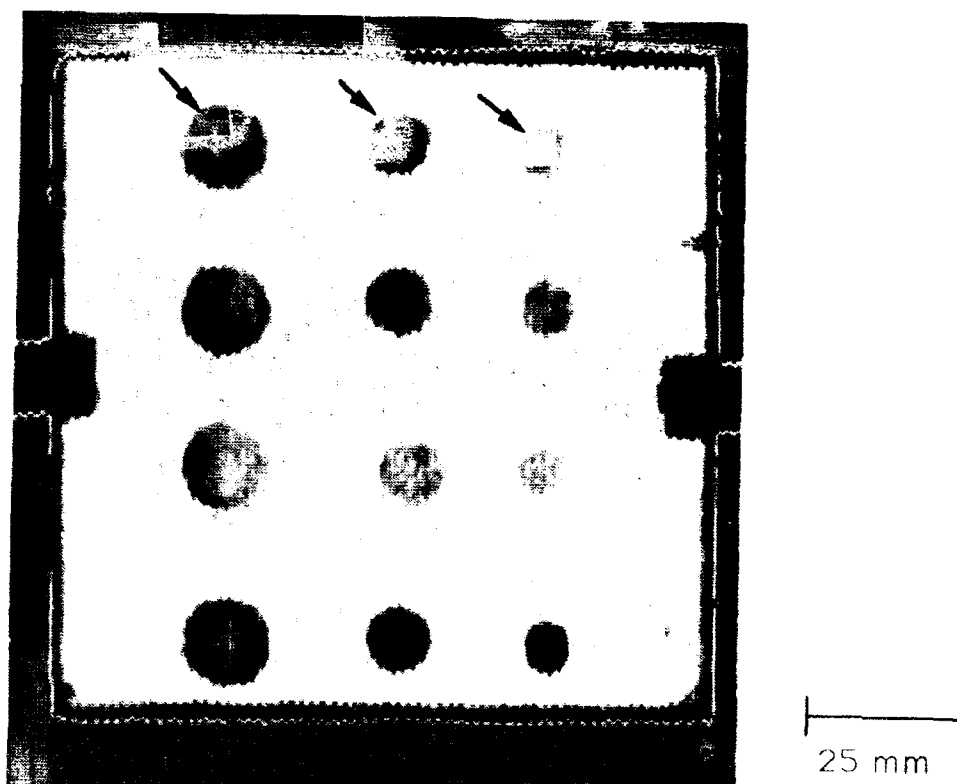
Figure 5.7 Ultrasonic through-transmission image of CAS/ Nicalon CMC panel N1 showing delaminations. Black circles represent delaminations.

Porosity

25 mm
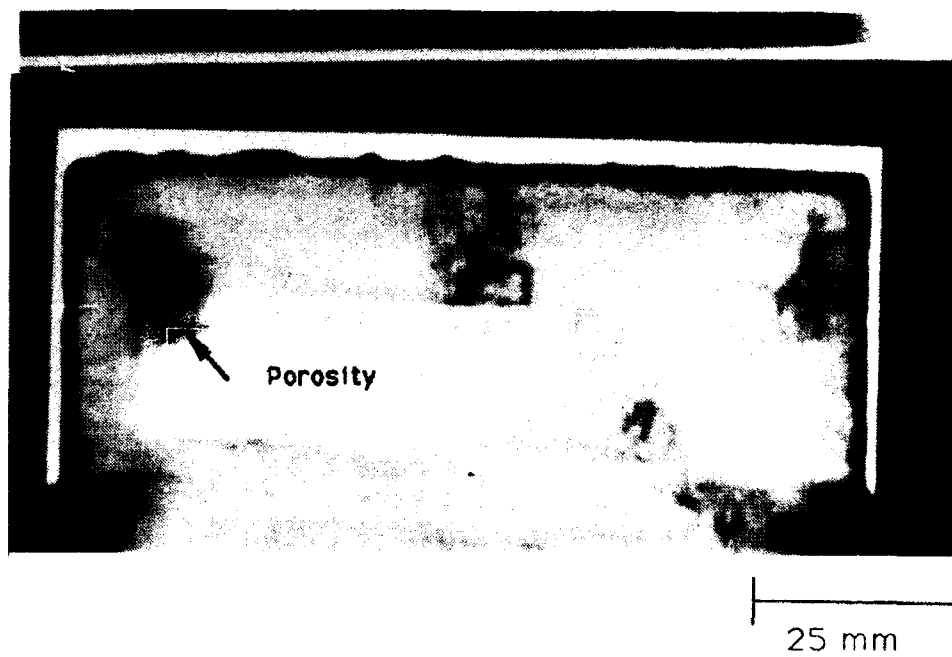
Figure 5.8 Ultrasonic through-transmission image of CAS/
Nicalon CMC panel N6 showing moderate porosity.
Dark regions are areas of higher porosity.

60
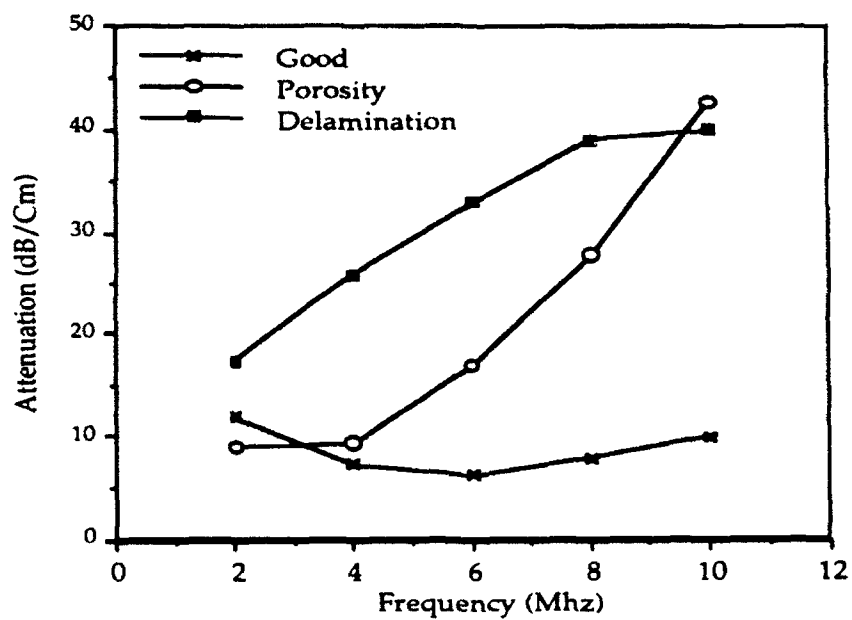
Figure 5.9 Attenuation vs. frequency plot for delaminations and porosity in CAS/Nicalon panels.

5.4 Ultrasonic Velocity

Basic Technique:
The velocity of sound within a material can be calculated by comparing the measured thickness of the specimen to the time elapsed between front and back surface echoes. Models were used to predict how much velocity variation would result from defect conditions. Two specific types of conditions which are expected to change the velocity are fiber volume fraction and porosity. The velocity of sound in fibers is greater than that of the matrix in CMC specimens, so increased incidence of fibers should increase the velocity of sound in the specimen. Porosity has a general tendency to decrease velocity in most materials.

Assessed Abilities of the Technique for MMCs:
This technique was not explored for MMCs.

Assessed Abilities of the Technique for CMCs:
Figure 5.10 shows how the modeled and measured velocities change as a function of fiber volume fraction. If the thickness of a specimen is well characterized, then a conventional time-of flight measurement between front and back surface echoes could be used to draw a velocity map. If that much data are not required, the specimen could be sampled at key locations to estimate velocity, and thus predict fiber/volume fraction. The one point in Figure 5.10 that does not fall in line with the other samples was influenced by porosity. This is an indication that porosity variations could have a more significant effect on on this measurement than fiber/volume fraction.

Limitations:
A significant consideration when using this technique is the difficulty of separating variables, because both porosity and fiber volume fraction can effect the measurement. Also, if the specimen material is dispersive, or if it preferentially attenuates specific frequency components of the incident waveform, then measuring the time of travel could be difficult.

5.5 Ultrasonic Backscatter

Basic Technique:
This technique is conceptually similar to pulse-echo ultrasonics, except that the transducer is placed at an angle with respect to the specimen surface. The received signal represents sound that has been scattered due to structural anomalies. This technique was devised to characterize small anomalies, which do not act as coherent reflectors, such as porosity and fiber characteristics. The transducer parameters should be selected in a manner similar to that for ultrasonic pulse-echo applications; with respect to desired penetration and size of defect.

62
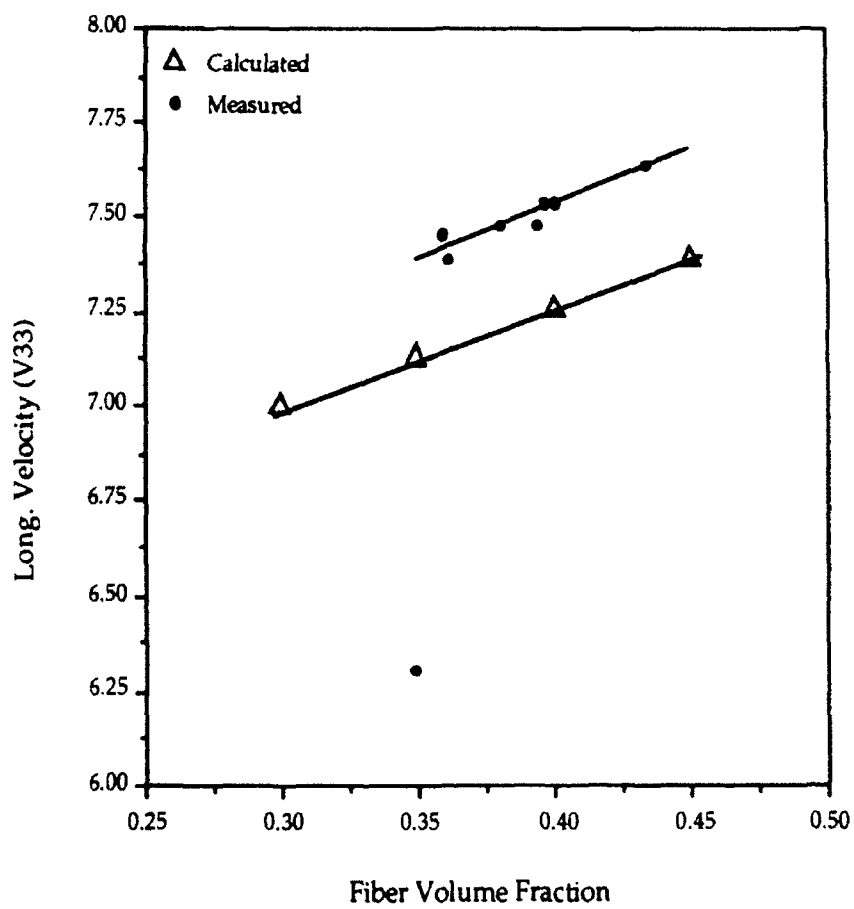
Figure 5.10 Variation of ultrasonic velocity with fiber volume
fraction for CAS/Nicalon panels.

63

Assessed Abilities of the Technique for MMCs.
Figure 5.11 shows how the backscatter signal is able to detect fiber orientation in a MMC with an unidirectional fiber layup. As the specimen is rotated 360 degrees, a strong incidence of scattered energy is received when the transducer is perpendicular to the fiber. The effect of angle of incidence, with respect to the specimen surface is shown, as the radial dimension of the circular scan represents the incidence angle ranging of 10 to 20 degrees.

Assessed Abilities of the Technique for CMCs:
Figure 5.12 shows how the backscatter signal is able to detect fiber orientation in a CMC with a 0/90 degree layup. As the specimen is rotated 360 degrees, a strong incidence of scattered energy is received when the transducer is perpendicular to the fiber. The effect of angle of incidence, with respect to the specimen surface is shown, as the radial dimension of the circular scan represents the incidence angle ranging of 10 to 20 degrees. Figure 5.13 shows how this technique is effective in detecting regional variations of porosity in a CMC specimen.

Limitations:
Scattered signals tend to be weak, and are therefore easily masked by noise. Especially difficult to characterize are the layers of a composite well below the surface, because scattering due to the outer fibers weaken the signals of the deeper fibers or deeper porosity.

5.6 Ultrasonic Surface Wave Velocity

Basic Technique:
When sound approaches a specimen at an angle greater than the Raleigh critical angle, the incident sound energy can only enter the specimen as a surface wave. As the surface wave travels along the specimen, sound energy leaks back into the coupling medium, which can then be detected. By using a transmitting and receiving transducer, and then comparing the distance traveled with the elapsed time between transmission and reception, the velocity of the surface wave in the specimen can be measured. This technique can be applied to measure absolute properties, or in a rotational manner, to measure directional variations in properties.

Assessed Abilities of the Technique for MMCs:
This technique was not explored for MMCs.

Assessed Abilities of the Technique for CMCs:
The surface wave velocity changes as a function of material density and modulus, and as a result, ultrasonic velocity is higher for fibers than the matrix in CAS/silicon carbide systems. As fiber fraction increases, velocity should increase as well. This effect is demonstrated in Figure 5.14, where the velocity is shown for three specimens of differing fiber fraction. Differences in velocity were noted as a

64
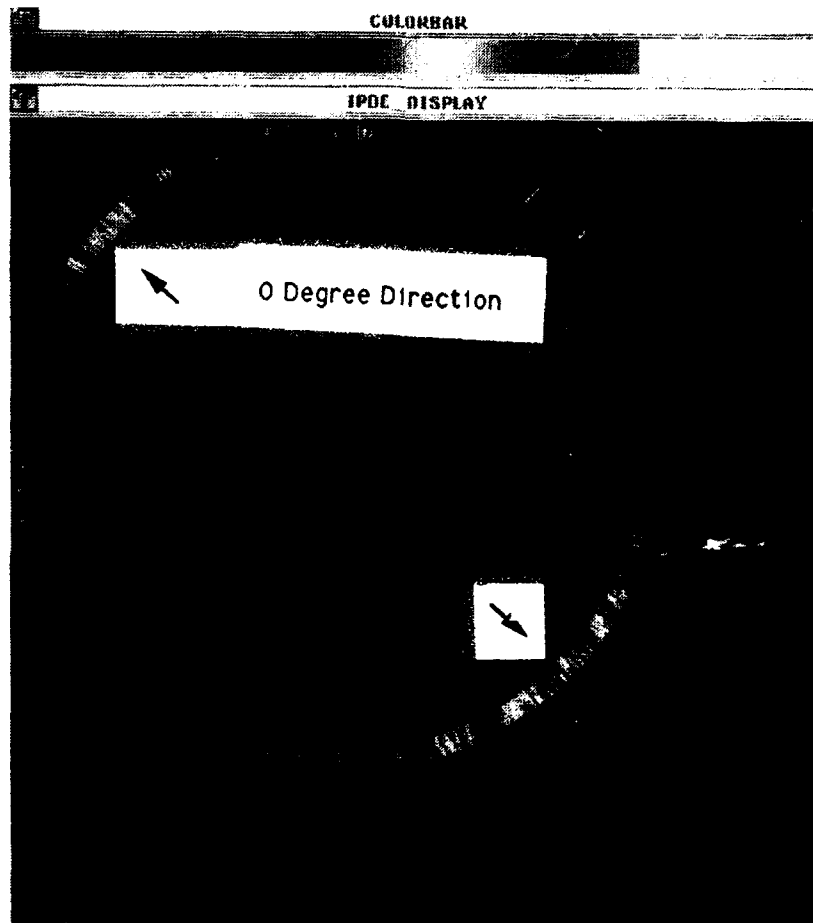
Figure 5.11 Ultrasonic polar backscatter scan showing unidirectional
fiber layup in a SiC/Ti MMC panel. Angular dimension
of plot corresponds to rotational angle of transducer
assembly. Radial dimension of plot corresponds to the
angle of incidence of sound to the panel, with the inner
value at 10 degrees and the outer value at 20 degrees.
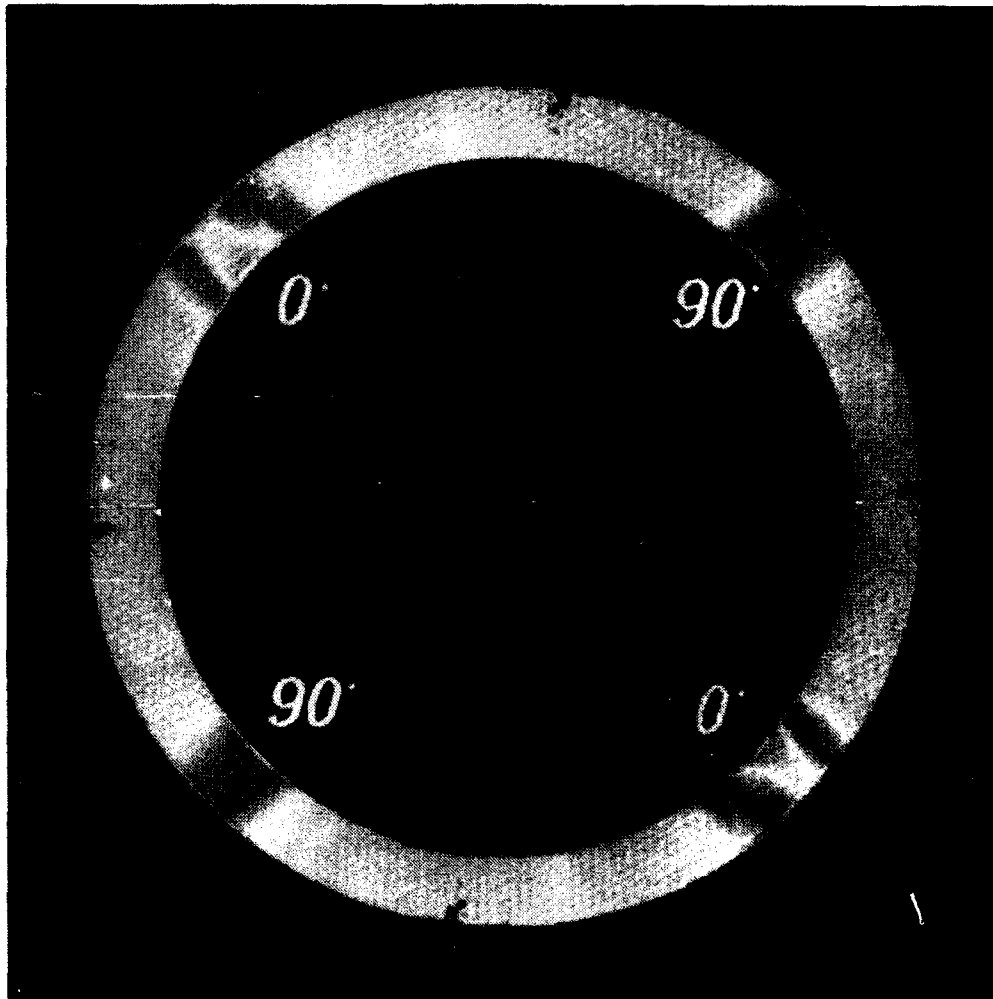
Figure 5.12 Ultrasonic polar backscatter scan showing 0/90 degree
fibers in a CAS/Nicalon panel. Angular dimension
of plot corresponds to rotational angle of transducer
assembly. Radial dimension of plot corresponds to the
angle of incidence of sound to the panel, with the inner
value at 10 degrees and the outer value at 20 degrees.
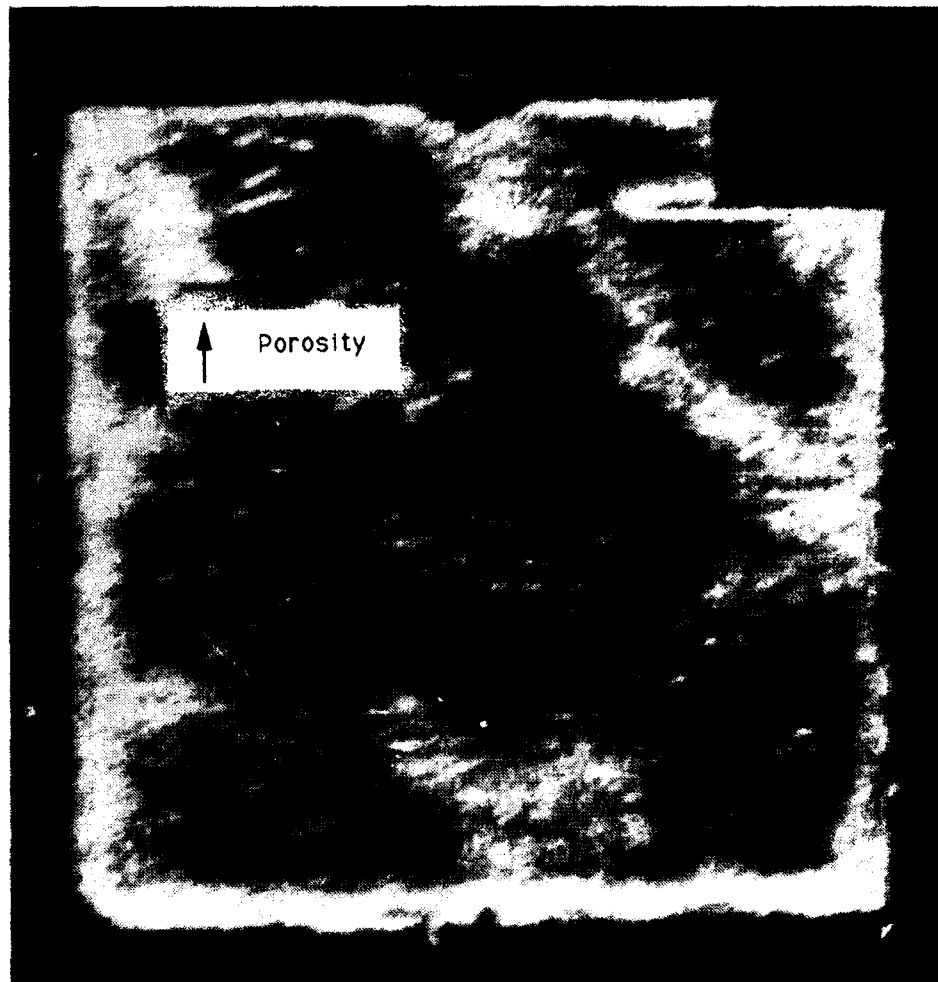
Figure 5.13 Ultrasonic backscatter scan of CAS/Nicalon CMC panel
N6 showing moderate porosity. White indications
correspond to higher porosity.
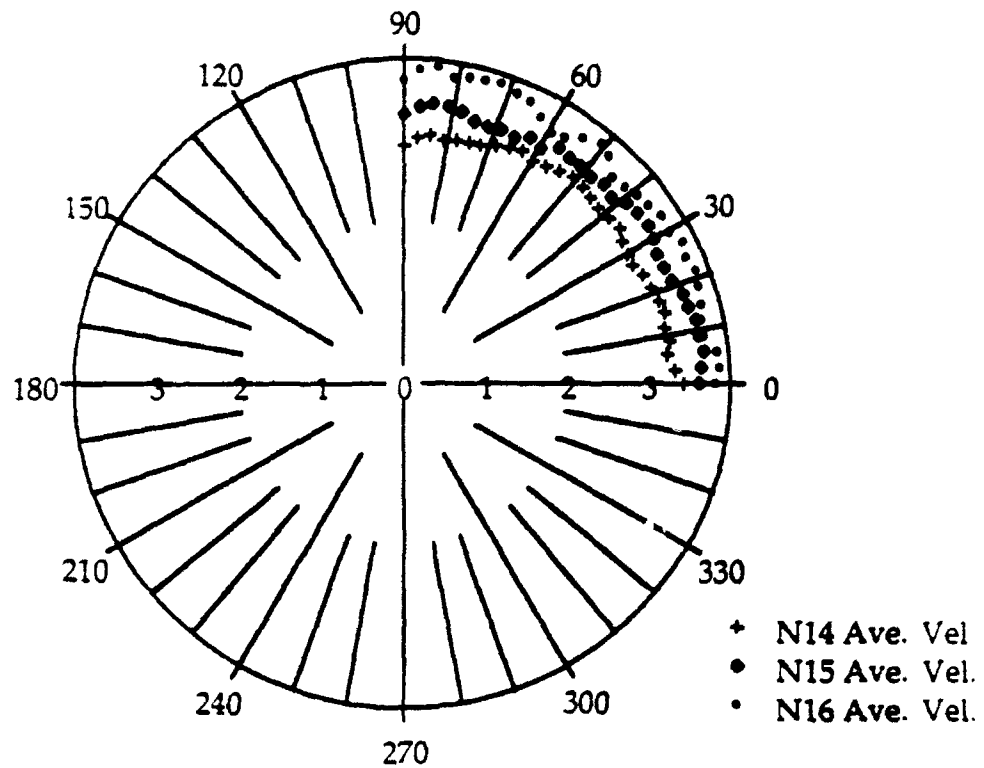
Figure 5.14 Polar plot of surface wave velocity for CAS/Nicalon panels N14, N15, and N16. Velocity increases with fiber volume fraction and tends to be higher along the direction of fiber orientation (0 degrees). Angular dimension of plot corresponds to rotational angle of transducer assembly, and radial dimension corresponds to velocity.

function of angle because sound travels faster along the direction of the fiber than across fibers. These differences, though slight, are shown in Figure 5.14 as a function of angle. This technique is applicable for interrogating volumes near the specimen surface, that are normally obscured by the front surface echo of a pulse-echo signal, or that are blended in with the full material volume in through-transmission inspections.

Limitations:
Structures well below the surface are not easily detected with this technique, because it relies on sound energy propagating along the specimen surface. The intensity of sound energy decreases logarithmically with depth, and is inversely proportional to frequency. The equivalent technique for looking at properties well below the specimen surface is described under Section 6.4 Ultrasonic Velocity. Also, surface anomalies strongly influence the received signal, so surface roughness interferes with subsurface structure indications.

One practical limitation to the use of this technique for the measurement of fiber orientation is that the measurement is only valid within the circle of rotation. If such a measurement is needed over the entire area of a specimen, a complex scan plan would be needed. Another practical limitation to this technique is the exacting requirements for the transducer positioning. To obtain an accurate measurement of distance traveled by the sound, the relative positions of the transducers must be well controlled.

5.7 Ultrasonic Surface Wave Attenuation

Basic Technique:
A single focused transducer was used to excite and receive a leaky surface wave, as described by Gilmore in [1]. Surface waves were automatically produced at the part surface, because the transducer used had a lens curvature greater than the Raleigh critical angle. By operating the transducer at a waterpath shorter than the focal length, the same transducer receives the surface wave energy as it is leaked back into the water. The amplitude of this received signal corresponds to the attenuative nature of the specimen under test.

Assessed Abilities of the Technique for MMCs:
This technique was not explored for MMCs.

Assessed Abilities of the Technique for CMCs:
Microcracks and variations in porosity in a CAS/Nicalon sample were easily detected using a 5-MHz transducer, as demonstrated by Figure 5.15. Other defects that attenuate sound in the ultrasonic through-transmission mode should also be detectable in the surface wave attenuation mode, as the same fundamental properties of detection are used. This technique is applicable for interrogating

69
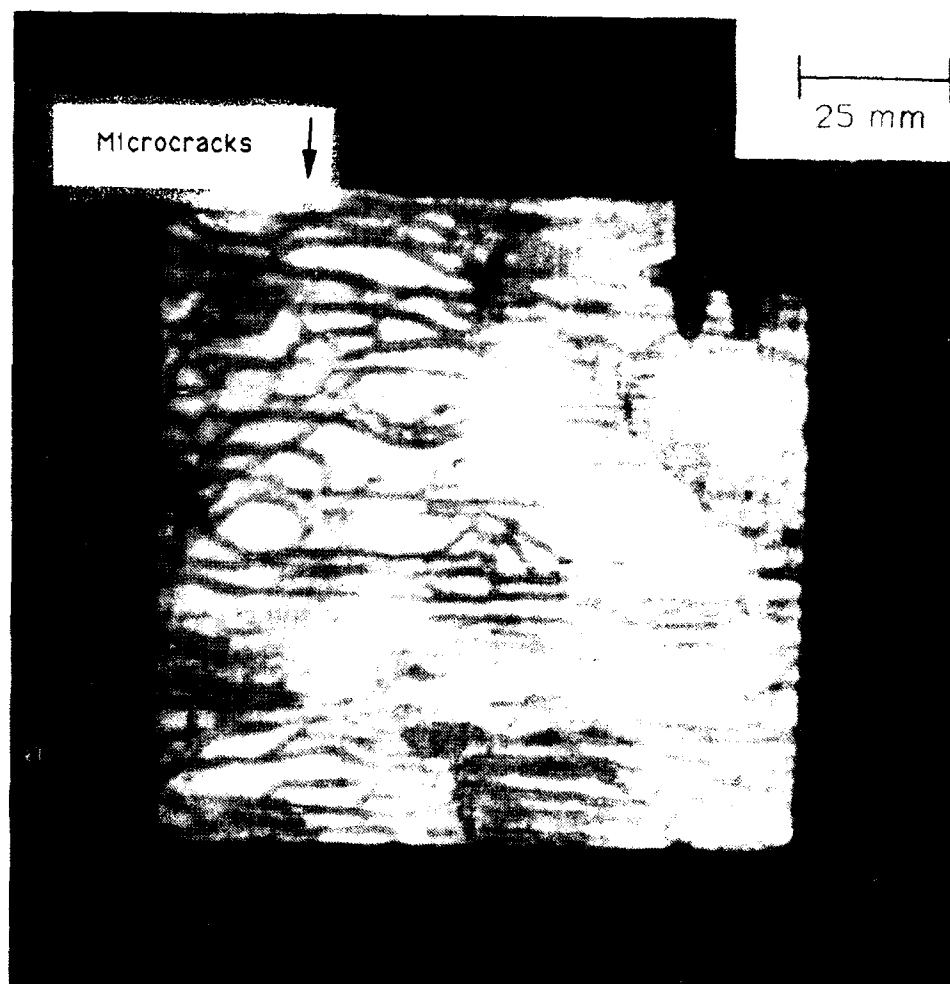
Figure 5.15 Ultrasonic surface wave image of CAS/Nicalon panel
N6 showing microcracks and moderate porosity. Black
line indications are microcracks and the dark patch
indications represent porosity.

volumes near the specimen surface, that are normally obscured by the front surface echo of a pulse-echo signal, or that are blended in with the full material volume in through-transmission inspections.

Limitations:
Only the outer layer of material can be inspected with this technique, because it relies on a surface wave. The depth of interrogation is on the order of 2 Raleigh wavelengths at the frequency of the transducer. Also, surface anomalies strongly influence the received signal, so surface roughness interferes with subsurface structure indications. Section 6.3, Ultrasonic Through-Transmission/Attenuation, discusses the inspection of internal volumes.

5.8 Film Radiography/Digital Radiography

Basic technique:
Any single-energy radiographic technique with the X-ray source fixed on one side of the specimen and the detector fixed on the opposite side should fall into this category. The transmitted radiation energy is attenuated according to the density of the specimen. High resolution detection of structural features can be optimized through improvements in the focus of the X-ray source, or in the size of the devices which detect the incident radiation. Improvements in the detectors are easiest to achieve, and can be implemented by using film with a finer grain than the detector, or by adjusting the design or placement of electronic X-ray detectors.

Assessed Abilities of the Technique for MMCs:
Changes in the composition or the thickness of the specimen are easily detected. Because the density of the silicon fiber is different from the Ti 6-4 matrix, the relative occurrence of fibers can be seen. The orientation of the fibers is clearly seen if the detector resolution is better than 140 microns, which indicates whether the plies have the correct layup. This orientation can be seen clearly in a 16-ply panel, as shown in Figure 5.16, which contains fibers at 0, +45, and -45 degrees. Inclusions or voids can be detected as well, as they will change the attenuation of the X-ray energy. Figure 5.17 shows indications in an 8-ply panel, (panel 2), where the only defects found destructively were broken fibers and a few voids associated with the breaks.

Assessed Abilities of the Technique for CMCs:
Changes in the composition or the thickness of the specimen are easily detected. Because the density of the fiber is different from the CAS matrix, the relative occurrence, and thus orientation of fibers can be seen. This indicates whether the plies have the correct orientation. This orientation can be seen clearly in an 8-ply panel, even for the detection of a few misplaced fibers, as is shown in Figure 5.18, which contains 10-micron Nicalon fibers at 0, 90, and +5 degrees. Inclusions or voids should be detectable as well, as they will change the attenuation of the X-ray energy. Changes in porosity can be detected, as shown in Figure 5.19, because

0 Degree Direction

-45 Degree Direction

+45 Degree Direction

100 mm
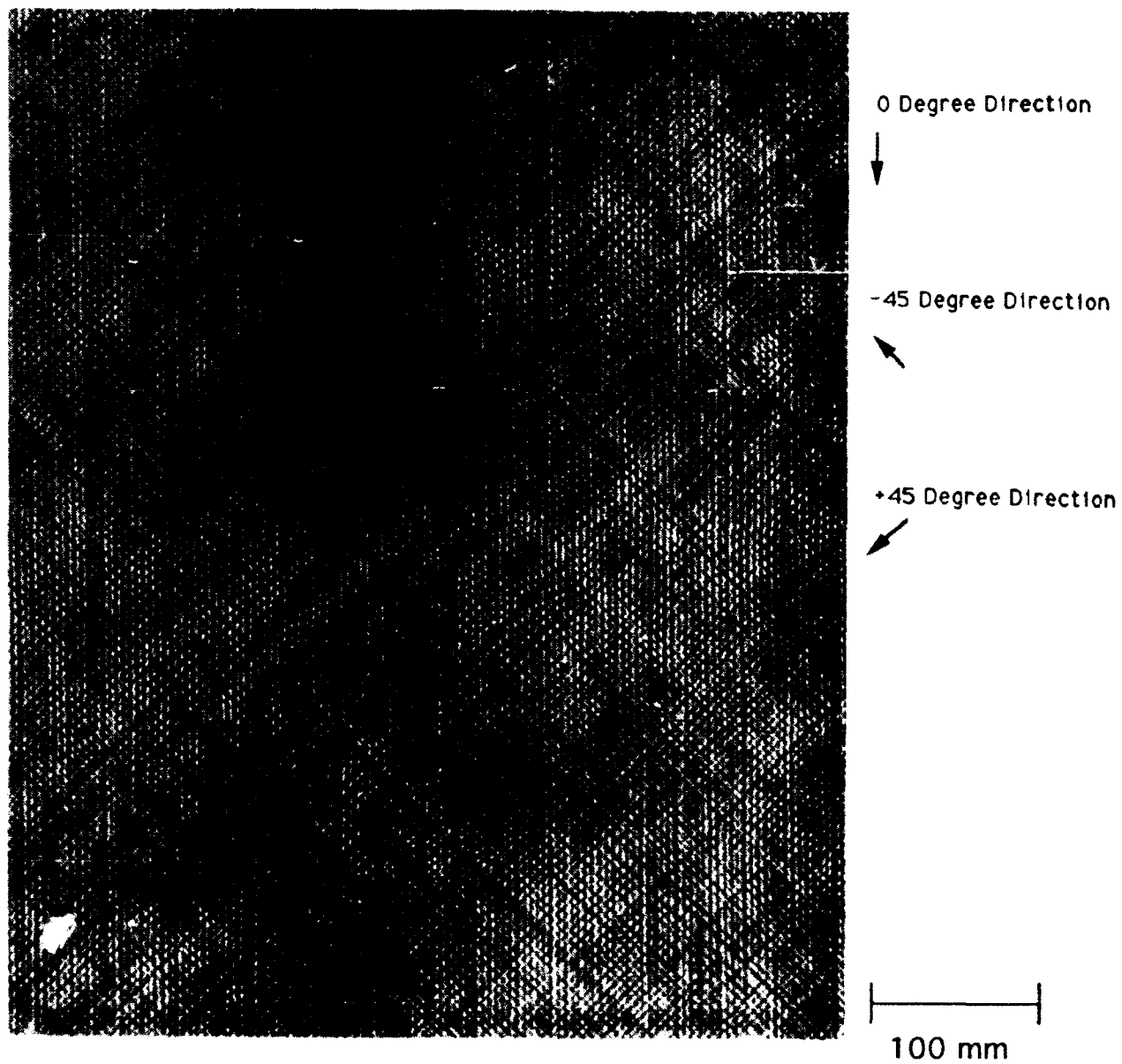
Figure 5.16 Film radiograph of MMC panel 7, with 0, +45, -45 degree
layup. Fiber orientation is clearly visible
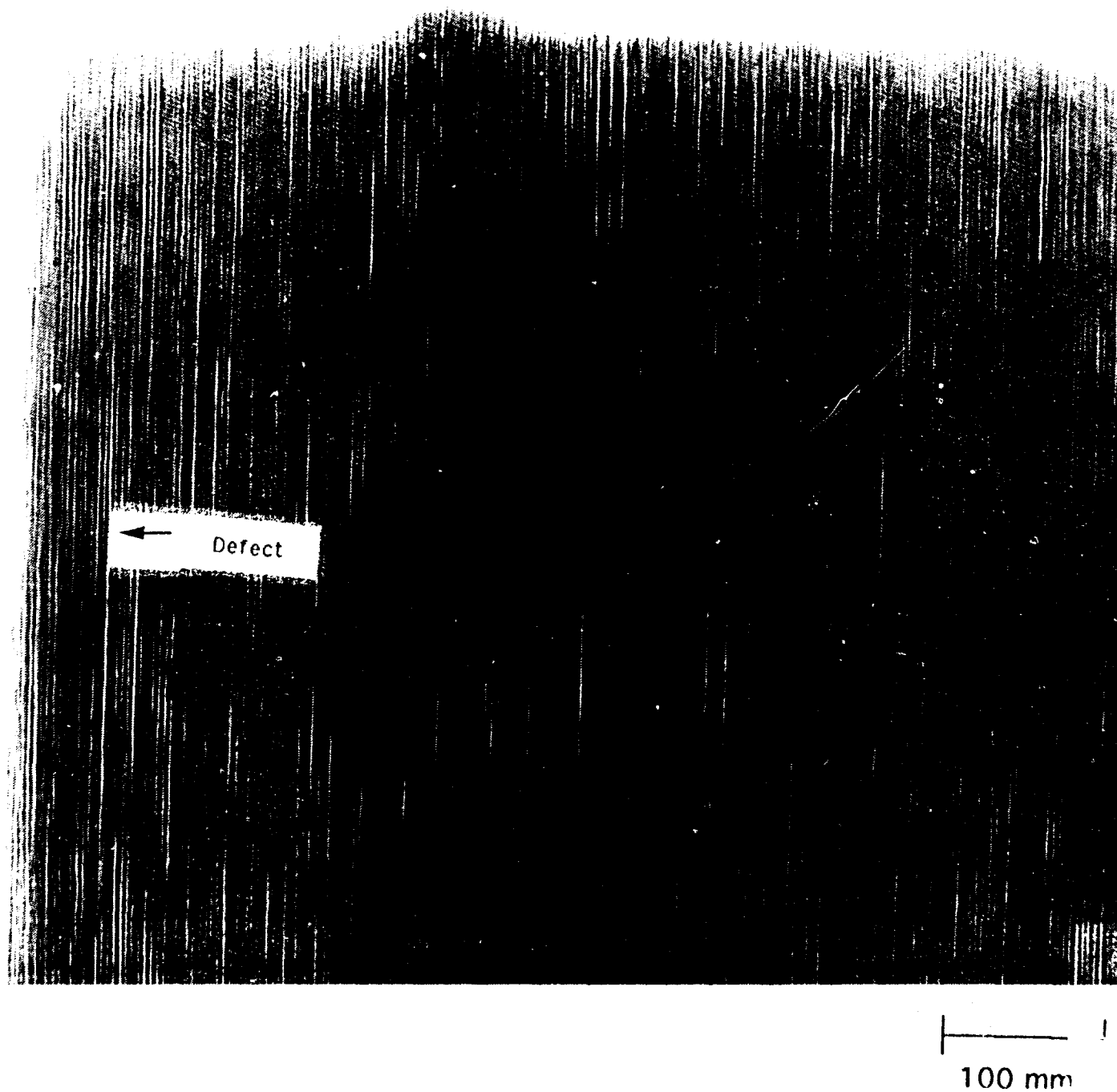
Figure 5.17 Film radiograph of MMC panel 2 showing defect
indications associated with fiber breaks.

CROSSED
FIBERS
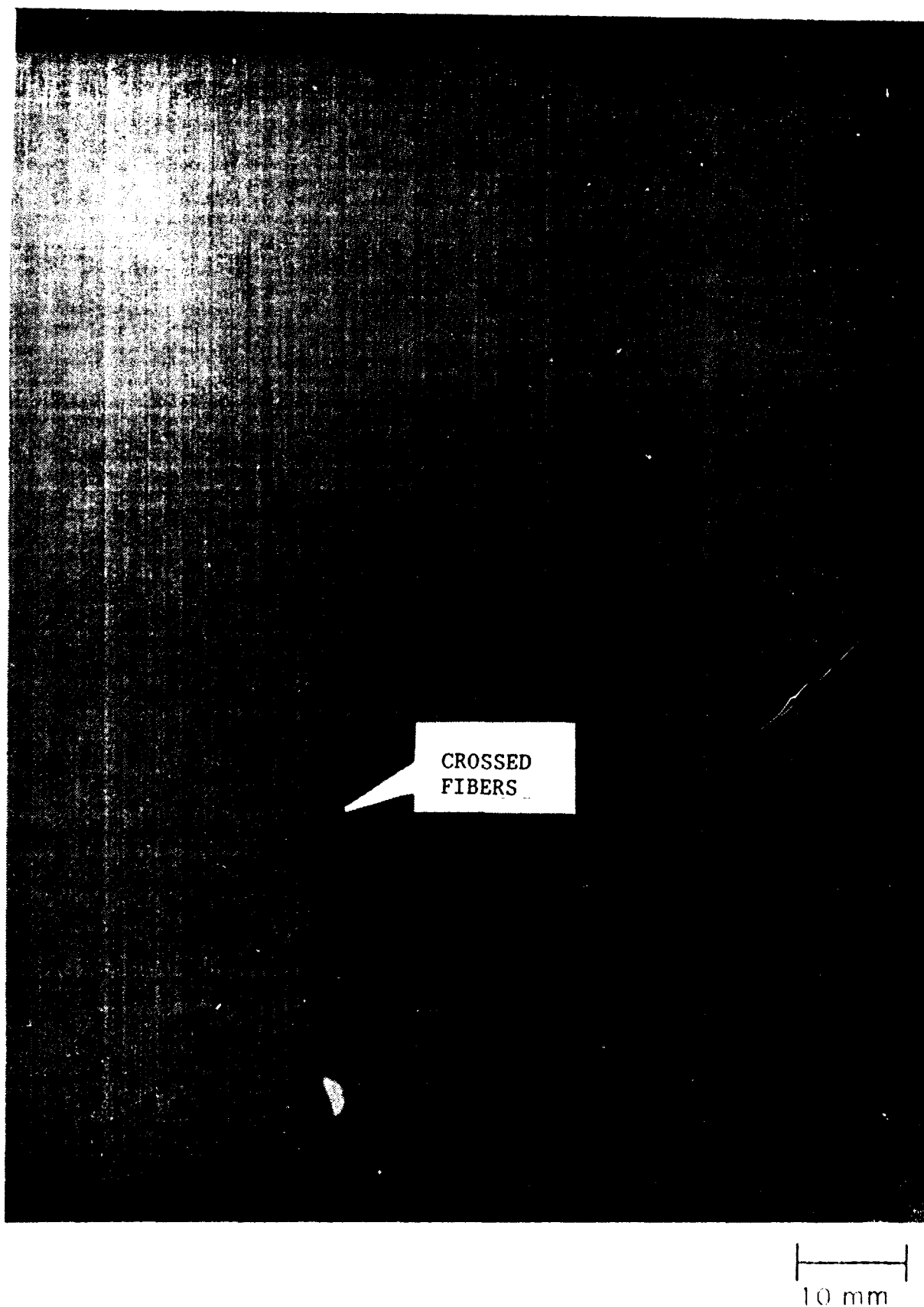
10 mm

Figure 5.18 Film radiograph image of CAS/SCS-6 CMC panel S3
showing fiber orientation. Fiber lay-up is 0/90 degree,
with several crossed fibers at approximately 5 degrees.
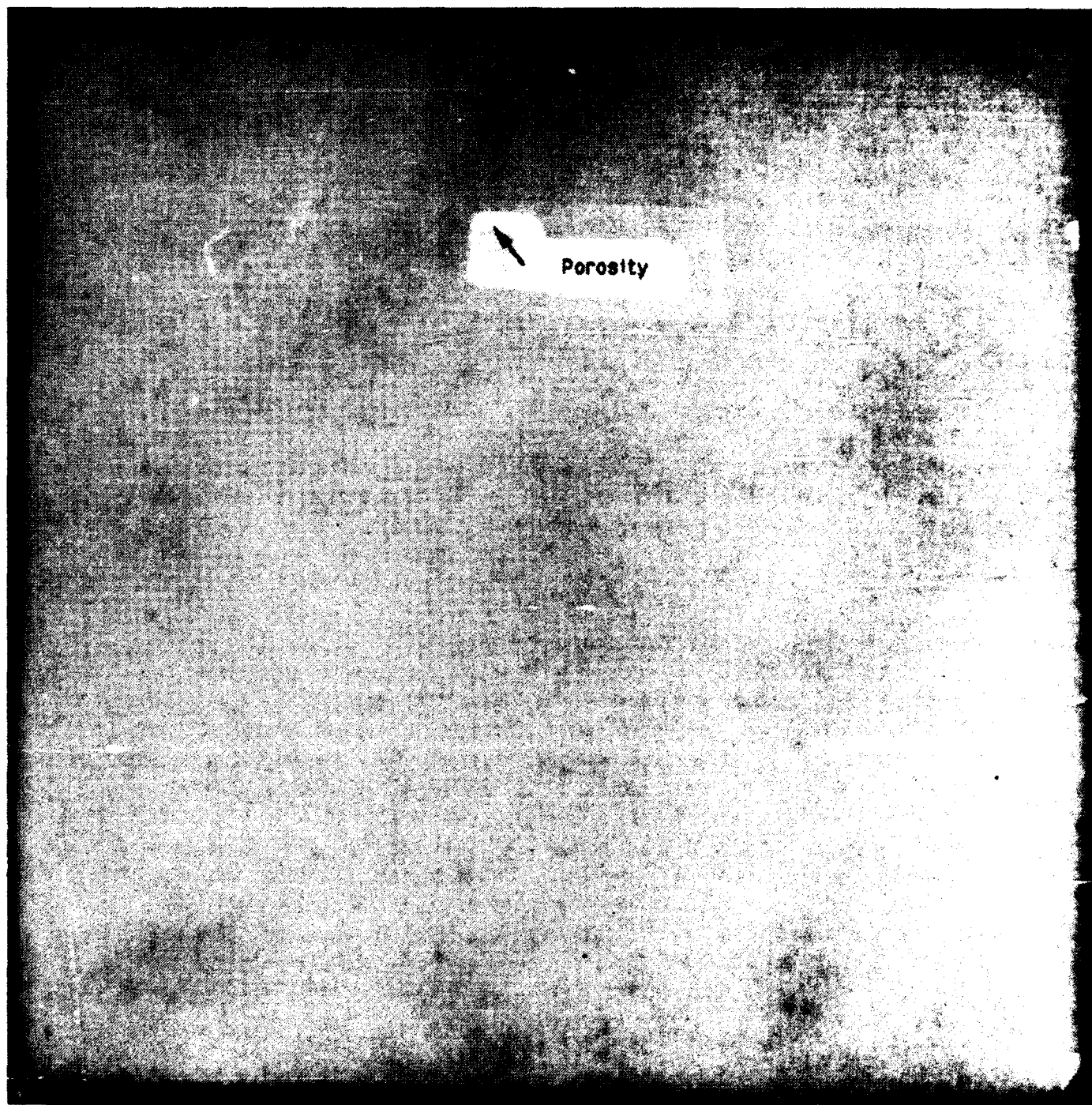
Figure 5.19 Film radiograph image of CAS/Nicalon CMC panel N6
showing moderate porosity. Dark regions represent
higher porosity.

porosity directly affects the specimen density. This ability leads to the conclusion that the absolute level of porosity might be measurable if an appropriate calibration technique is developed. Figure 5.20 shows that delaminations can also be detected with this technique.

Limitations:
The one problem with using this technique to determine ply lay-up is that it can only tell whether a given orientation exists, not the specific order of the lay-up. Another potential difficulty is that surface roughness can worsen the signal-to-noise ratio of the data.

5.9 X-Ray Microtomography

Basic Technique:
A focused beam of radiographic energy was used to scan small specimens, while they were rotated 360 degrees. The computed tomography algorithm is able to reconstruct the data so that a detailed cross section of the specimen is imaged. In general, this technique detects the same type of variations as film radiography, except that the data are displayed as a cross section rather than as a projection, so individual layers are not superimposed. High resolution is obtained by adjusting the beam parameters or by choosing detectors with higher resolution.

Assessed Abilities of the Technique for MMCs:
A microfocus computed tomography system, (a device with the registered trademark name 'Tomoscope', located at Wright laboratory, Materials Directorate X-Ray Computed Tomography Research Facility at Wright Patterson Air Force BAse), with a resolution approaching 25 microns was used to discern the 140-micron silicon carbide fibers from the matrix in the MMCs tested. For an example of the type of resolution available, see Figure 5.21. This technique can determine the location of the fibers, which indicates fiber spacing and orientation, on a ply-by-ply (fiber-by-fiber) basis. Breaks and voids larger than 50 microns should also be easily detected. The Synchrotron yields similar results, except that it has a resolution of the order of 5 microns, and significantly longer scan times. This resolution enables it to discern the 30-micron carbon core of the fibers, as well as smaller fiber breaks, cracks and voids. The resolution available from this technique is described below, under Assessed Abilities of the Technique for CMCs.

Assessed Abilities of the Technique for CMCs:
A microfocus computed tomography system with a resolution approaching 25 microns was used to discern the 140 micron SCS-6 fibers from a CAS matrix. This capability allows one to locate the fibers, which indicates fiber spacing and orientation, on a ply-by-ply (fiber-by-fiber) basis. Breaks and voids larger than 50 microns should also be easily detected. The Synchrotron yields similar results, except that it has a resolution of the order of five microns, and significantly longer scan times. This resolution enables it to discern the 30 micron carbon core of the

76
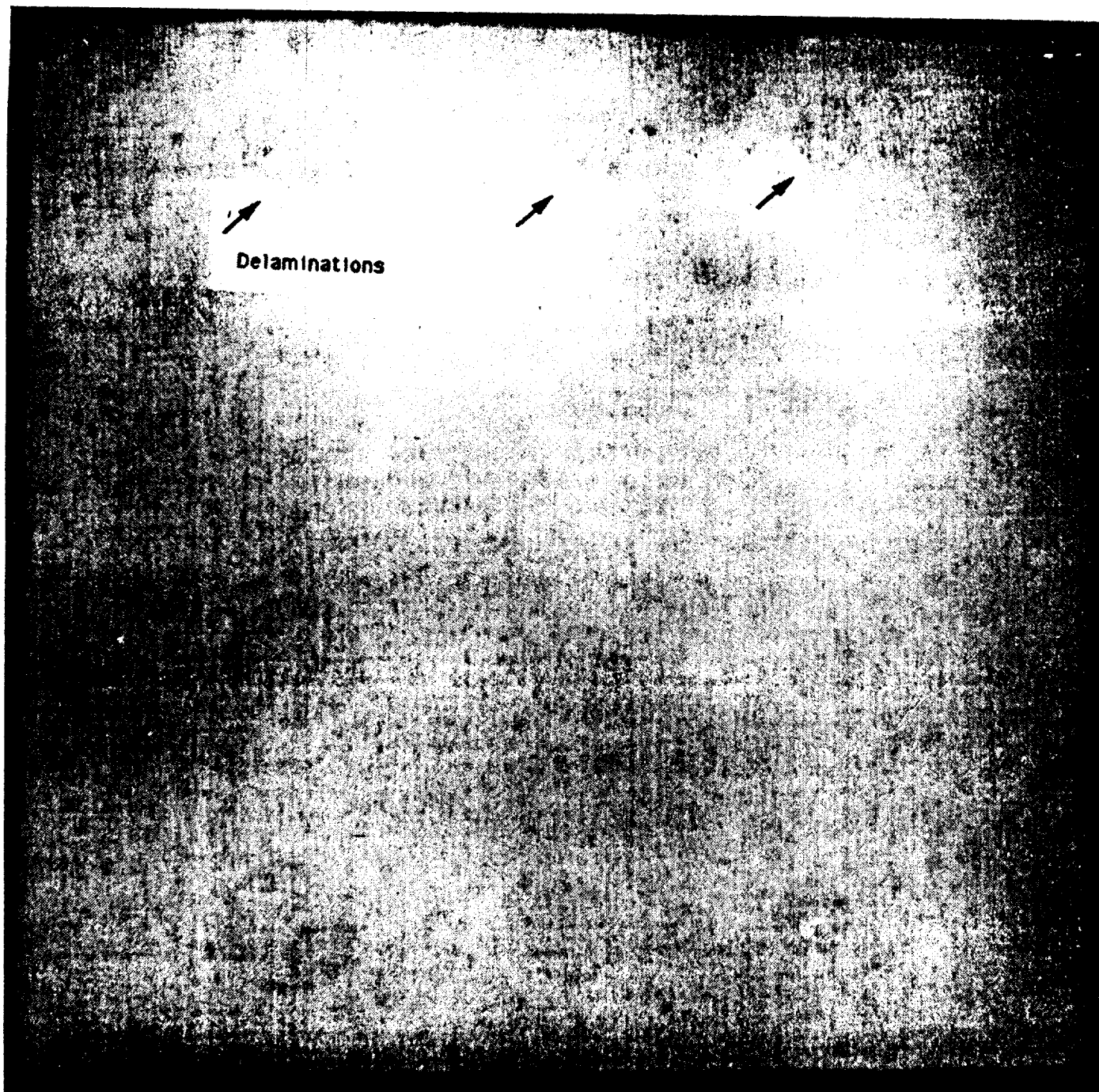
Figure 5.20 Film radiograph image of CAS/Nicalon CMC panel N1
showing delaminations. Dark circles are delaminations
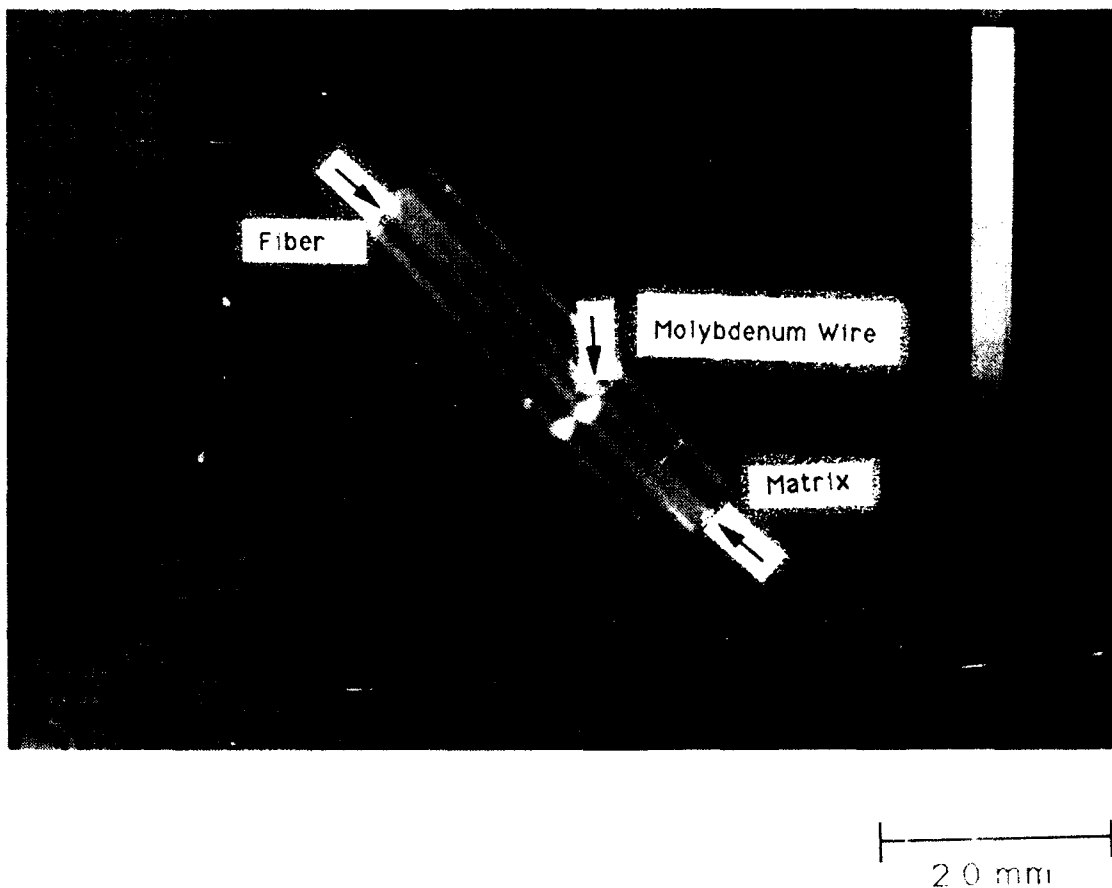
Figure 5.21 Microtomographic image of TiAl/SCS-6 sample, showing resolution of Tomoscope system for MMC structures.

fibers, as well as smaller fiber breaks and cracks. This capability is demonstrated in Figures 5.22 and 5.23, for the SCS-6 fiber and CAS matrix system.

Limitations:
Only the gross details of the fibers were visible, because the resolution of the Tomoscope was of the order of 25 microns. For the Synchrotron, only details as small as the fiber cores were visible, because its resolution was of the order of 5 microns. Coatings and interfaces were not characterized.

Cost is a significant limitation for the application of this technique, in the same manner as for the acoustic microscope. Extreme scan times are required for large volumes of material, in order to acquire the large quantity of data. In addition, geometric limitations of the Tomoscope limit saample sizes to less than 80 mm in diameter. The source energy limitations of the Tomoscope often limit sample diameters to much less than 80 mm. Obviously, because the Synchrotron is a higher resolution, lower energy device than the Tomoscope, its cost and size limitations are more severe.

5.10 Dual Energy X-Ray Microtomography

Basic Technique:
This technique is based on the microtomographic technology described earlier in this report, (Section 5.9), except that energy selective techniques are used to provide information about the composition (effective atomic number), and electron density of the material, as opposed to the simple density measurement of conventional radiographic techniques. This technique is based on the fact that the X-ray attenuation coefficient of an object can be decomposed into two basic physical effects, (or basis materials coefficients). These two parameters can be separated by scanning the material at two radiation energies.

This technology needed development in several areas: calibration techniques, error correction techniques, and error elimination. The technique has been developed to the point where data have been acquired at two energies, as shown in Figures 5.24, and 5.25, but has not yet been correlated for parameter separation. The instrument energy level was calibrated with respect to carbon and copper attenuation properties, to acquire the data in Figures 5.24 and 5.25. As the development of this technique progresses, these data are expected to provide estimates of chemical composition, microstructure, defect states in the matrix, distribution and condition of the contained fibers, and characteristics of the fiber/matrix interface.

Assessed Abilities of the Technique for CMCs and MMCs:
This technique was not fully developed in time to be applied under this program.
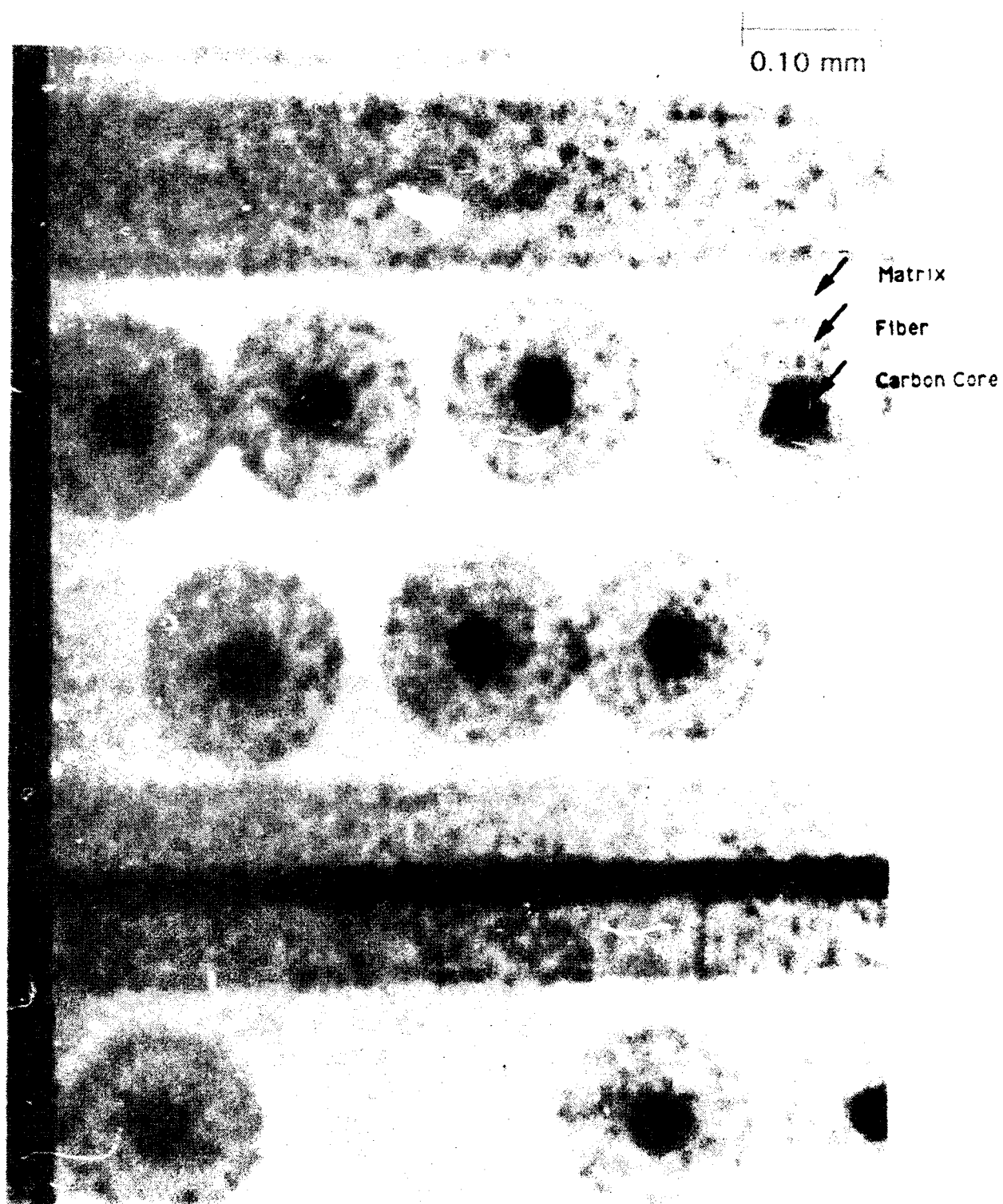
Figure 5.22 Synchrotron image of CAS/SCS-6 system, showing
details as fine as the fiber core

80
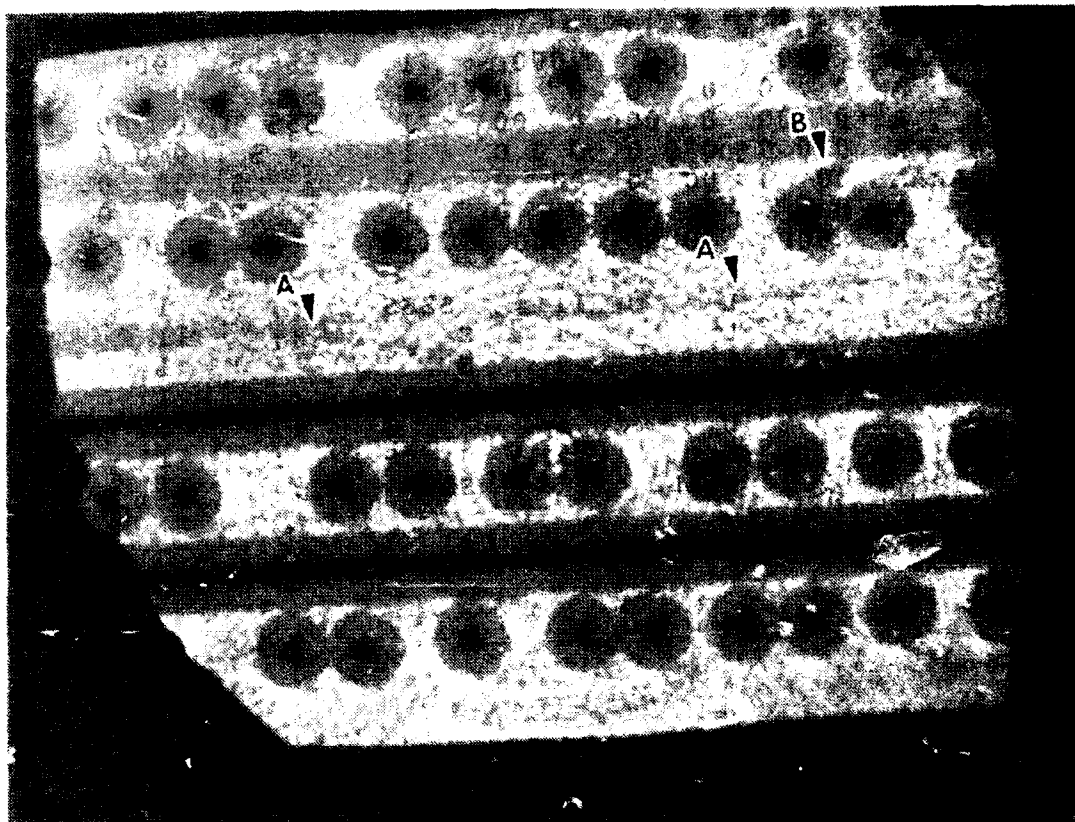
Figure 5.23 Synchrotron image of CAS/SCS-6 system, showing broken fiber and matrix cracks. Arrows A points to a matrix crack traveling the length of the specimen, its maximum width was 1.5 microns. Arrow B points to a broken fiber.

81
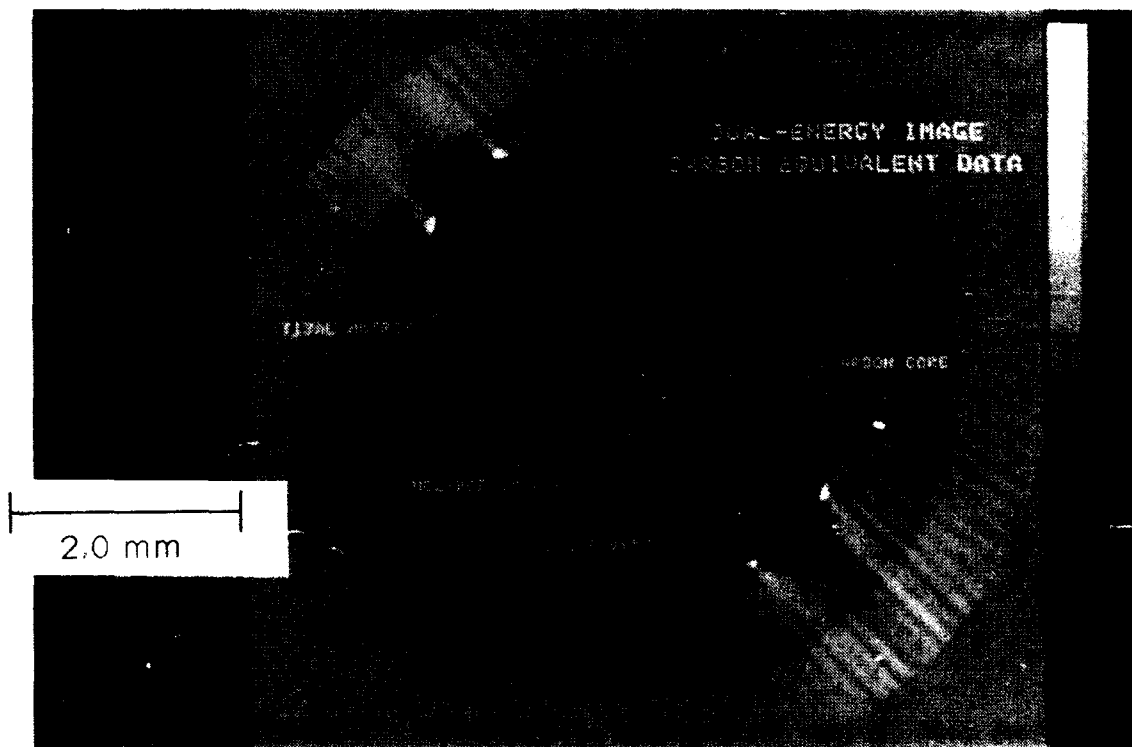
Figure 5.24 Dual Energy image of TiAl/SCS-6 sample: carbon
equivalent data
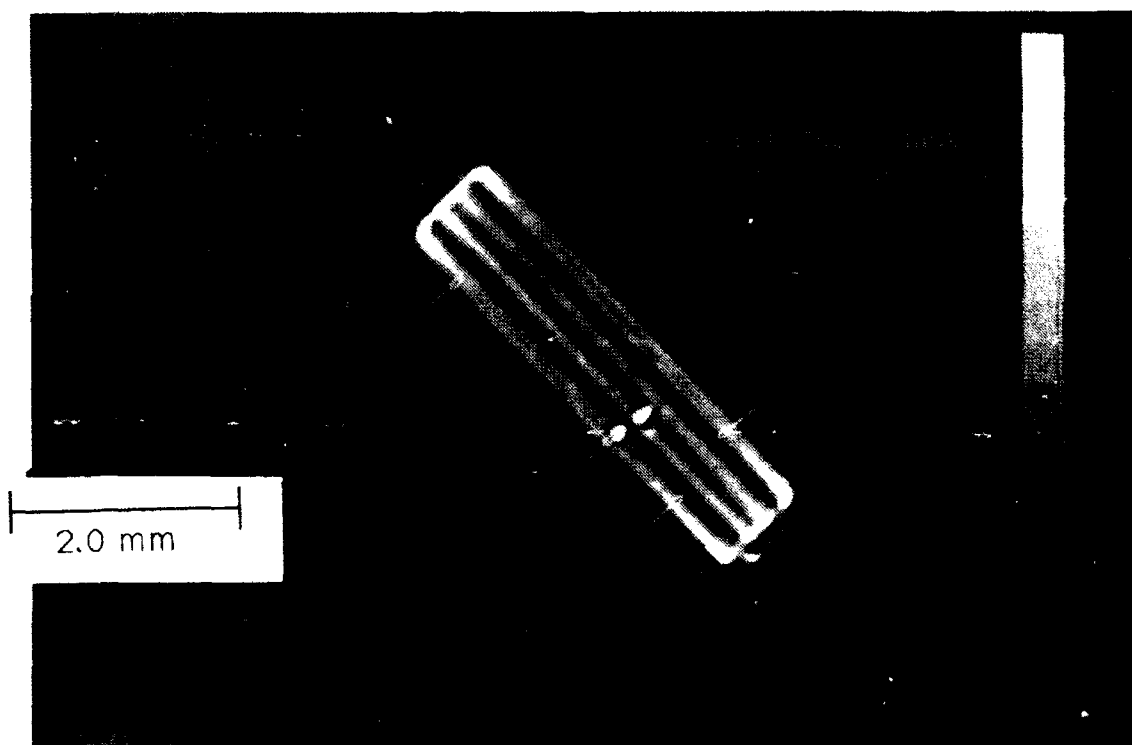
Figure 5.25 Dual Energy image of TiAl/SCS-6 sample: copper
equivalent data

Limitations:
Because this technique is still in the development phase, limitations are difficult to predict. Current difficulties include the limited accuracy and stability of the electronic data acquisition system, that can obscure the data by increasing noise.

6.0 Preferred Methods of Composite Defect Detection

This section describes NDE techniques that are able to detect a given type of anomaly. A tabulated summary of these techniques is provided in Table 6.1. Some of the defects listed in this section can be detected with a wide variety of techniques, while others do not have as many options. For each defect class listed, the most effective and least costly techniques are described, and then some alternative techniques are listed for reference. For a more detailed description on how to apply the techniques, refer to Section 5.0.

6.1 MMC Defects

6.1.1 Delaminations

Ultrasonic pulse-echo is the most effective technique for the detection of delaminations in MMCs. It should be applied by gating only the volume of material within the focal zone of the transducer. The cost of this technique is minimized by selecting the transducer having the largest beam diameter and the longest depth of field for the inspection, which will minimize inspection time. The limits on the transducer beam size are determined by the size of the delamination that must be detected. Delaminations that are smaller than the beam diameter may be obscured by the scattering effects of the fibers. Furthermore, depth of penetration is a consideration. Delaminations that are as small as the constituent fibers may not be detectable more than a few plies deep, due to the scattering from the fibers. To increase depth of penetration, lower frequency transducers and less sharply focused lenses will allow the coverage of a wide spectrum of delamination detection requirements. Figure 5.5 shows some examples of the types of indications which can be expected.

Another technique that has been shown to work is ultrasonic through-transmission, although it does not have the sensitivity of pulse-echo. A technique which can detect delaminations in small specimens is X-ray microtomography, but this technique would be impractical for full sized components.

6.1.2 Broken Fibers

Acoustic microscopy is the only technique which has demonstrated the ability to reliably detect fiber breaks in MMCs. By using a 25- to 40-MHz, sharply focused transducer, and placing the focal spot on the ply of interest, breaks are detected as indications similar to air-backed interfaces. Single fiber breaks that are several plies below the part surface are difficult to detect for the same reason that small delaminations are difficult to detect: scattering of sound by fibers. Figure 4.14 shows the type of indications which are produced by broken fibers.

85

Table 6.1 Summary of NDE Techniques for MMC and CMC Materials

Defect Type	CMC NDE Techniques	MMC NDE Techniques
Delamination	Ultrasonic Pulse-Echo Ultrasonic Through-Trans. Film Radiography Microtomography	Acoustic Microscopy Ultrasonic Pulse-Echo Ultrasonic Through-Trans. Microtomography
Voids/Porosity	Ultrasonic Through-Trans. Ultrasonic Velocity Ultrasonic Backscatter Film Radiography Surface Wave Attenuation Surface Wave Velocity	Acoustic Microscopy Film Radiography
Fiber Fraction	Ultrasonic Velocity Surface Wave Velocity Microtomography	Acoustic Microscopy Microtomography
Fiber/Matrix Interface	(Dual Energy Radiography)	Acoustic Microscopy (Dual Energy Radiography)
Fiber Orientation	Ultrasonic Backscatter Surface Wave Velocity Film Radiography Microtomography	Acoustic Microscopy Ultrasonic Backscatter Microtomography
Fiber Breaks	Microtomography	Acoustic Microscopy Microtomography
Matrix Cracks	Ultrasonic Through-Trans. Surface Wave Attenuation Microtomography	Acoustic Microscopy Microtomography
Matrix Properties	(Dual Energy Radiography)	(Dual Energy Radiography)

86

Microtomographic techniques (Synchrotron) should have the resolution to detect fiber breaks, as was demonstrated for a CMC specimen, (Section 6.9). Although film radiography has detected indications which correlate with broken fibers, consistent detectability with this technique has not been demonstrated, and further verification is needed.

6.1.3 Fiber Spacing/Volume Fraction, Orientation

Film radiography is the simplest and most cost effective method for detecting fiber orientation in MMCs, as shown in Figure 5.16. This technique can be used to inspect large areas of material of 16 plies or more thick in short period of time.

Acoustic microscopy is able to view individual fibers in the outer plies, and fiber spacing can be calculated by counting the number of fibers in a given area. Ultrasonic backscatter can determine fiber orientation, as shown in Figure 5.11. Microtomography is able the show the specific location of fibers in a cross section, which can then be used to calculate fiber volume fraction. These techniques are inherently limited in scope; acoustic microscopy and backscatter are only able to look at the outer few plies, and microtomography is only able to look at small samples such as edge trimmings.

6.1.4 Fiber/matrix Interface (Coatings)

Acoustic microscopy is the only technique which has demonstrated a capability to detect variations in fiber/matrix interface integrity for MMCs. Although differences in fiber coatings have not been characterized, fiber/matrix debonds have been clearly detected, as can be seen in Figure 5.3. The application of this technique has the same limitations as for broken fibers.

Dual energy microtomography holds promise for characterizing the interface characteristics in terms of chemical composition. The composition can be correlated with mechanical tests to suggest the properties of the interfacial bond strength.

6.1.5 Matrix Cracks

Acoustic microscopy can find any air-backed interface, as long as the interface provides a coherent back-reflected signal, from an area equal in size to the sound beam diameter. For MMC cracks that are perpendicular to the specimen surface, a special application of microscopy must be used: shear mode. Figure 6.1 shows how this technique is able to find matrix cracks in a MMC specimen.

SHEAR WAVE IMAGE: CRACKS CLEARLY VISIBLE

Crack

3.0 mm
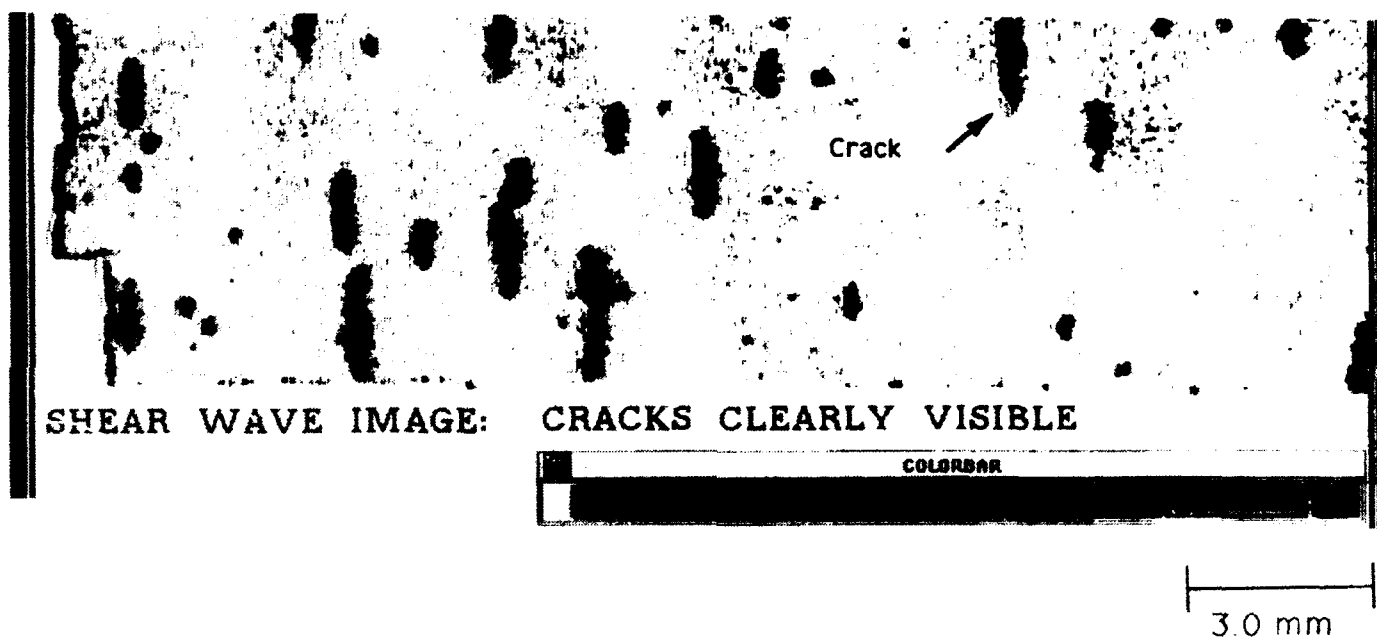
Figure 6.1 Acoustic microscope image of SiC/Ti MMC specimen
showing matrix cracks to demonstrate capability of
technique developed under this program. The black
vertical indications represent cracks, and are best
detected using a shear mode.

6.1.6 Voids/Porosity

As with any other air-backed interface, voids in MMCs can be detected with acoustic microscopy. Their reflected signal strength is a function of the reflecting area and depth below the surface. Near surface voids whose diameter is of the order of 50 microns, as shown in Figure 5.4, have been detected.

Film radiography can also pick up small local variations in density, as might be produced by voids, as seen in Figure 5.17. Microtomographic techniques should also be able to detect voids larger than 25 microns in small specimens.

6.2 CMC Defects

6.2.1 Delaminations

Ultrasonic through-transmission is able to detect delaminations in CMCs, as shown in Fig 5.7. Furthermore, a frequency analysis of the attenuation is able to discern attenuation caused by delaminations from that caused by porosity, as demonstrated in Figure 5.9.

Ultrasonic pulse-echo can also detect delaminations in the same way as described for MMC delaminations. Film radiography has also demonstrated the capability for detecting delaminations, as evidenced by Figure 5.20, although the reliability of the application of this technique is not known. Finally, microtomography should be able to detect delaminations, as long as they have significant width.

6.2.2 Broken Fibers/Tows

Microtomography, (Synchrotron), was able to detect broken SCS-6 fibers, as shown in Figure 5.23.

Acoustic microscopy should not be ruled out as a technique for this class of defect. Although no CMC fibers were imaged under this program, specimens with smoother surfaces may produce better results.

6.2.3 Fiber Spacing

Ultrasonic velocity can be used to estimate overall volume fraction, and ultrasonic surface wave velocity can be used to estimate volume fraction for just the outer plies. Figures 5.10 and 5.14 show how velocity is a function of volume fraction.

6.2.4 Fiber Orientation

Film radiography is the simplest and most cost effective method for detecting fiber orientation, as shown in Figure 5.18. This technique can be used to inspect large areas of material of 16 plies or more thick, in a short period of time.

Other effective ultrasonic techniques include backscatter, as shown in Figure 5.12, and surface wave velocity measurements. These techniques are appropriate for the outer plies, and require significant set-up time to obtain data over a small region. Nonetheless, these techniques are available when film radiography cannot be applied. Microtomography can be applied to a small specimen, to map the locations of fibers, which can be used to determine fiber orientation.

6.2.5 Fiber/matrix Interface (Bonding)

No techniques were found to be successful for the evaluation of the fiber/matrix bond characteristics. Dual energy microtomography, however, may provide a solution, as it should be able to describe the atomic composition at that location, and thus predict bond properties. This technique may not be applicable to engine components, however, because it can only be applied to small specimens.

6.2.6 Matrix Cracks

Ultrasonic surface wave attenuation proved effective in detecting microcracks at the surface of these materials, as shown in Figure 5.15. Large cracks can be detected with through transmission, as shown in Figure 6.2. Microtomography is also able to detect cracks in small specimens.

6.2.7 Voids/Porosity

Film radiography has been effective in detecting regions of porosity, as demonstrated in Figure 5.19. This technique is fast and extremely cost effective.

Ultrasonic through-transmission is believed to be the most efficient technique for the detection of slight variations in porosity. An example of this can be seen in Figure 5.8. This technique is particularly useful in characterizing the nature of an attenuated indication through frequency analysis. Porosity preferentially attenuates high frequency signals, while delaminations tend to attenuate all frequencies equally. In the same manner, ultrasonic surface wave attenuation is also an effective technique for evaluating the porosity near the specimen surface, as shown in Figure 5.15.

Other techniques that have detected porosity include backscatter, ultrasonic velocity, and ultrasonic surface wave velocity.
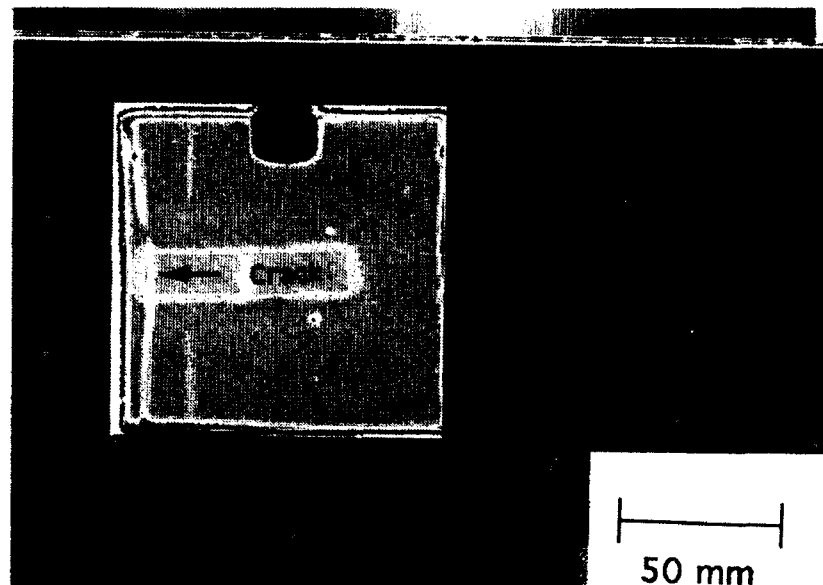
Figure 6.2 Ultrasonic through-transmission attenuation image
of CAS/Nicalon CMC panel N11 showing matrix cracks.
White vertical indications represent cracks.

91

7.0 Conclusions

This program has demonstrated that advanced NDE processes can detect a wide variety of indications in ceramic and metal matrix composites. To detect very small, air-backed features near a specimen surface, acoustic microscopy is the technique of choice. This technique has demonstrated the clear ability to detect minute voids, broken fibers, matrix cracks, and fiber/matrix disbonds in MMCs. To detect larger regions of defective material, ultrasonic pulse echo is often quite effective. The detection of CMC/MMC delaminations and CMC porosity has been demonstrated with this technique. To determine fiber orientation, a wide variety of techniques are available, but film radiography is the simplest, most cost effective and most reliable technique. To examine the details of fiber/matrix structure, microtomographic radiography is the most appropriate technique. This technique shows the exact locations of fibers and can image the more severe cases of fiber breaks.

The advances in NDE technology provided by this program have resulted not only in the ability to screen specimens to verify manufacturing quality, but have also provided a valuable tool for understanding mechanical properties of composites. The high resolution NDE techniques, such as acoustic microscopy and microtomographic radiography are able to detect mechanical damage, in addition to manufacturing defects. As a result, the propagation of damage can be mapped in detail, as a function of preexisting defects and/or mechanical test parameters. This can be used to identify the defects which are severe and to identify the operating conditions (e.g., temperatures or strains) which limit composite component life. Finally, by mapping the propagation of damage, detailed analyses of the modes of composite failure can be compared to model predictions for verification or improvement of the composite models. Such detailed information can greatly boost the confidence in these materials for application to strategic engine components.

8.0 Recommendations for Future NDE Development Work

Although this program has made great progress in understanding how to characterize composite materials, much work remains to be done to provide robust NDE capability for composite components and to advance the ability to fully characterize small specimens. The ISC program specifically addressed the investigation and development of NDE techniques for determination of the internal characteristics of composites. Work that remains to be done includes an investigation of untested techniques, an exercise of material characterization techniques to establish their limitations and the scale-up of the developed techniques for component manufacture.

8.1 Additional Basic NDE Development Needed

The most significant NDE technique that still needs basic development is dual-energy microtomography. Single-energy microtomographic techniques have shown significant results, and in so doing, have demonstrated the mechanical feasibility of dual-ergy microtomography. The expected capability of this technique to describe the chemical composition at a 25-micron resolution will make it a powerful technique for characterization of composite specimens.

Other techniques that have not been fully investigated, and might hold promise for specialized needs of composite inspection include holography, eddy current and thermography. These techniques were not investigated under the ISC program because the information they are expected to yield would be of little value for most material characterization needs, but they should nonetheless be kept in mind for unusual applications.

8.2 Additional NDE Development Needed for Material Characterization

Before these materials can be utilized in propulsion systems, their mechanical properties and failure characteristics must be well understood. Acoustic microscopy and microtomography provide two non-invasive methods to document the behavior of small test specimens while undergoing mechanical tests. While these techniques have already demonstrated significant abilities, their exact limitations need to be better understood to determine which defect/damage conditions are not detectable. To achieve this characterization of NDE methods, specimens with subtle structural variations would need to be manufactured. These specimens could then be used in an iterative process of mechanical and nondestructive tests to determine the detectability of the initial subtle variation and the resulting damage, for correlation with mechanical properties. Those conditions which result in significant mechanical degradation could then provide the focus for further development of high resolution NDE techniques.

93

8.3 Scale-up of NDE for Components

In order to reduce the developed techniques to a practical, manufacturing level, the following efforts must be undertaken: the determination of defects that are critical to component performance, the establishment of calibration procedures and the reduction of inspection costs. These steps are critical for the inspection of manufactured hardware. Without knowing the mechanical effects of defects, components are likely to be either over-inspected at great cost, or under-inspected at great risk. Without a calibration procedure, the certainty of defect detection will not be known. Without a cost reduction effort, NDE requirements could make these composite components prohibitively expensive.

In order to specify the NDE requirements for manufactured hardware, the defect conditions that are critical to component performance must be determined. This information is necessarily linked to the individual components, as requirements will change with the type of hardware, but certain generalities can be established up front. By knowing the effect of commonly occurring defects, general NDE scale-up can be directed towards the most severe defects, and then specific levels of inspection can be selected for the hardware of interest.

Although a wide variety of techniques have been developed to detect a wide variety of defects in composite materials, defect severity information may lead to detection requirements which extend beyond the current NDE capability. Further NDE development may be required to augment the techniques available for the inspection of manufactured hardware, specifically in the areas of development of new NDE methods and adaptation of high resolution techniques to large volume components. Such development can only come after the defect detection requirements are fully understood.

Calibration procedures are required to provide consistency and confidence in inspections. Current techniques rely on variations in defect severity to provide indications for detection. This philosophy is not adequate for the inspection of hardware slated for engine application. Because composite materials are more difficult to inspect than monolithic materials, the calibration techniques need to be specially designed to take into account the unique variability of a fiber/matrix system, while minimizing inspection cost and complexity.

Although this program has developed methods for detecting many of the defects that are expected to be critical in the performance of composite materials, most of the techniques are time consuming and costly. Once the inspection requirements are established, the requisite inspection techniques will need to be made economical. This might be achieved through increased automation, parallel systems, or lowered inspection resolution.

94

9.0 References

1. Gilmore, R.S., Tam, K.C., Young, J.D., and Howard, D.R., "Acoustic Microscopy From 10 to 100 MHz For Industrial Applications," Phil. Trans. Royal Society Lond., A320, 215-235 (1986).

2. Irving, R.R., Iron Age 228--23, 45 (1985).

3. Chimenti, D.E., and Crane, R.L., AFML-TR-79-4214 (Air Force Materials Laboratory, 1980).

Appendix Publications

Bashyam, M, "Ultrasonic NDE for Ceramic- and Metal- Matrix Composite Material Characterization," Review of Progress in Quantitative Nondestructive Evaluation, Vol. 10, Edited by D.O. Thompson and D.E. Chimenti, Plenum Press, NY 1991.

Bashyam, M, and Rose, J.L., "Low Frequency Directional Acoustic Microscope for Nondestructive Evaluation," 1991 Ultrasonics Symposium Proceedings. Edited by G.K. Montress, Institute of Electrical and Electronic Engineers, NY 1991.

Bashyam, M, and Rose, J.L., "Surface Acoustic Wave Techniques for Ceramic Matrix Composite Materials Characterization," Review of Progress in Quantitative Nondestructive Evaluation, Vol. 11, Edited by D.O. Thompson and D.E. Chimenti, Plenum Press, NY 1992.

ULTRASONIC NDE FOR CERAMIC- AND METAL- MATRIX COMPOSITE

MATERIAL CHARACTERIZATION

Manohar Bashyam
GE - Aircraft Engines
One Neumann Way, Mail Drop - Q45
Cincinnati, Ohio 45215.

INTRODUCTION

A brief summary of the progress of the research in the internal structural characterization of metal matrix (MMC) and ceramic matrix (CMC) composite materials is presented here. These materials show great potential for improving turbine engine performance by enabling operation at higher temperatures and stresses than now possible [1]. However, the application of these materials requires advances in NDE capability in order to characterize material parameters that are likely to affect performance. Several ultrasonic methods are being developed to characterize the internal structure of these anisotropic, inhomogeneous materials.

Our research focuses on characterizing one metal-matrix and two ceramic-matrix composites. The chosen MMC manufactured by Textron, consists of relatively large diameter (140 μm) silicon carbide (SCS6) ceramic fibers in a plasma sprayed titanium 6-4 (Ti64) matrix. Both the CMC materials made by Corning Glass, have a calcium aluminum silicate (CAS) glass-ceramic matrix. One series was reinforced with SCS6 fibers and the other with 15 μm diameter silicon carbide (Nicalon) fibers. The micrographs of these composites are shown in Figs. 1a - 1c to illustrate the relative size of the fibers. Various types of defects were deliberately introduced into these panels by the manufacturer, to simulate delamination, porosity, fiber breakage and matrix cracking etc.

A desirable composite should contain layered, uniformly spaced fibers. Fig. 1 illustrates one potential defect condition of interest, where the fiber distribution is uneven. Note that incomplete bonding or cracking between fibers is also present to some extent. We are also concerned with defects such as fiber breakage, misaligned fibers, incorrect fiber volume fraction, porosity in the matrix and delamination.

This paper discusses ultrasonic velocity, attenuation, backscatter and surface wave techniques to characterize the internal structural features of the MMC and CMC materials.

1423

VELOCITY MEASUREMENTS

The key to reliable ultrasonic measurements is the thorough understanding of the material properties and the resulting wave propagation modes. For this a previous wave propagation model developed by Murakami & Hegamier [2] was used as the basis of our analyses. This model was used to calculate laminate elastic constants and various ultrasonic wave velocities. Table 1 shows a comparison of the theoretically computed and experimental wave velocities.

The experimental values for the MMC and CMC were lower than the theoretical values predicted by the model with a nominal 35% and 45% fiber volume fraction respectively. We estimated from the micrographs that the actual volume fractions were lower than the nominal, this resulted in lower experimental wave velocities. This led us to calculate the variation in velocity as a function of fiber volume fraction. Thus varying the fiber volume fraction of the CMC (with Nicalon fibers) between 30% - 45% to compute V_{33} resulted in the graph shown in Fig. 2. The corresponding experimental results are also plotted on the same graph. Note that the fiber volume fractions associated with these results are based on manufacturing estimates. It was seen that a 2% change in volume fraction produced a 1% change in velocity. This clearly indicates a potential NDE method to characterize the fiber volume fraction which is an important variable affecting both the strength and the modules.

To better understand the anisotropic behavior of the composite materials, the Christofel's equation [3] was solved for these materials. The slowness plot (inverse of the velocities) shown in Fig. 3 for two different materials (graphite-epoxy and Ti64-SCS6) for 0° azimuthal angle, i.e. along the fiber direction, illustrates the degree of anisotropy of the materials. The corresponding wave propagation modes for these materials are shown in Fig. 4.

Table 1. Comparison of the computed theoretical and experimental wave velocities.

Direction (Km/Sec)	Theoretical Ti64-SCS6 (35% FF)	Measured	Theoretical CAS-Nicalon (45% FF)	Measured
V_{11}	8.0	~	7.6	~
V_{33}	7.2	7.0	7.4	7.2
V_{44}	3.9	3.9	4.5	4.1
V_{55}	4.1	3.7	4.4	4.1
V_{s1}	3.8	3.6	4.0	3.6
V_{s2}	3.8	3.6	4.0	3.6

~ - Not measured.

V_{11} - Longitudinal along fibers. V_{33} - Longitudinal across fibers.

V_{44} - Shear perpendicular to fiber. V_{55} - Shear along the fiber.

V_{s1} - Surface wave velocity along fiber. V_{s2} - Surface wave velocity across fiber.

Fig. 1a. Micrograph of a Ti64-SCS6
MMC with 35% fiber volume
fraction.
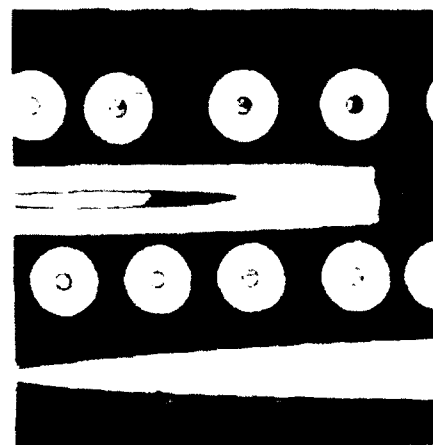
Fig. 1b. Micrograph of a CAS-SCS6
CMC with 45% fiber volume
fraction.
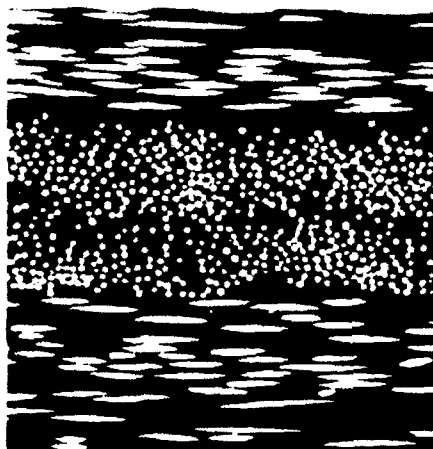
Fig. 1c. Micrograph of a
CAS-Nicalon CMC with 45%
fiber volume fraction.
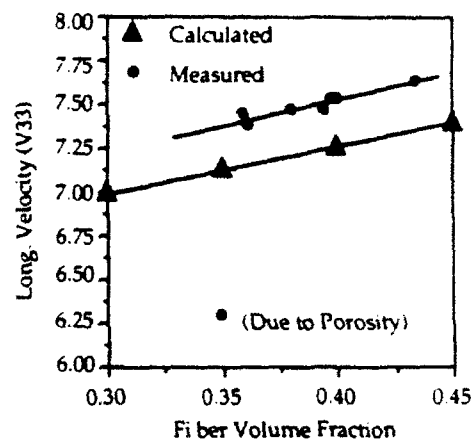
Fig. 2. Theoretical and experimental
velocity (V33) for CAS-Nicalon.

These modes are computed by taking the dot product of the particle velocity and the wave vector, for 0° azimuthal angle, where the value of 1 clearly represents a pure longitudinal mode, value of 0 represents a pure shear mode (PT) and values between 0 and 1 correspond to quasi modes (QL & QT). From these figures it was concluded that the materials are mildly anisotropic when compared to a graphite-epoxy composite material. The slowness and mode plots for CAS-SCS6 and CAS-Nicalon materials were very similar to that of the Ti64-SCS6 plots shown.

ATTENUATION MEASUREMENTS

Previous studies indicate that planar defects such as delaminations should produce attenuation which is relatively independent of frequency. Scatter sources such as porosity produce attenuation which is highly frequency-
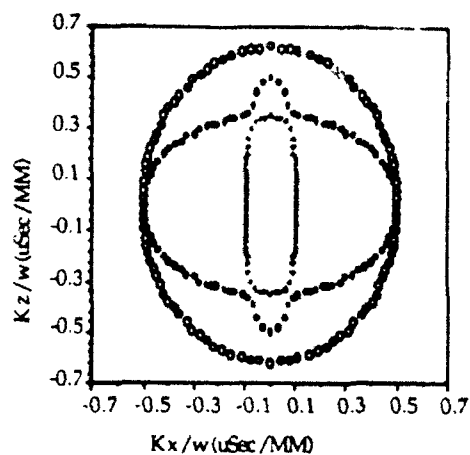
Fig. 3a. Slowness plot for
graphite-epoxy - 60% fiber
volume fraction at 0°
azimuthal angle.
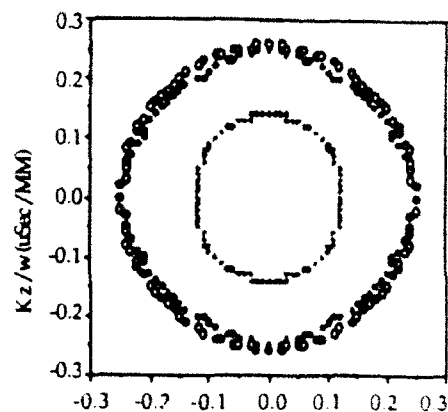
Fig. 3b. Slowness plot for Ti64 -SCS6 -
35% fiber volume fraction at
0° azimuthal angle.
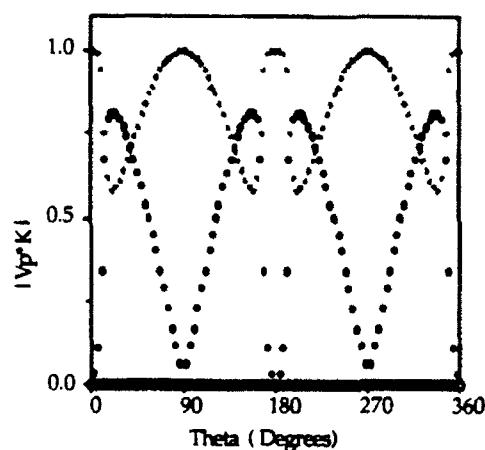
Fig. 4a. Wave propagation mode
plot for graphite-epoxy
- 60% fiber volume fraction
at 0° azimuthal angle.
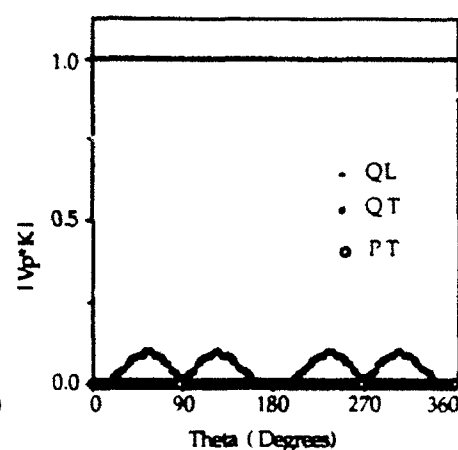
Fig. 4b. Wave propagation mode plot
for Ti64-SCS6 - 35% fiber
volume fraction at 0°
azimuthal angle.

dependent. Obviously we need to understand the frequency-dependent attenuation characteristics to determine the optimum frequencies for routine inspection.

Two different system configurations were set up for data acquisition, both with broadband transducers. The single-transducer method uses echoes from the front and back surfaces at normal incidence while the through-transmission method uses signals transmitted through the water path as a reference signal. The latter configuration has a wider application since it can be used in attenuative regions where there is no distinct back wall echo.

5

The reference signal data for a CAS-Nicalon ceramic plate was collected with only water between the transducers. The plate was then inserted and the through-transmitted signal data was collected. The relevant portions of each signal were gated and a FFT was performed to obtain an amplitude versus frequency spectrum for each signal. We then applied a bandpass filter to select the frequency range, typically 2 to 10 MHz. The attenuation versus frequency plot obtained by the division of the two spectra is shown in Fig. 5.

The lower curve shows the averaged attenuation characteristics for non-defective regions obtained from six different CAS-Nicalon plates. This curve was used to compare with the other areas which had programmed defects. Delaminations were produced by replacing a local single layer disc of composite with a layer of dry fibers without the glass-ceramic matrix. Porosity was introduced by varying the conditions of the "burn-out" stage in which organic components are driven from the laminate. It can be seen in Fig. 5 that the attenuation for the non-defective material is very low, with a maximum of 10 dB/cm implying that scattering from the fibers is not predominant. The porosity curve shows the expected increase in attenuation with frequency resulting from scattering from the voids. The curve associated with delamination is not flat, as may be expected from a simple planar defect but is less dependent on frequency than the porosity curve. This may be due to the fact that delamination is not a true planar discontinuity but is a single layer with partial transmission through the fibers and this causes some frequency-dependent characteristics to surface.

OBLIQUE INCIDENCE

In order to solve fiber-related problems such as fiber alignment, ply layup orientation, to improve porosity detection and to detect subsurface cracks, the oblique incidence technique was explored as a viable solution. This technique [4,5,6] has been proven to be very sensitive to fiber orientation and porosity level. The Surface Acoustic Wave (SAW) technique was utilized to find subsurface cracks.

A schematic of the experimental setup for backscatter measurement is shown in Fig. 6. By measuring the backscattered signal, fiber orientation and other fiber related defects can be detected [6].

In Fig. 7, a $[0/90]_{4s}$ CAS-Nicalon panel was scanned to show the four sharp backscattered signals associated with the 0° and 90° fibers. The fibers were initially aligned 45° to the transducer. The specimen was then rotated 360° (shown circumferentially) while the transducer was swept from 10° to 20° (shown radially) past the second critical angle. The layers closer to the front surface showed a higher backscatter amplitude than the ones further down. This proved to be quite useful in identifying the overall layup sequence. This technique could be further improved to show the total number of plies and their orientation. We observed that the material was not sensitive to the incidence angle ($\alpha = 10° - 20°$). This made the detection of the fiber orientation much easier than expected.

Fig. 8 displays a through-transmission C-scan that was generated using a pair of of 10 MHz (1/2" diameter) broadband transducers. Using the results from the scan in Fig. 7, a raster scan of a CMC specimen was performed with a chosen optimum incident angle (α) of 14°, to map the backscattered
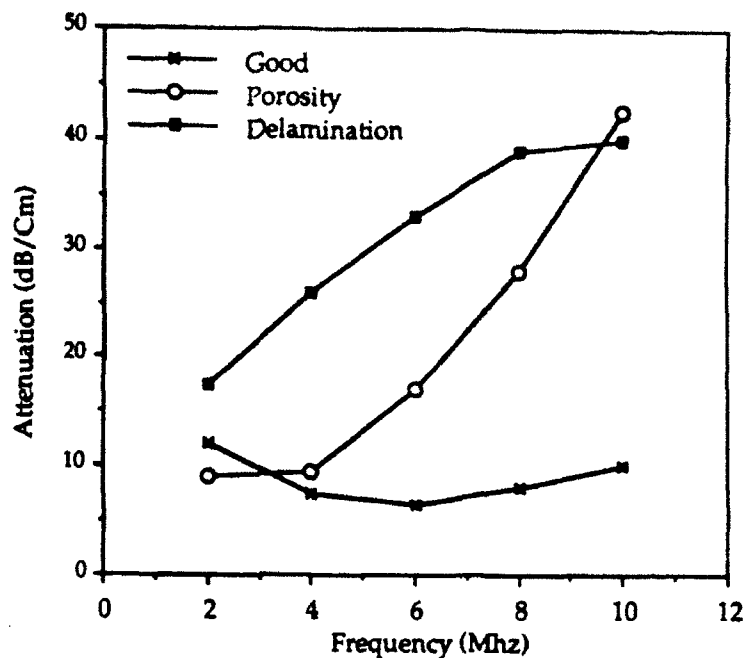
Fig. 5. Attenuation vs frequency plot for CAS-Nicalon CMC material.
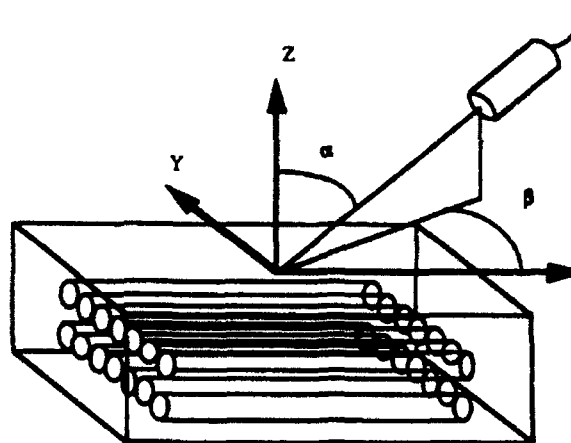
Fig. 6. Experimental setup used for backscatter measurement.

amplitude (Fig. 9). The comparison of Figs. 8 and 9 indicated that the backscatter method has a higher sensitivity to porosity detection than the through-transmission method.

To detect the subsurface cracks that may be present, we used a low frequency (5 MHz, 1.0" focus) SAW transducer to perform a through-transmission image of the sub-surface. Several researchers have shown the use of the SAW transducer to generate subsurface waves [7]. This approach was taken to image the CMC material with Nicalon fibers. This C-scan (Fig. 9) revealed considerable crack-like indications. On examining the micrographs of

102
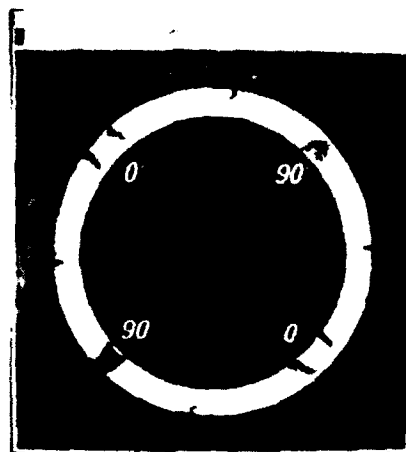
Fig. 7. Polar backscatter scan
showing the 0/90° fibers in a
[0/90] 4s CAS-Nicalon CMC.
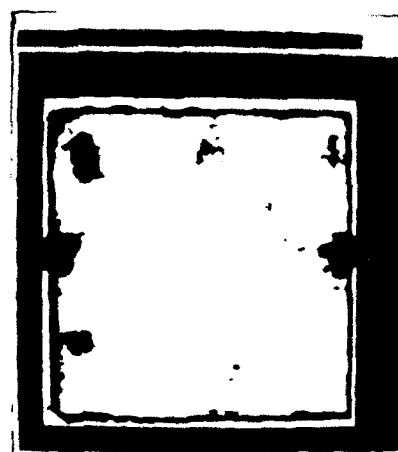
Fig. 8. Through transmission C-scan
of a [0/90]4s CAS-Nicalon
CMC with moderate porosity.

Fig.9. Backscatter scan of a
[0/90]4s CAS-Nicalon CMC
with moderate porosity.

Fig. 10. Surface acoustic wave scan
of a [0/90]4s CAS-Nicalon
CMC with moderate porosity
and subsurface defects.

this material we concluded that these indications were due to the cracks and/or
due to the inhomogenieties in the matrix. We expect that the further
development of this technique will aid in determining the complete material
stiffness matrix.

SUMMARY

We have a theoretical model to calculate elastic properties and ultrasonic
velocities for a variety of materials. This model has proven suitable for
parametric studies to examine effect of varying fiber volume fractions and
porosity among other things.

The materials used in experiments seem to be mildly anisotropic in contrast with graphite-epoxy composites. The low attenuation properties of the MMC and CMC materials make it practical to measure sound velocities. We also noted that the velocity transverse to the fibers is an useful indicator of the fiber volume fraction.

The measurement of frequency-dependent attenuation has proven to be very useful to classify defects. We have a practical method to acquire and process signals and our results indicate that this method has the potential to distinguish between porosity and planar type defects. For large scale operations, it would be necessary to optimize this inspection procedure. One rewarding approach could be the use of real-time DSP filtering techniques to extract two or three frequencies of interest instead of analyzing the entire waveform and spectrum.

We have identified polar backscatter technique to analyze fiber orientation and other fiber related defects. The backscatter technique has contributed to improving the sensitivity of porosity detection for the MMC and CMC materials. We have demonstrated that low frequency SAW has the potential to detect sub-surface def xcts, porosity and material inhomogeniety.

In our on-going research we have identified several potential techniques that can be implemented from the practical standpoint of NDE of advanced composites. We propose to utilize the frequency dependent backscatter signal in characterizing other difficult to detect fiber related defects. We anticipate that further developments in surface wave technique will aid in determining the complete material stiffness constants.

REFERENCES

1. McConnell, V.P., 1990, "Metal Matrix Composites: Materials in Transition - Part I", Advanced Composites, May/June, Vol. 5, No. 3.

2. Murakami, H., and Hegamier, G.A., 1986, "A Mixture Model for Unidirectionally Fiber-Reinforced Composites.", ASME Journal of Applied Mechanics, Vol. 53.

3. Auld, B.A., 1973, "Acoustic Fields and Waves in Solids", Vol. I and Vol. II, (John Wiley & Sons, N.Y.).

4. Rose, J.L., Pilarski, A., and Huang, Y., 1988, "Surface Wave Utility in Composite Material Characterization", Symposium, ASME AMD, Vol. 9D.

5. Rose, J.L., Nayfeh, A., and Pilarski, A., 1989, "Surface Waves for Material Characterization", ASME AMD.

6. Bar-Cohen, Y., and Crane, R.L., 1982, "Acoustic-Backscattering Imaging of Subcritical Flaws in Composites",Materials Evaluation, Vol. 40.

7. Gilmore, R.S., Tam, K.C., Young, J.D., and Howard, D.R., 1986, "Acoustic microscopy from 10 to 100 MHz for industrial applications", Phil. Trans. Royal Society, A320.

LOW FREQUENCY DIRECTIONAL ACOUSTIC MICROSCOPE FOR NONDESTRUCTIVE EVALUATION

Manohar Bashyam,
GE Aircraft Engines, Cincinnati, OH 45215.

&

Joseph L. Rose,
Pennsylvania State University, University Park, PA 16802.

ABSTRACT

The main thrust of this work was to develop a technique for measuring the anisotropic properties of materials. A low frequency (5MHz) technique was developed using a single transducer similar to the one used in acoustic microscopy, to measure anisotropic properties of ceramic matrix composite (CMC) materials. Experiments were conducted to verify that the velocity of the SAW is a function of the fiber orientation and fiber content of unidirectional CMC. Several important anomalies were imaged and compared to the results obtained from destructive analysis.

BACKGROUND

A brief literature survey on the current NDE practices used in evaluating ceramic and CMC materials is presented [1]. The CMC material chosen for this research consists of calcium aluminum silicate glass-ceramic matrix, reinforced with 15 μm diameter silicon carbide and silicon oxide based fibers and was made by Corning Glass. The size of the fibers are illustrated in [2]. Various types of defects were deliberately introduced into these panels by the manufacturer, to simulate delamination, porosity, fiber breakage, matrix cracking, etc.

PRINCIPLES OF SAW VELOCITY MEASUREMENT

The principle of operation of a highly convergent (spherically focused) transducer for the generation of surface acoustic waves is discussed [1]. The output of this type of transducer pulse is due to the contribution of both the direct axial reflection from the material's top surface and the subsurface leaky Rayleigh waves. These two contributions are received on the same electrical channel. Therefore, they interfere to give rise to periodic maxima and minima as the lens is moved in and out of focus, yielding the well-known $V(z)$ curves. The velocity of surface acoustic waves (v_R) can be calculated by measuring the interval between the minima of these $V(z)$ curves [3]. This technique has been extremely successful in the high frequency tone burst mode for the measurement of leaky wave velocity in several monolithic ceramics. However, it is not a precise technique in the practical NDE of CMC, especially while using the low frequency surface wave transducers, because the presence of material noise and superposition of waveforms make it difficult to pinpoint the exact location of the minima. To overcome this, both the absolute and the perturbation of the surface acoustic wave velocity can be measured without scanning in the z direction, using a broad-band impulse converging beam, which is given by the following expression [4],

$$v_R = \left(\Delta t_R / v_0 z - \Delta t_R^2 / 4z^2 \right)^{-\frac{1}{2}} \quad (1)$$

where, v_0 is the velocity of the acoustic waves in the coupling media, z represents the defocus distance of the transducer and Δt_R is the time interval between the arrival of the axial and the surface waves at the transducer.

It is important to remember that the surface waves are formed by the intersection of the highly convergent beam of sound. When this cone of sound intersects with the specimen, it forms a circular entry. This formation occurs only if the wave velocity is equal in all directions around the entry circle, which is the case for isotropic materials. But, when the surface wave velocity varies with direction in the plane of the surface, then the travel time along each entry-exit path is different, and

the received amplitude is dependent on both the length of each path and the summation of all the arrival times back to the transducer with respect to both their amplitude and phase. This situation which occurs in anisotropic materials can be overcome by using a transducer in which the focus forms a line entry, that is, by cylindrically focusing. The advantage of the line-focus is that it will enable the measurement of absolute velocity in any direction with respect to fiber orientation in the specimen. This unique transducer at a low frequency of 5 MHz with 12 mm diameter and 12 mm line focus was specially built for this purpose.

The surface acoustic wave velocities of the CMC specimens N14, N15 and N16 (fiber content 35, 40 and 51% respectively) were measured using the 5 MHz cylindrically focused transducer, by gating the axial reflection and the leaky wave pulses at various locations of each of the specimens. The leaky wave velocity was computed from equation (1) with data collected at every 3°, with respect to fiber orientation on the top surface. Figure 1 shows the polar plot of the average of the velocities taken at five locations from 0° (along the fiber) to 90° (across the fiber) for each of the three unidirectional specimens. From this polar plot of the surface wave profile, the variations in velocity due to the anisotropic influence and fiber orientation can be observed. By noting the variations in velocities as a function of fiber orientation, it can be concluded that the cylindrically focused probe is capable of measuring the surface wave velocity in anisotropic materials.
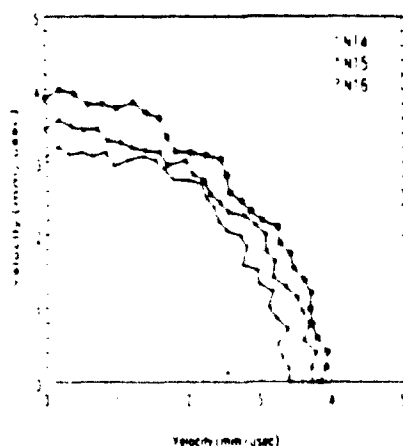
Figure 1. The SAW velocity obtained for the CMC specimens N14, N15 and N16. Each point represents the average of five data points with a standard deviation of 0.04 mm/µsec.

FEATURE MAPS

An imaging technique using a single 5 MHz transducer with 12 mm diameter and 12 mm spherical focus was developed to image quantitatively the inhomogeneities in the CMC anisotropic materials. The axial reflection and leaky surface wave signals were collected at each scanned location and the surface acoustic wave velocity was calculated using the velocity computations discussed earlier in equation (1). Figure 2a shows a scan obtained for a small section of the N6 test panel. The changes in velocity (3.0 - 3.4 mm/µsec) enabled the characterization of anomalies including porosity and changes in fiber fraction in the CMC specimen.

Similar experiments were conducted using the innovative 5 MHz cylindrically focused transducer at different SAW propagation directions of 0°, 45° and 90° with respect to fiber orientation. It is evident from these velocity maps shown in Figures 2(b-d) that certain material inhomogeneities are detectable only under specific wave propagation directions, signifying the need for quantitative evaluation of the material properties in various different directions. Furthermore, the potential of the cylindrically focused probe for this type of inspection is exploited.

Another important material inhomogeneity is the formation of micro-cracks during the manufacturing and in-service life cycle of CMC. Traditional techniques of inspection using bulk waves are unable to image these defects because the size of the micro-cracks is very small (100 µm). The problem of detection is further aggravated by the presence of these cracks close to the top surface of the material. These micro-cracks can, however, be detected by conventional bulk wave techniques provided high frequency (100 - 300 MHz) ultrasonic inspection methods are used. The presence of large fibers in these materials cause large amounts of scatter at these high frequencies. This makes the detection of cracks which are a few times larger than the size of the fibers in the material (10-15 times size of the fiber diameter) extremely difficult. In contrast, since the surface acoustic waves travel along the surface of the fibrous material, they are quite capable of detecting inhomogeneities in the materials, such as micro-cracking, even when they are very small and close to the top surface. This capability is demonstrated

106

(a)   (b)

(c)   (d)
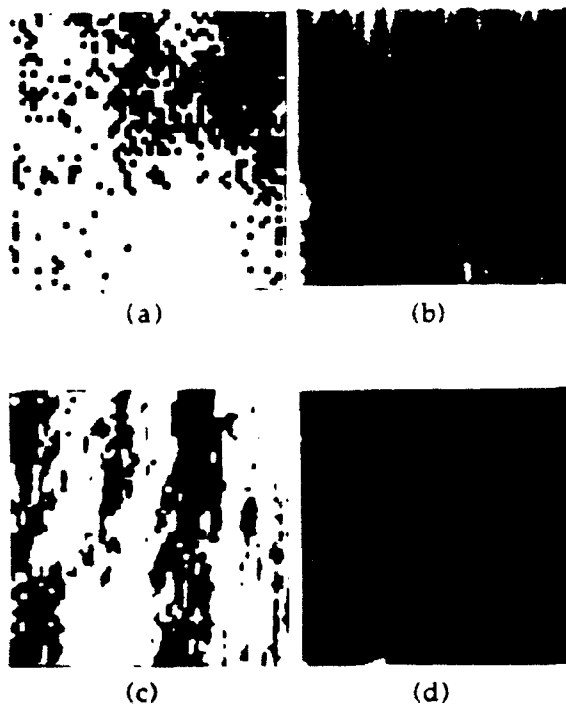
Figure 2. SAW velocity maps.

(a) Illustrate the presence of porosity which is indicated by the low amplitude, obtained using a 5MHz spherically focused transducer.

(b-d) Shows the presence of material inhomogeneity which significantly affects the SAW velocity in certain propagation directions of 0°, 45° and 90° respectively, obtained using a 5MHz cylindrically focused transducer.

(a)

(b)

Figure 3. C-scan of surface acoustic wave amplitude for the CMC specimen obtained by gating leaky surface waves using a 50 MHz SAW transducer (1.27 mm defocus). Linear indications represent micro-cracking.

(a) CMC specimen N6, revealing high degree of micro-cracking.

(b) CMC specimen N5, revealing traces of micro-cracking.

using surface acoustic wave transducers at 5 MHz [2] and 50 MHz frequencies, with a noticeable improvement in the depth of penetration while using the lower frequency probe. In Figure 3, a surface acoustic wave image of the CMC specimen N6 is shown, which was obtained by gating the leaky surface waves using the 50 MHz spherically focused transducer at 1.27 mm defocus. This CMC specimen N6 was created with moderate porosity and micro-cracking. Another CMC specimen N5 with low porosity and traces of micro-cracking was scanned to compare changes in SAW amplitude due to variations in micro-cracking. The interaction of a micro-crack with the entry circle varies depending on the position of the entry circle. When the entry circle is positioned over the crack, the surface acoustic wave amplitude is completely blocked. But, when the entry circle is positioned partially over the micro-crack, defects that are much smaller than the entry circle allow the interaction of a few of the rays. Some of the energy is transmitted while there is still a significant loss of SAW energy. As a result of this loss of surface acoustic wave energy and the small entry circle, the transducer can be used to image the micro-cracks that are smaller than the entry circle by scanning over the entire specimen.

107

To summarize, it can be stated that the low frequency transducer is adequate for imaging CMC specimens, since it provides a greater depth of penetration when compared to the high frequency transducer and it is recommended for imaging specimens with high degree of inhomogeneities that are typically found in composite laminates.

BENEFITS OF THE SPHERICALLY FOCUSED TRANSDUCER TECHNIQUES

Inspection with the SAW at normal incidence can be achieved since the transducer is a single transducer with a highly focused beam. This provides an accurate measure of isotropic leaky wave velocities and a relative measure of anisotropic wave velocities. This setup results in a single sided inspection which is an useful tool for material characterization. For example, the properties of a single layer or few layers of a quasi-isotropic structure made up of several layers can be obtained, by careful selection of the ultrasonic transducer frequency and defocus. The large pulse width at the low ultrasonic frequencies while using the pulse-echo and through transmission techniques prevents the observation of near surface defects. This limitation in resolving near surface defects is minimized here, since the surface acoustic waves are not limited by the pulse width and are sensitive only to the inhomogeneities at a small depth into the material. Anisotropic effects are cancelled due to the integrated effect of the 360° beam entry.

BENEFITS OF THE CYLINDRICALLY FOCUSED TRANSDUCER TECHNIQUES

A significant improvement of the cylindrical focusing over the spherically focused surface wave transducer is that due to the line-focus; it is possible to measure anisotropic properties of materials, especially the SAW velocity as a function of fiber orientation. This allows the quantitative characterization of the anisotropic materials by a single sided normal incidence technique as a function of the rotational angle of the probe. This transducer unlike the spherically focused probe, cannot create images with good resolution due to the fairly large line focus when the line focus is across the defects, in noting however, the image accuracy is better since there is no integration over the 360° circular entry path. Regardless, it can still produce images with improved resolution to map the inhomogeneities in the anisotropic material when compared to the

traditional dual transducer techniques.

SUMMARY

In summary, low frequency transducers similar to the transducers used in acoustic microscopy were explored to characterize anisotropic CMC materials. Quantitative measurements of the SAW velocities in the low frequency were made, to characterize the fiber and porosity content of the CMC specimens. Material inhomogeneities such as micro-cracking, porosity, fiber distribution delaminations, etc. were imaged using the amplitude of the reflected SAW signals. The results thus obtained were compared with the results of the high frequency surface acoustic waves. A technique that was developed to image the variations in the near surface characteristics of a specimen by measuring the local perturbation of the Rayleigh wave velocity, was discussed. A novel line-focused transducer that was used to measure the directional propagation of SAW in the anisotropic CMC material was presented. In conclusion, the use of the spherically focused transducer was recommended for quantitative imaging to map inhomogeneities in the material while the cylindrically focused probe should be preferred to measure absolute leaky surface wave velocities and to characterize anisotropic properties of materials such as ceramic matrix composites.

ACKNOWLEDGEMENT

REFERENCES

1. Bashyam, M., Rose, J.L., "Surface Acoustic Wave Techniques for Ceramic Matrix Composite Materials Characterization," *Review of Progress in Quantitative NDE*, Vol. 11, Plenum Press, NY., 1991.

2. Bashyam, M., "Ultrasonic NDE for Ceramic- and Metal- Matrix Composite Material Characterization," *Review of Progress in Quantitative NDE*, Vol. 10, Plenum Press, NY., 1990.

3. Atalar, A., *J. Appl. Phys.* Vol. 50, pp. 8237, 1979.

4. Yamanaka, K., "Surface Acoustic Wave Measurements using Impulse Converging Beam," *J. Appl. Phys.* Vol. 54 (8), pp. 4323-4329, Aug. 1983.

SURFACE ACOUSTIC WAVE TECHNIQUES FOR CERAMIC MATRIX COMPOSITE

MATERIALS CHARACTERIZATION

Manohar Bashyam and Joseph L. Rose*

GE - Aircraft Engines
One Neumann Way. Mail Drop - Q45
Cincinnati, Ohio 45215

* Pennsylvania State University, University Park. PA 16802

INTRODUCTION

A brief summary of the progress of the research in the internal structural characterization of ceramic matrix composite (CMC) materials is presented. The objective of this research is to focus on the classification of the various anomalies such as delamination, porosity and inhomogeneity in CMC. It will also address the issues of anisotropy and quantification of fiber fraction. Two types of surface acoustic wave (SAW) techniques are explored to characterize CMC materials, a line-source technique in contact mode and the use of a single transducer similar to that used in acoustic microscopy. The generation of surface acoustic waves with low frequency transducers is emphasized in this work; results obtained are compared with the results of high frequency surface acoustic waves. Quantitative measurements of the surface acoustic wave velocities are made to characterize the fiber and porosity content of various CMC specimens. Material inhomogeneities such as micro-cracking, porosity, fiber distribution, etc. are imaged using the amplitude of the reflected surface acoustic wave signals. A novel line-focused transducer is used to measure the directional propagation of SAW in anisotropic CMC materials. This highly convergent line-focused probe significantly alleviates the difficulties encountered while using the two transducer contact mode setup to characterize CMC materials.

The CMC material chosen for this research was made by Corning Glass, with calcium aluminum silicate glass-ceramic matrix, reinforced with 15 μm diameter silicon carbide (Nicalon™) fibers. The size of the fibers are illustrated in [1]. Various types of defects were deliberately introduced into these panels by the manufacturer, to simulate delamination, porosity, fiber breakage and matrix cracking etc.

A brief literature survey on the current NDE practices used in evaluating ceramic and CMC materials is presented. To detect and evaluate reflections from discrete flaws in monolithic ceramics, traditional ultrasonic measurement methods like the pulse-echo technique at 50 MHz [2-5] are used which include measurements of attenuation and velocity of ultrasonic waves as a function of ultrasonic frequency. These results reveal correlation to the location and size of anomalies in monolithic ceramic materials such as silicon nitride (Si_3N_4) and silicon carbide (SiC). To detect small (50 μm) near-surface flaws of the composite, high frequency ultrasonic SAW have been studied. Kunerth and Walter [6] developed an acoustic microscopy technique using high frequency (50 MHz) focused ultrasonic transducers. Preliminary studies were conducted by Bashyam [1] on two types of CMC and a metal matrix composite to demonstrate the influence of frequency dependent attenuation on anomalies such as porosity and delamination. It was also shown that backscatter can be used to detect fiber orientation in a bidirectional composite layup.

CMC were modeled to show that they were mildly anisotropic in comparison to polymeric composites that are being investigated extensively by other researchers. From this literature survey it is evident that research on monolithic ceramics and CMC has been focused on the problems relating to the location and characterization of localized defects, but little emphasis has been placed on the effect of global inhomogeneities while evaluating the overall material properties such as elastic constants, degrees of failure and degradation. All these issues need to be addressed together with detailed local inspection, taking into consideration the anisotropic influence and inhomogeneities of the ceramic matrix composites.

GENERATION OF SAW BY THE CONTACT LINE SOURCE METHOD

To overcome the difficulty associated with the generation of surface acoustic waves in materials where the SAW velocity is close to the longitudinal velocity of the coupling medium, Rose et al. [7] adopted a line source method similar to the one presented by Auld [8] with some modifications. The transducers are coupled with the mediator in such a way that the transducer's incident angle is at the third critical angle of the mediator. This enables the generation of SAW within the mediator which in turn produces surface waves in the composite test specimen (Figure 1). As the surface wave travels down the mediator, its thickness is decreased to form a wedge which is equivalent to a sharp line source placed on the composite. This line source is able to generate surface waves as well as other modes within the composite material. To steer the propagation direction of the generated surface waves, an oblique configuration was utilized. This type of surface wave generation method was explored for the CMC materials in this research. Fortunately, traditional techniques of surface wave generation using a coupling medium alone also worked well since the surface wave velocity in ceramic composites is in the range of 3500 - 3900 m/s, significantly higher than the surface wave velocity in graphite-epoxy materials. But, the use of the line source technique was still preferred because of the robust fixturing and consistent data collection procedure compared to the more traditional approach.

In the experimental setup to measure surface wave velocity, the surface waves from the line source (that is the edge of the mediator that is attached to the transmitter), are generated on the specimen and received by the edge of another mediator which is attached to the receiving transducer and is separated from the line source by a known distance. The measurements of the surface wave velocity were performed with a differential measurement technique. A small measurement distance was chosen due to large attenuation (0.6 dB/mm in the fiber direction and 1.0 dB/mm in the perpendicular direction at 2.25 MHz center frequency) and to avoid any difficulties in the interpretation of the received signals that might arise due to the finite thickness of the composite layer and the possible occurrence of the reflected waves from the far side.
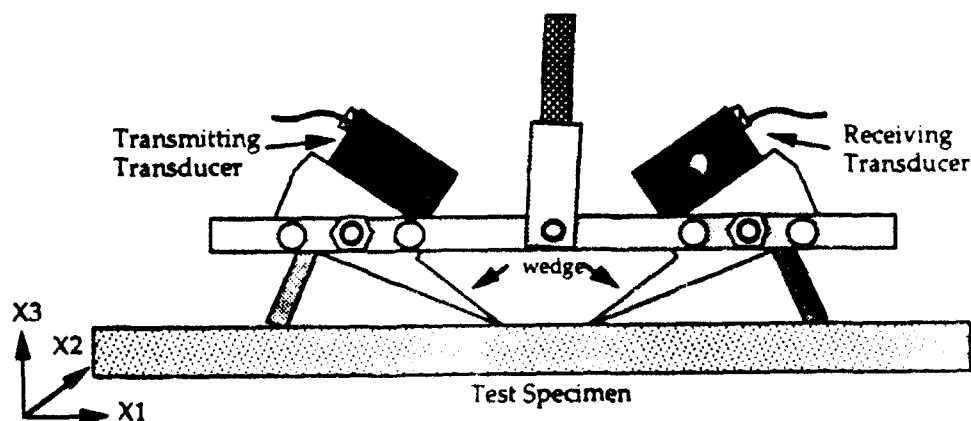

Figure 1. Experimental configuration for SAW velocity measurement in contact mode using a modified line source method to generate surface waves.

MEASUREMENT OF FIBER CONTENT AND FIBER ORIENTATION

Surface wave velocity measurements were carried out on three CMC specimens with unknown material properties. The specimens used were N14, N15 and N16 which were blocks of unidirectional ceramic matrix composite with varying fiber fraction estimated (by photo-micrographs) to be 35%, 40% & 51% respectively. Five different areas on the surface (X1-X2) of the specimen were selected to generate surface waves. The sending and receiving transducers were kept at a known distance d apart and the received surface wave RF signal was collected with an analog-to-digital (A/D) recorder. The receiver probe was then moved a small distance Δd apart and the RF signal was collected again. The data of these two waveforms were then sent through an envelope detection (Hilbert Transform) program that accurately calculated the time between the peaks of the envelopes of the two signals and directly computed the velocity with the known value Δd. Data was collected with a 2.25 MHz transducer (0.8 MHz -6dB bandwidth) while varying the propagation direction from along the fibers to across the fibers in small increments of $3°$ on the X1-X2 plane. Figure 2 presents a polar plot of the average of the velocities obtained at five locations for each of the three different CMC specimens N14, N15 and N16.

This illustrates the relative change in magnitude of these average velocities for different fiber fractions. It is clear from this plot that an increase in the fiber fraction of a material causes the surface wave velocity to increase. The area under these curves could be an useful feature which can be used in feature-based systems to characterize and classify these materials. It was also observed that the degree of anisotropy was mild since the change in velocity between $0°$ and $90°$ was small. The range of the velocity data for the CMC test specimen N14 was between 3.2 - 3.5 mm/μsec, while the average was 3.4 mm/μsec and the standard deviation was 0.07 mm/μsec in the $0°$ direction. This variation can be explained by the following statements. The assumption is made that the material is homogeneous with both depth and in-plane distance through which the surface wave propagates. The relatively large distance used for transducer separation will significantly influence the surface wave velocity measurement if there is any material inhomogeneity within that distance. The errors associated with the mechanical fixturing, transducer separation, contact pressure and inadequate coupling could influence the velocity measurements.
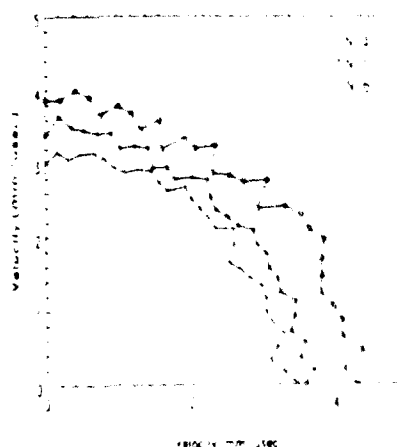

Figure 2. Experimental surface acoustic wave velocity in the X1-X2 plane, obtained by using the contact mode method with a pair of 2.25 MHz transducers, for CMC specimen N14, N15 and N16. Each point represents the average of five data points with a standard deviation of 0.07 mm/μsec.

GENERATION OF SAW BY A HIGHLY CONVERGENT TRANSDUCER

The principle of operation of a highly convergent transducer for the generation of surface acoustic waves is discussed. Consider Figure 3, in which a transducer with a highly focusing lens is placed over the test specimen in such a way that the focal point of the transducer is within the specimen. The lens and the test specimen are acoustically coupled through a coupling medium which is typically water. When this acoustic lens is placed with its focal point below the surface of the substrate, the most significant contributions to the electrical output of the piezo-electric transducer are the on-axis ray (direct axial reflection) and the outer rays that impinge on the water-solid interface at the Rayleigh angle θ_R, which excite leaky surface waves that are reradiated back to the acoustic lens. The use of this architecture is proposed in this research, in place of the traditional dual transducer techniques that are cumbersome to characterize CMC materials. It was found that the sensitivity to subsurface features could be increased by defocusing [9]. Defocusing is achieved by moving the transducer closer to the test material, so that, the transducer focus is located within the sample, under the assumption that the sample does not affect the acoustic fields. In Figure 3, the distance z represents the defocus of the transducer.

PRINCIPLES OF SAW VELOCITY MEASUREMENT

The output of the transducer pulse is due to the contribution of both the direct axial reflection from the material's top surface and the subsurface leaky Rayleigh waves. These two contributions are received on the same electrical channel. Therefore, they interfere to give rise to periodic maxima and minima as the lens is moved in and out of focus, yielding the well-known $V(z)$ curves. The velocity of surface acoustic waves (v_R) can be calculated by measuring the interval between the minima of these $V(z)$ curves [10]. This technique
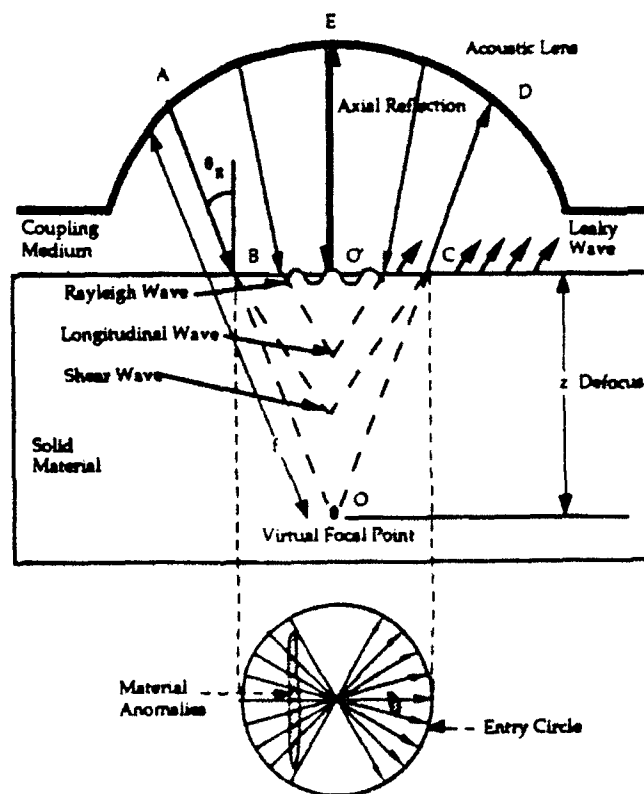

Figure 3. A ray model of the acoustic fields of the converging beam and the axially reflected waves from a highly convergent transducer. The leaky surface wave component is excited by the incident ray at the Rayleigh critical angle θ_R.

112

has been extremely successful in the high frequency tone burst mode for the measurement of leaky wave velocity in several monolithic ceramics. However, it is not a precise technique in the practical NDE of CMC, especially while using the low frequency surface wave transducers because the presence of material noise and superposition of waveforms make it difficult to pinpoint the exact location of the minima. To overcome this, both the absolute and the perturbation of the surface acoustic wave velocity can be measured without scanning in the z direction, using a broad-band impulse converging beam, which is given by the following expression [11],

$$v_R = \left(\Delta t_R / v_0 z - \Delta t_R^2 / 4z^2 \right)^{1/2} \qquad (1)$$

where, v_0 is the velocity of the acoustic waves in the coupling media and Δt_R is the time interval between the arrival of the axial and the surface waves at the transducer.

It is important to remember that the surface waves are formed by the intersection of the highly convergent beam of sound. When this cone of sound intersects with the specimen, it forms a circular entry. This formation occurs only if the wave velocity is equal in all directions around the entry circle, which is the case for isotropic materials. But, when the surface wave velocity varies with direction in the plane of the surface then the travel time along each entry-exit path is different, and the received amplitude is dependent on both the length of each path and the summation of all the arrival times back to the transducer with respect to both their amplitude and phase. This situation occurs in anisotropic materials. This situation can be overcome by using a transducer in which the focus forms a line entry. This can be achieved by using a cylindrically focused transducer which produces a line-focused beam. The advantage of the line-focus is that it will enable the measurement of absolute velocity in any direction with respect to fiber orientation in the specimen. This unique transducer at a low frequency of 5 MHz with 12 mm diameter and 12 mm line focus was specially built for this purpose. This cylindrically focused transducer will enable the propagation of surface waves in a manner similar to the conventional oblique incidence techniques with dual transducer setup.

The surface acoustic wave velocities of the CMC specimens N14, N15 and N16 were measured using the 5 MHz cylindrically focused transducer, by gating the axial reflection and the leaky wave pulses at various locations of each of the specimen. The leaky wave velocity was computed from equation (1) with data collected at every 3°, with respect to fiber orientation on the X1-X2 plane. Figure 4 shows the polar plot of the average of the
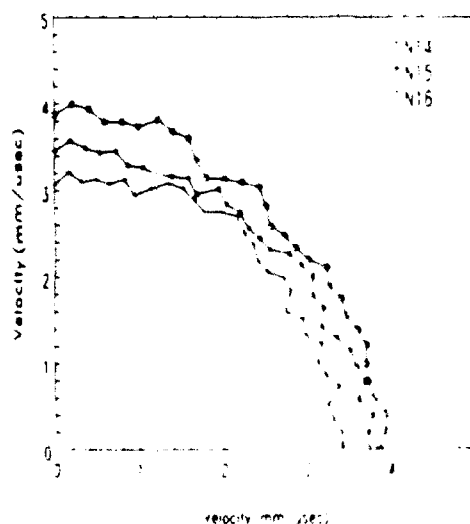

Figure 4. The SAW velocity obtained for the CMC specimen N14, N15 and N16. Each point represents the average of five data points with a standard deviation of 0.04 mm/μsec.

velocities taken at five locations from 0° (along the fiber) to 90° (across the fiber) for each of the three specimens. From this polar plot which is the surface wave profile, the variations in velocity due to the anisotropic influence and fiber orientation can be observed. By noting the variations in velocities as a function of fiber orientation, it can be concluded that the cylindrically focused probe is capable of measuring the surface wave velocity in anisotropic materials. The scatter in the SAW velocity data was significantly reduced when compared to the contact SAW method.

FEATURE MAPS

An imaging technique using a single 5 MHz transducer with 12 mm diameter and 12 mm spherical focus was developed, to image quantitatively the inhomogeneities in the CMC anisotropic materials. The axial reflection and leaky surface wave signals were collected at each scanned location and the surface acoustic wave velocity was calculated using the velocity computations discussed earlier in equation (1). Figure 5a shows a scan obtained for a small section of the N6 test panel. The changes in velocity (3.0 - 3.4 mm/μsec) enabled the characterization of anomalies including porosity and changes in fiber fraction in the CMC specimen

Similar experiments were conducted using the innovative 5 MHz cylindrically focused transducer at different SAW propagation directions of 0°, 45° and 90° with respect to fiber orientation. It is evident from these velocity maps shown in Figures 5(b-d) that certain material inhomogeneities are detectable only under specific wave propagation directions, signifying the need for quantitative evaluation of the material properties in various different directions. Furthermore, the potential of the cylindrically focused probe for this type of inspection is exploited.

Another important material inhomogeneity is the formation of micro-cracks during the manufacturing and the in-service life cycle of CMC. Traditional techniques of inspection using bulk wave and surface acoustic waves are unable to image these defects because the size of the micro-cracks is very small (order of 100 μm). The problem of detection is further aggravated by the presence of these cracks close to the top surface of the material. These micro-cracks can, however, be detected by conventional bulk wave techniques provided high frequency (100 - 300 MHz) ultrasonic inspection methods are used. The presence of large fibers in these materials cause large amounts of scatter at these high frequencies. This makes the detection of cracks which are a few times larger than the size of the fibers in the material (ten to fifteen times size of the fiber diameter) extremely difficult. But, since the surface acoustic waves travel along the surface of the fibrous material, they are quite capable of detecting inhomogeneities in the materials, such
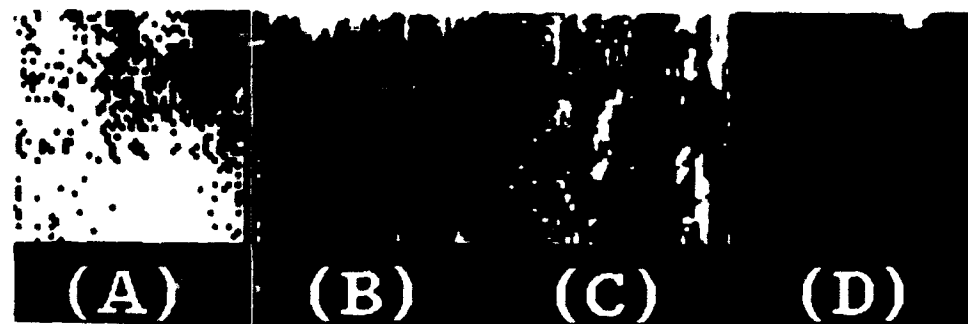

Figure 5. SAW velocity maps with the 5MHz spherical and cylindrical transducers.
    (a) Illustrate the presence of porosity which is indicated by the low amplitude.
    (b-d) Shows the presence of material inhomogeneity which significantly affects the SAW velocity in certain propagation directions of 0°, 45° and 90° respectively.
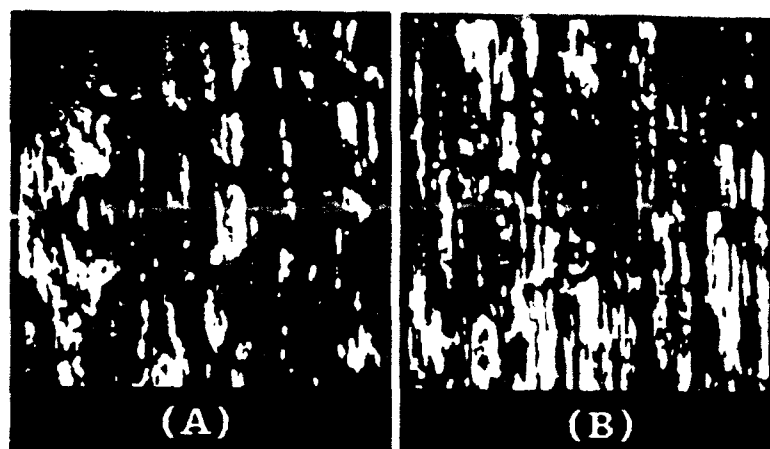
Figure 6. C-scan of surface acoustic wave amplitude for the CMC specimen obtained by gating leaky surface waves using a 50 MHz SAW transducer (1.27 mm defocus). Linear indications represent micro-cracking.
(a) CMC specimen N6, revealing high degree of micro-cracking.
(b) CMC specimen N5, revealing traces of micro-cracking.

as micro-cracking, even when they are very small and close to the top surface. This capability is demonstrated using surface acoustic wave transducers at 5 MHz and 50 MHz frequencies, with a noticeable improvement in the depth of penetration while using the low frequency probe. The SAW images from the CMC specimen which have varying degree of micro-cracking, that were obtained using the 5 MHz probe [1] were compared with the SAW images obtained using the 50 MHz probe. In Figure 6, a surface acoustic wave image of the CMC specimen N6 is shown, which was obtained by gating the leaky surface waves using the 5 MHz spherically focused transducer at 1.27 mm defocus. This CMC specimen N6 was created with moderate porosity and micro-cracking. Another CMC specimen N5 with low porosity and traces of micro-cracking was scanned to compare changes in SAW amplitude due to variations in micro-cracking. The interaction of a micro-crack with the entry circle varies depending on the position of the entry circle (Figure 3). When the entry circle is positioned over the crack, the surface acoustic wave amplitude is completely blocked. But, when the entry circle is positioned partially over the micro-crack, defects that are much smaller than the entry circle allow the interaction of a few of the rays and some of the energy is transmitted while there is still a significant loss of SAW energy. As a result of this loss of surface acoustic wave energy and the small entry circle, the transducer can be used to image the micro-cracks that are smaller than the entry circle by scanning over the entire specimen.

To summarize, it can be stated that the low frequency transducer is adequate for the imaging of the CMC specimen, since it provides a greater depth of penetration when compared to the high frequency transducer and it is recommended for imaging of specimens with high degree of inhomogeneities that are typically found in composite laminates.

BENEFITS OF THE SPHERICALLY FOCUSED TRANSDUCER TECHNIQUES

Inspection with the SAW at normal incidence can be achieved since the transducer is a single transducer with a highly focused beam. This provides an accurate measure of isotropic leaky wave velocities and a relative measure of anisotropic wave velocities. This setup results in a single sided inspection which is an useful tool for material characterization. For example, the properties of a single layer or few layers of a quasi-isotropic structure made up of several layers can be obtained, by careful selection of the ultrasonic transducer frequency and defocus. The large pulse width at the low ultrasonic frequencies while using the pulse-echo and through transmission techniques prevents the observation of near surface defects. This limitation in resolving near surface defects is minimized here, since the surface acoustic waves are not limited by the pulse width and are sensitive only to the inhomogeneities at a small depth into the material. Anisotropic effects are cancelled due to the integrated effect of the 360° beam entry.

BENEFITS OF THE CYLINDRICALLY FOCUSED TRANSDUCER TECHNIQUES

A significant improvement of this type of focusing over the spherical focused surface wave transducer is that due to the line-focus, it is possible to measure anisotropic properties of materials, especially the SAW velocity as a function of fiber orientation. This allows the quantitative characterization of the anisotropic materials by a single sided normal incidence technique as a function of the rotational angle of the probe. This transducer unlike the spherically focused probe, cannot create images with good resolution due to the fairly large line focus when the line focus is across the defects, in noting; however, the image accuracy is better since there is no integration over the 360° circular entry path. But, it can still produce images with improved resolution to map the inhomogeneities in the anisotropic material when compared to the traditional dual transducer techniques.

SUMMARY

In summary, the contact mode technique proved to be quite useful in characterizing material inhomogeneities. The use of several single transducers similar to the transducer used in acoustic microscopy, were also explored to characterize the anisotropic CMC materials. Quantitative measurements of the SAW velocities in the low frequency were made, to characterize the fiber and porosity content of the CMC specimen. Material inhomogeneities such as micro-cracking, porosity, fiber distribution delaminations, etc. were imaged using the amplitude of the reflected SAW signals. The results thus obtained were compared with the results of the high frequency surface acoustic waves. A technique that was developed to image the variations in the near surface characteristics of a specimen by measuring the local perturbation of the Rayleigh wave velocity, was discussed. A novel line-focused transducer that was used to measure the directional propagation of SAW in the anisotropic CMC material was presented. In conclusion, the use of the spherically focused transducer was recommended for quantitative imaging to map inhomogeneities in the material while the cylindrically focused probe should be preferred to measure absolute leaky surface wave velocities and to characterize anisotropic properties of materials such as ceramic matrix composites.

ACKNOWLEDGEMENT

REFERENCES

1. Bashyam, M., "Ultrasonic NDE for Ceramic- and Metal- Matrix Composite Material Characterization," *Review of Progress in Quantitative NDE*, Vol. 10 (B), Editors. Thompson, D.O. and Chimenti, D.E., Plenum Press, NY., 1990.
2. Chou, C.H., Khuri-Yaqub, B.T., Liang, K. and Kino, G.S., "High-Frequency Bulk Wave Measurements of Structural Ceramics," *Review of Progress in Quantitative NDE*, La Jolla, CA., pp. 663-670, Jul. 8-13, 1979, AFWAL-TR-80-4078, 1980.
3. Kino, G.S., Khuri-Yaqub, B.T., Murakami, Y. and Yu, K.H., "Defect Characterization in Ceramics Using High-Frequency Ultrasonics," *Review of Progress in Quantitative NDE*, La Jolla, CA., pp. 242-245, Jul. 1978, AFML-TR-78-205, 1979.
4. Derkacs, T., "High-Frequency Longitudinal and Shear Wave Inspection of Gas Turbine Ceramics," *Review of Progress in Quantitative NDE*, pp. 251-266, 1978.
5. Derkacs, T., Matay, M., and Brentall, W.D., "Nondestructive Evaluation of Ceramics," Final Technical Report, TRW-ER-7798-F, Apr. 1976.
6. Kunerth D.C., and Walter., J.B., "Time-of-Flight Acoustic Microscopy of Silicon Carbide," submitted to *Advanced Ceramics Materials*, Idaho National Engg. Lab., ID.
7. Rose, J.L., Pilarski, A. and Huang, Y., "Surface Wave Utility in Composite Material Characterization," *Research in Nondestructive Evaluation*, Vol. 1 (4), pp. 247-265, 1990.
8. Auld, B.A., Acoustic Fields and Waves in Solids, John Wiley, Vol. 2, pp. 163-167, 1973.
9. Khuri-Yakub, B.T., Reinholdsten, P., Chou, C-H. and Arnaud, J.L., "Acoustic Imaging of Subsurface Defects in Composites and Samples with Rough Surfaces," *1985 IEEE Ultrasonics Symposium*, 1985.
10. Atalar, A., *Journal of Applied Physics*, Vol. 50, pp. 8237, 1979.
11. Yamanaka, K., "Surface Acoustic Wave Measurements using Impulse Converging Beam," *Journal of Applied Physics*, Vol. 54 (8), pp. 4323-4329, Aug. 1983.